Ultrafast nonlinear optics in semiconductors

Walmsley, M.

ULTRAFAST NONLINEAR OPTICS IN SEMICONDUCTORS

by

M. Walmsley, B.Sc., B.Sc.

A thesis

submitted for the degree of

Doctor of Philosophy

at the University of Durham.

1993

ABSTRACT

The nonlinear optical phenomena which occur in semiconductor materials on a femtosecond to picosecond timescale have recently generated much interest, especially in the field of telecommunications where the development of all-optical switching devices based on semiconductors promises a considerable reduction in the complexity of design coupled with a large increase in the speed of operation. This thesis examines the underlying ultrafast physical processes with the aim of providing a clear understanding of the mechanisms involved.

The two main regimes of operation are investigated, namely off-resonance excitation where virtual processes are important and on-resonance excitation where real carriers are photogenerated, and in each case a particular system of interest is studied. For the virtual regime of operation, a recent proposal is examined which suggests the use of bandstructure engineering for a semiconductor quantum well in order to enhance the nonlinear optical response by the introduction of additional resonant transitions between subbands. A number of descriptions of the device are presented, and it is concluded that the technique does not necessarily lead to an improved response. An example of on-resonance phenomena is provided by the modelling of the fast refractive index changes in semiconductor laser amplifiers which have been observed in recent experiments. A simple physical model is developed which predicts the behaviour seen in the experimental observations. The nonlinear optical response of the laser amplifier promises the development of fast all-optical switching based on these devices.

The thesis also examines the difficulties associated with describing the interaction of semiconductor material and electromagnetic field, and in particular looks at the formulation of a gauge invariant procedure for calculating values of the susceptibility. The propagation of a light beam along the plane of a semiconductor quantum well is discussed, and the gauge invariance of susceptibility calculations performed in the so called $\mathbf{A}.\mathbf{p}$ and $\mathbf{E}.\mathbf{r}$ gauges is explicitly demonstrated. Finally, a brief exploration is undertaken of the effects of bandstructure on the optical response of a semiconductor, and two quantum well models for the calculation of a more realistic bandstructure are presented which employ infinite and finite wells respectively.

DECLARATION

I declare that this thesis and all original material contained within it (except as otherwise acknowledged) are solely the work of the author, and that no part of the thesis has previously been submitted for a degree at this or any other university.

Ph.D. Candidate

Ph.D. Supervisor

ACKNOWLEDGEMENTS

I would like to thank my academic supervisor Dr. R.A. Abram and my industrial supervisor Dr. M.G. Burt for their many helpful suggestions and constructive criticisms throughout the course of my studies at Durham and in the preparation of this thesis. I also gratefully acknowledge the financial support of a CASE studentship provided by BT and the Science and Engineering Research Council.

Much of the material in chapter four has previously appeared in the paper 'Ultrafast nonlinear optical response of quantum wells ...', M. Walmsley *et al.* (Semicond. Sci. Technol. **8** 268 (1993)). The work on the infinite quantum well model which appears in chapter six was developed in collaboration with Mr. G.C. Crow, whilst the finite quantum well model is a development of the earlier work of Dr. A.C.G. Wood.

Finally, I would like to thank Robert Kelsall, John French, David Hall, Andrew Wood, Graham Warren, David Hughes, Mark Leeson, Martyn Chamberlain, Stuart Brand, Dick Abram, Stephen Wilson, Gavin Crow and especially David Hoare for each contributing in their own way to the total Durham experience.

à la France

'God said, "Let there be light."

And there was light.'

Genesis **1** 3

CONTENTS

CHAPTER ONE

Introduction

The advent of the laser with the inherent strong fields that it provides has provoked much interest in the study of nonlinear optics in various material systems. Of particular interest here are semiconductor materials and microstructures and their potential use in integrated all-optical switching systems for applications in the field of telecommunications. The current approach is to use transducers to interface optical and electronic subsystems but an integrated all-optical design would reduce the overall complexity of the system and also promises much faster speeds of operation. Electronic technology currently limits transmission rates to around one gigahertz, but switching with optical pulses of picosecond duration or less is theoretically practicable. In this thesis a study is made of the so called ultrafast nonlinear processes in semiconductor materials and microstructures (which typically occur on the timescale of 10fs to 10ps), with the aim of understanding these processes for eventual use in novel all-optical switching devices.

The second chapter of the thesis is devoted to providing a basic understanding of the theoretical concepts and calculation techniques required in the study of ultrafast nonlinear optical phenomena. In chapter three, consideration is given

to the problem of describing the interaction of the semiconductor material system with the electromagnetic field of an intense light beam. In particular the issues relating to the choice of electromagnetic gauge are examined and the gauge invariance of the susceptibility calculations is demonstrated in an example of practical importance.

Chapters four and five contain the major investigations of the thesis. Chapter four looks at off-resonance phenomena where optical excitation of the semiconductor is produced by radiation at a frequency slightly below the absorption band of the material, and a detailed discussion of the response in this so called virtual carrier regime is presented by employing a perturbative approach. In chapter five, on-resonance phenomena are considered where the excitation occurs within the absorption band of the material. In this case the perturbative approach of chapter four is no longer satisfactory and the use of the Bloch equations to model the resonant excitation is necessary. Chapter five is dedicated to modelling the fast refractive index changes in semiconductor laser amplifiers that have been observed in recent experiments, and it considers the effects of thermal relaxation of carriers within the device to equilibrium energy distributions.

In chapter six, the approximation of parabolic bands is questioned and a more realistic bandstructure is calculated for a typical quantum well structure. The chapter also examines the variation of optical response over the Brillouin zone and how this is influenced by the plane of the polarisation of the light beam.

Throughout the thesis the Coulombic interactions which lead to the formation of excitonic states are neglected, but chapter seven outlines how such effects may be included within the framework presented here. Also the thermal relaxation processes discussed in chapter five are modelled using a number of phenomenological time constants, and chapter seven briefly examines some theoretical techniques for the calculation of the scattering rates involved in these processes.

CHAPTER TWO

Fundamentals of ultrafast nonlinear optics

This chapter provides a brief introduction to the basic concepts and methods of calculation applicable to a study of ultrafast nonlinear optics. The first section describes the wave equation for a light beam propagating through a semiconductor material and extends the ideas of linear optics to the nonlinear regime. The constitutive relation between electric field and induced polarisation is presented, and the susceptibility coefficients $\chi^{(r)}$ are defined. Next the density matrix formalism is developed and the calculation of the density matrix from the Liouville equation is discussed. For a semiconductor illuminated by a light beam, the density matrix permits the determination of the electronic state occupation probabilities and also of the optically induced polarisation for the semiconductor material. A diagrammatic approach for the rapid calculation of the maximally resonant contributions to the density matrix is described. The final section examines ultrafast pulses and introduces the notion of optically generated virtual carriers.

Section 2.1. The wave equation and the constitutive relation.

The wave equation [1-3] in free space is given by

$$\nabla \times (\nabla \times \mathbf{E}) + \varepsilon_0 \mu_0 \frac{\partial^2 \mathbf{E}}{\partial t^2} = \mathbf{0} \tag{2.1}$$

where the electric field vector $\mathbf{E}(\mathbf{r}, t)$ is a function of position $\mathbf{r}$ and time t, and ε_0 and μ_0 are the permittivity and permeability of free space respectively. Now consider a field $\mathbf{E} = \mathbf{E}_0 \exp[i(\mathbf{k}_0.\mathbf{r} - \omega t)]$ which propagates in the direction defined by $\mathbf{k}_0$ perpendicular to $\mathbf{E}_0$. From the wave equation (2.1) it follows that the field travels at the velocity of light

$$c = \frac{\omega}{k_0} = \frac{1}{\sqrt{\varepsilon_0 \mu_0}} \tag{2.2}$$

However when a light beam is incident on a material, the electric field of the light is responsible for inducing a displacement of charge within the material which varies in sympathy with the incident field. This polarisation of the material can be described for sufficiently low values of the incident field by a linear relationship between the incident field $\mathbf{E}(\mathbf{r}, \mathbf{t})$ and the induced polarisation $\mathbf{P}(\mathbf{r}, \mathbf{t})$ namely

$$\mathbf{P} = \varepsilon_0 \chi \mathbf{E} \tag{2.3}$$

where the constant of proportionality χ is known as the susceptibility. The oscillating polarisation of charge corresponds to a current

$$\mathbf{J} = \frac{\partial \mathbf{P}}{\partial t} \tag{2.4}$$

which modifies the wave equation

$$\nabla \times (\nabla \times \mathbf{E}) + \varepsilon_0 \mu_0 \frac{\partial^2 \mathbf{E}}{\partial t^2} = -\mu_0 \frac{\partial^2 \mathbf{P}}{\partial t^2} \tag{2.5}$$

to account for the current source term. However, substituting for $\mathbf{P}$ from equation (2.3) reproduces the wave equation in free space but with the free space permittivity ε_0 replaced by $\varepsilon_0(1+\chi)$. Thus the presence of the material increases the effective permittivity by a factor $\varepsilon_r = 1+\chi$, the relative permittivity, which in semiconductors typically has a value of $\varepsilon_r = 3.5$. The effect of the polarisation is to alter the velocity of the light propagating through the material via the relations

$$v = \frac{\omega}{k} = \frac{1}{\sqrt{\varepsilon_0 \varepsilon_r \mu_0}} = \frac{c}{n} \tag{2.6}$$

where $n = \sqrt{\varepsilon_r}$ is the refractive index of the material. If a light beam propagates a given distance L in the material it undergoes a phase shift $\Delta\phi$ which depends directly on the refractive index. For the plane wave solution $\mathbf{E} = \mathbf{E}_0 \exp[i(\mathbf{k}.\mathbf{r} - \omega t)]$ of equation (2.5) the phase shift is $\Delta\phi = kL = nk_0L$. As described in chapter one this refractive index dependent phase shift is useful in optical switching devices. Further if the frequency of the light is such that the photon energy lies in the absorption band of the material this results in a component of the polarisation oscillating in quadrature to the applied electric field. The corresponding component of the current is in phase with the field as would be expected for a dissipative process. The quadrature component of the polarisation contributes an imaginary part to the relative permittivity ε_r and equation (2.6) shows that the wavevector

k of the light is consequently a complex quantity. Now $k = nk_0 + i\alpha$ so that after a distance L the exponential term in the plane wave solution contributes a factor $\exp[i\Delta\phi - \alpha L]$. Hence the real part of the wavevector determines the velocity of propagation of the light, whilst the imaginary part describes the absorption of the light beam with 2α being the intensity absorption coefficient.

Now if the intensity of the light beam is increased the relationship between the electric field and the induced polarisation becomes nonlinear. However, the polarisation may be expressed as a power series in the electric field

$$P = \varepsilon_0\chi^{(1)}E + \varepsilon_0\chi^{(2)}E^2 + \varepsilon_0\chi^{(3)}E^3 + \ldots \tag{2.7}$$

which is known as the constitutive relation [4-6], and where $\chi^{(r)}$ is the r^{th} order susceptibility. It is assumed that in the semiconductor materials considered the induced polarisation is collinear with the electric field so that the tensorial nature of the susceptibility may be neglected. It is further assumed that the materials possess inversion symmetry so that if a field $\mathbf{E}$ induces a polarisation $\mathbf{P}$ then a field $-\mathbf{E}$ will induce a polarisation $-\mathbf{P}$ and consequently $\chi^{(2)} = 0$. In this case

$$P = \varepsilon_0(\chi^{(1)} + \chi^{(3)}E^2)E \tag{2.8}$$

to third order. The response of the material at the driving frequency of the electric field is of concern here so that, for example, the description of third harmonic generation by $\chi^{(3)}$ is not considered. Thus the nonlinear relative permittivity may be defined as

$$\varepsilon_r = \varepsilon_r^{(0)} + \varepsilon_r^{(2)}E^2 \tag{2.9}$$

and has a constant component $\varepsilon_r^{(0)}$ together with a term which depends on the intensity of the incident field. Hence by varying the intensity of the light beam (or perhaps by employing a separate control beam) it is possible to influence the refractive index or the absorption experienced by the beam as it passes through the material. Later chapters of this thesis concentrate on examining these particular effects in more detail, although it should be noted that many other processes [4,7] (such as harmonic generation, Raman frequency shifting and parametric amplification) are also possible in the nonlinear regime.

Section 2.2. Liouville's equation and the density matrix.

The evolution of the quantum mechanical state of a semiconductor system subject to illumination by a light beam may be described by the system wavefunction $\Psi(t)$ calculated from the Schrödinger equation [8,9]

$$i\hbar\frac{d\Psi(t)}{dt} = (H_0 + H_I)\,\Psi(t) \tag{2.10}$$

where H_0 is the Hamiltonian of the unperturbed material system whose eigenstates $\{\Psi_n\}$ are used as basis states and where H_I is the interaction Hamiltonian which describes the influence of the electromagnetic field on the material system. The wavefunction $\Psi(t)$ may be used in the calculation of the expectation value of some observable with corresponding quantum mechanical operator O through the standard relation

$$\langle O(t)\rangle = \int \Psi^*(x,t)O(t)\Psi(x,t)dx \tag{2.11}$$

where the wavefunction $\Psi(x,t)$ is normalised to unity

$$\int \Psi^*(x,t)\Psi(x,t)dx = 1 \tag{2.12}$$

Alternatively the evolution of the system may be described in terms of the density matrix [7-9] of the system whose operator in the Schrödinger picture is

$$\rho_S = \sum_{n,m} \rho_{nm}|\Psi_n\rangle\langle\Psi_m| \tag{2.13}$$

This is particularly useful in the problems considered here as there is a clear correspondence between certain elements of the density matrix and the light-induced

polarisation of a material with inversion symmetry. Also the density matrix formalism allows external effects (such as electron-hole pair recombination and thermal scattering processes) to be easily included in the equations. The matrix elements in the basis $\{\Psi_n\}$ are clearly ρ_{nm}. The interpretation of the density matrix elements is best made by considering an ensemble of identical systems. Then the diagonal matrix element ρ_{nn} describes the probability of finding a system in the basis state Ψ_n whilst the off-diagonal matrix element ρ_{nm} describes the probability of finding a system whose wavefunction includes a coherent mixture of the basis states Ψ_n and Ψ_m.

Now if the system wavefunction is Ψ then the density matrix may be written as

$$\rho_S = |\Psi\rangle\langle\Psi| \tag{2.14}$$

Also the Schrödinger equation is

$$i\hbar\frac{d|\Psi\rangle}{dt} = H_S|\Psi\rangle \tag{2.15}$$

and its complex conjugate is

$$-i\hbar\frac{d\langle\Psi|}{dt} = \langle\Psi|H_S \tag{2.16}$$

where $H_S = H_0 + H_I$ is the total Hamiltonian in the Schrödinger picture. It follows from equations (2.14) to (2.16) that

$$i\hbar\frac{\partial\rho_S}{\partial t} = i\hbar\frac{d|\Psi\rangle}{dt}\langle\Psi| + i\hbar|\Psi\rangle\frac{d\langle\Psi|}{dt}$$

$$= H_S|\Psi\rangle\langle\Psi| - |\Psi\rangle\langle\Psi|H_S$$

$$= H_S\rho_S - \rho_S H_S$$

$$= [H_S, \rho_S] \tag{2.17}$$

where use is made of the commutator notation. This is the Liouville equation [7-9] for the density matrix which will be used extensively throughout this thesis to describe the evolution of the quantum mechanical state of a semiconductor system subjected to pulsed electromagnetic radiation. Further the expectation value of an observable O as defined in equation (2.11) may be calculated as

$$\langle O\rangle = \langle\Psi|O|\Psi\rangle$$

$$= \sum_n \langle\Psi|O|\Psi_n\rangle\langle\Psi_n|\Psi\rangle$$

$$= \sum_n \langle\Psi_n|\Psi\rangle\langle\Psi|O|\Psi_n\rangle$$

$$= \sum_n \langle\Psi_n|\rho_S O|\Psi_n\rangle$$

$$= Trace\,(\rho_S O) \tag{2.18}$$

so that once the density matrix has been determined the expectation value of the observable may be obtained directly by using the trace operation. Hence the density matrix provides a complete description of a quantum mechanical system and offers an alternative to the wavefunction approach. The Liouville equation is employed in preference to Schrödinger's equation when external events influence the development of the state of some otherwise isolated system. The advantages of the Liouville equation are particularly apparent in chapter five where thermal

effects are considered.

Now to establish the connection between the density matrix and the polarisation of the material system noted previously, consider the simple example of a two-level system perturbed by a periodic electromagnetic interaction $\mathbf{E} = \mathbf{E}_0 \cos \omega_p t$ with photon energy $E_p = \hbar\omega_p$ close (but not equal) to the energy separation $E_g = \hbar\omega_g$ of the two states. The ground state Ψ_0 is assumed to have odd parity (as for a p-like valence state in a semiconductor) and the excited state Ψ_1 is assumed to have even parity (as for an s-like conduction state). The system is initially in the ground state, and at time t the system wavefunction consists of a mixture of the two states

$$\Psi(t) = \Psi_0 e^{-i\omega_0 t} + \alpha(t)\Psi_1 e^{-i\omega_1 t} \tag{2.19}$$

where $\alpha(t)$ is small for a low intensity electric field and $\hbar\omega_i$ is the energy of state Ψ_i. From elementary time-dependent perturbation theory [8,9] $\alpha(t)$ is given by

$$\alpha(t) \simeq \frac{\langle \Psi_1 | H_I(\omega_p) | \Psi_0 \rangle}{\hbar(\omega_p - \omega_g)} e^{-i(\omega_p - \omega_g)t} \tag{2.20}$$

where $H_I(\omega_p)\exp(-i\omega_p t)$ is the interaction Hamiltonian written to explicitly show the periodic time dependence at frequency ω_p. The current operator (discussed further in chapter three) may be written as $\mathbf{J} = -(e/m)\mathbf{p}$ and equation (2.18) may be used to calculate the expectation value

$$\langle \mathbf{J} \rangle = -(e/m)(\rho_{01}\mathbf{p}_{10} + \rho_{10}\mathbf{p}_{01}) \tag{2.21}$$

Also from equations (2.14) and (2.19) it follows that $\rho_{10} = \overline{\rho_{01}} = \alpha(t)\exp(-i\omega_g t)$ where the bar denotes complex conjugation. Thus the first term in equation (2.21) describes the response at frequency $-\omega_p$ whilst the second term describes the response at frequency $+\omega_p$, and the current oscillates at the driving frequency in sympathy with the electric field. The induced current is in fact in quadrature with the driving field (see equation (3.56)) and so the interaction produces a refractive index change with no absorption.

The mixing of the basis states is a coherent effect and is subject to external influences (for example the interaction of an electron with other electrons or with phonons) which tend to force the system wavefunction to correspond to definitely one or other of the two states. This destruction of mixing between states is known as dephasing [4]; in the above example it removes the phase coherence of the two states Ψ_0 and Ψ_1 apparent in equation (2.19) which is induced by the electromagnetic interaction. With a system comprising a number of individual subsystems (as with electrons in a semiconductor), the total polarisation is the resultant of all individual polarisations and once the applied field has been removed it decays to zero under the influence of dephasing.

Section 2.3. Introduction to double Feynman diagrams.

The Liouville equation (2.17) presented in section 2.2 is described as being in the Schrödinger picture [8,9] which is denoted by the subscripts S. The relations

$$\Psi_I = U^\dagger \Psi_S \tag{2.22}$$

and

$$O_I = U^\dagger O_S U \tag{2.23}$$

where

$$U = \exp(H_0 t/i\hbar) \tag{2.24}$$

transform the wavefunctions Ψ and the operators O from the Schrödinger picture to the interaction picture [8,9]. Applying the transformation in equation (2.23) to the operators $O_S = H_I$ and $O_S = \rho_S$ allows the Liouville equation to be written in the interaction picture

$$i\hbar \frac{\partial \rho_I}{\partial t} = [H_I, \rho_I] \tag{2.25}$$

In a similar fashion to the expansion (2.7) of the polarisation in powers of the electric field, the density matrix may also be expanded in a perturbation series

$$\rho_I = \rho_I^{(0)} + \rho_I^{(1)} + \rho_I^{(2)} + \rho_I^{(3)} + \dots \tag{2.26}$$

where $\rho_I^{(r)}$ depends on the r^{th} power of the electric field E^r. Now omitting the I subscript on the density matrix elements and concentrating on just r^{th} order terms in the Liouville equation gives

$$i\hbar \frac{d\rho_{nm}^{(r)}}{dt} = \left[H_I, \rho_I^{(r-1)}\right]_{nm} \tag{2.27}$$

which may be integrated to obtain

$$\rho_{nm}^{(r)} = \frac{1}{i\hbar}\int_{t_0}^{t}\sum_{l}\left(H_{nl}\rho_{lm}^{(r-1)} - \rho_{nl}^{(r-1)}H_{lm}\right)dt \tag{2.28}$$

In this form the Liouville equation may be particularly easily solved through the use of a pictorial method involving double Feynman diagrams. Single Feynman diagrams [10] represent the evolution of a wavefunction in time by a series of smooth propagations (shown as straight line segments) interrupted by perturbing interactions (shown as nodes between line segments). Double Feynman diagrams [7,11-14] represent the evolution of the density matrix in a similar fashion, but with the evolution of both the ket-vector $|\Psi\rangle$ and the bra-vector $\langle\Psi|$ depicted.

Thus for the perturbation calculation of the density matrix elements ρ_{nm}, the Feynman diagrams consist of a pair of vertical lines representing the bra and ket parts of the density matrix together with one electromagnetic interaction node for each stage of the perturbation calculation. At the r^{th} stage of the calculation the $(r-1)^{\text{th}}$ order density matrix $\rho_I^{(r-1)}$ has already been determined and equation (2.28) is used to calculate the r^{th} order density matrix $\rho_I^{(r)}$. The term involving $H_{nl}\rho_{lm}^{(r-1)}$ represents an interaction with the ket part of the density matrix causing a transition from the ket-state $|\Psi_l\rangle$ to the ket-state $|\Psi_n\rangle$. This is depicted by the diagram in figure 2.1a where the optical field at frequency Ω acts via the operator $H_{nl}(\Omega) \equiv \langle\Psi_n|H_I(\Omega)|\Psi_l\rangle$ on the $(r-1)^{\text{th}}$ order density matrix element $\rho_{lm}^{(r-1)}$ to produce the r^{th} order density matrix element $\rho_{nm}^{(r)}$. The photon involved in the interaction has frequency Ω and is depicted in the figure by the wavy photon

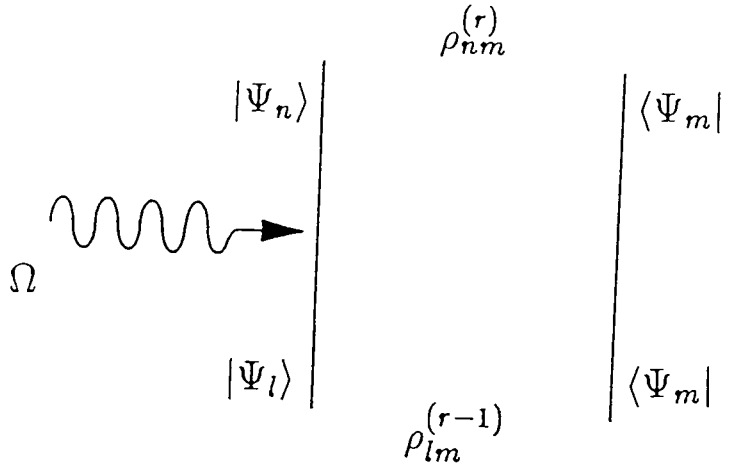

Figure 2.1a. Interaction involving a photon of frequency Ω (represented by the wavy photon arrow) which results in a transition of the density matrix from ket-state $|\Psi_l\rangle$ to ket-state $|\Psi_n\rangle$. The vertical lines depict the propagation through time of the bra- and ket-parts of the density matrix.

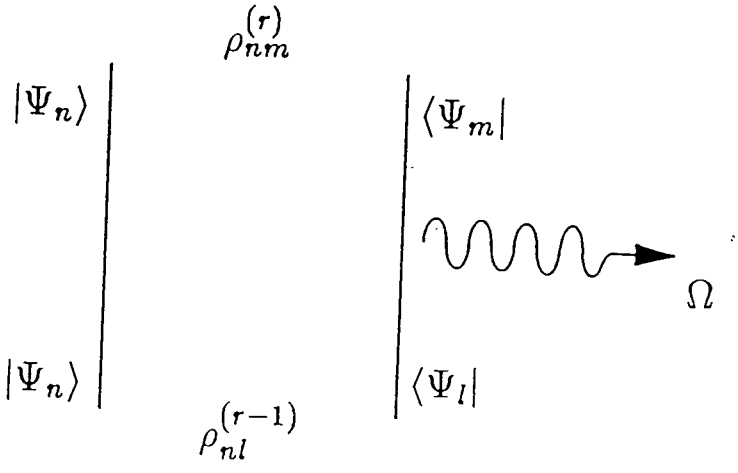

Figure 2.1b. Interaction involving a photon of frequency Ω which results in a transition of the density matrix from bra-state $\langle\Psi_l|$ to bra-state $\langle\Psi_m|$.

arrow. The convention adopted is that Ω is positive when the direction of the photon arrow is towards the right. Similarly the term involving $\rho_{nl}^{(r-1)} H_{lm}$ is depicted in figure 2.1b where the interaction operator is $H_{lm}(\Omega)$. Note that interactions occuring on the right of the diagram introduce a minus sign in the corresponding algebraic expression. Higher order density matrix elements may be obtained by extending the diagram upwards, adding an interaction on the left or on the right of the diagram at each stage.

To illustrate the above ideas consider as an example the two-level system of section 2.2 with the ground state initially occupied and no coherence between states so that $\rho_{00}^{(0)}$ is the only non-zero density matrix element to zero order. Suppose that the system is illuminated by light with electric field vector $\mathbf{E} = \mathbf{E}_0 \cos \omega_p t$ where $E_p = \hbar\omega_p$ is close (but not equal) to the energy separation $E_g = \hbar\omega_g$ of the two states. Then the frequency components of the interaction Hamiltonian are $H_I(\omega_p)$ and $H_I(-\omega_p)$. The calculation of the first order density matrix element $\rho_{10}^{(1)}$ uses the double Feynman diagram shown in figure 2.2a which depicts an interaction of the ket-state with the electromagnetic field at the frequency Ω_1. The magnitude of the first order interaction depends on the energy difference $\hbar(\omega_p - \omega_g)$ which appears in the denominator of equation (2.20). For $\omega_p \simeq \omega_g$ the magnitude of the interaction becomes large and this is consequently termed a resonant interaction. In fact the expression in equation (2.20) neglects a non-resonant term which involves the denominator $\hbar(\omega_p + \omega_g)$. Thus in figure 2.2a a resonant interaction

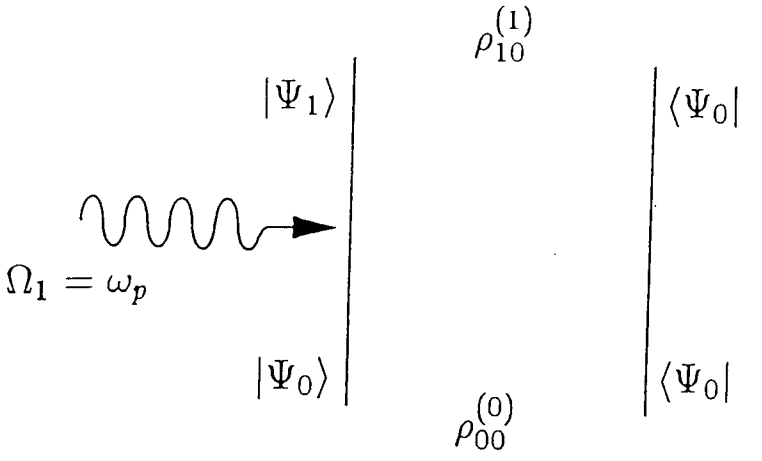

Figure 2.2a. Feynman diagram depicting the resonant contribution to the first order density matrix element $\rho_{10}^{(1)}$.

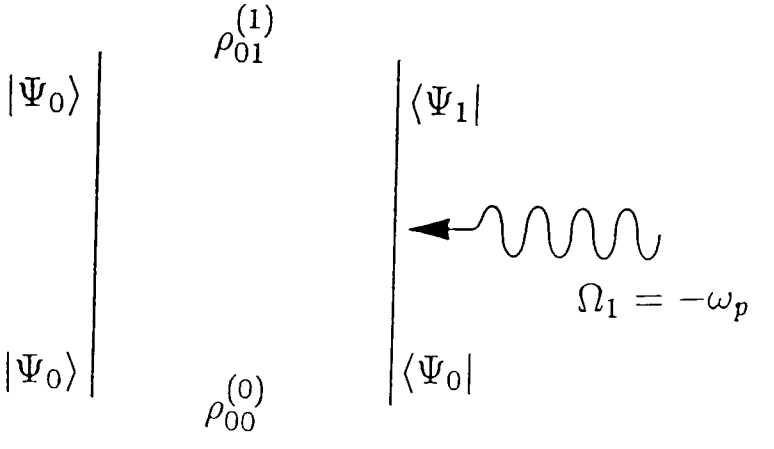

Figure 2.2b. Feynman diagram depicting the resonant contribution to the first order density matrix element $\rho_{01}^{(1)}$.

is obtained with $\Omega_1 = \omega_p \simeq \omega_g$ and a non-resonant interaction is obtained with $\Omega_1 = -\omega_p$. The calculation of the first order density matrix element $\rho_{01}^{(1)}$ uses the double Feynman diagram shown in figure 2.2b. In this case $\Omega_1 = -\omega_p \simeq -\omega_g$ gives the resonant interaction and $\Omega_1 = \omega_p$ gives the non-resonant interaction. The general rule is that the sum of the frequencies $\sum_{i=1}^{r} \Omega_i$ from the bottom of a diagram to the top must be compared with the frequency difference $\omega_{nm} \equiv \omega_n - \omega_m$ associated with the density matrix element $\rho_{nm}^{(r)}$ at the top of the diagram in order to determine if the diagram represents a resonant interaction. In figure 2.2a the frequency difference associated with the matrix element $\rho_{10}^{(1)}$ is $\omega_{10} = \omega_g$ whilst in figure 2.2b the frequency difference associated with $\rho_{01}^{(1)}$ is $\omega_{01} = -\omega_g$. It is possible to calculate higher order density matrix elements retaining only resonant diagrams at each stage; the resultant matrix elements are termed maximally resonant. For example figure 2.3 shows a maximally resonant contribution to $\rho_{11}^{(2)}$ where $\Omega_1 = \omega_p$ and $\Omega_1 + \Omega_2 = 0$.

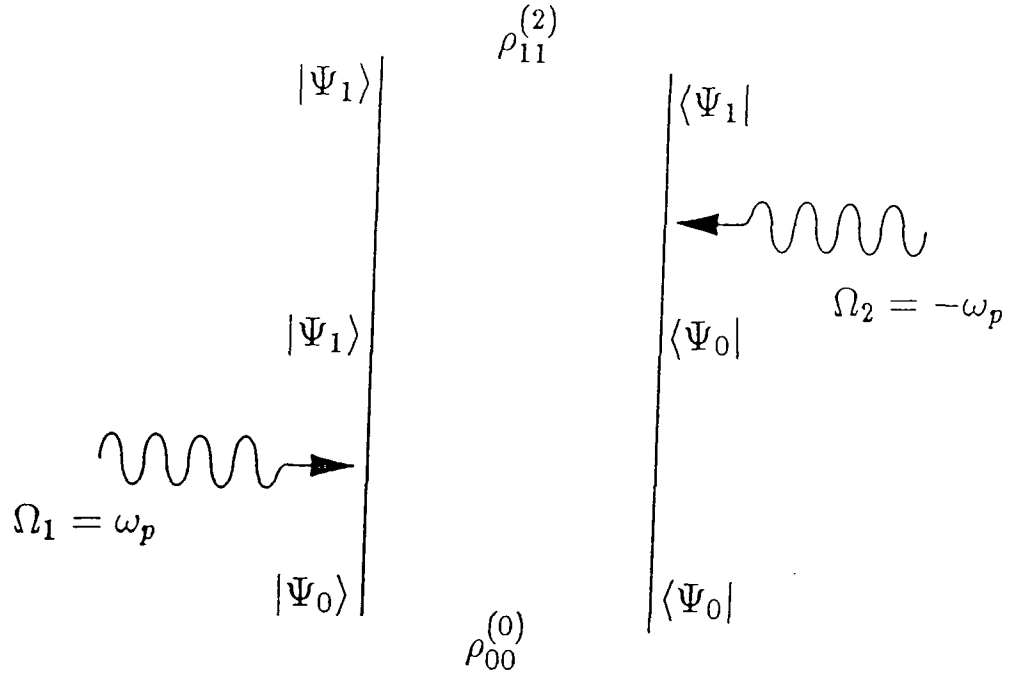

Figure 2.3. Feynman diagram depicting a maximally resonant contribution to the second order density matrix element $\rho_{11}^{(2)}$.

Section 2.4. Fermi's Golden rule and ultrashort pulses.

This section examines the applicability of Fermi's Golden rule [15] to the description of pulsed excitations. For a semiconductor excited by continuous-wave electromagnetic radiation at a single frequency ω_p the rate R of transfer of an electron from an initial state Ψ_0 to some final state Ψ_1 is given by Fermi's Golden rule

$$R = \frac{2\pi}{\hbar^2} \int |H_{10}|^2 \delta(\omega_1 - \omega_0 \pm \omega_p) \rho(\omega_1) d\omega_1 \tag{2.29}$$

where $H_{10} = \langle \Psi_1 | H_I | \Psi_0 \rangle$ is the interaction Hamiltonian, $\hbar\omega_0$ and $\hbar\omega_1$ are the energies of initial and final states, and $\rho(\omega_1)$ is the density of final states.

Now consider the excitation of the two-level system of previous sections by a pulsed electromagnetic interaction having gaussian envelope with time constant τ

$$\mathbf{E} = \mathbf{E}_0 \cos \omega_p t \exp(-t^2/\tau^2) \tag{2.30}$$

And following the method of derivation of Fermi's Golden rule suppose that

$$H_{10}(t) = H_{10}(0) \mathrm{e}^{-i\omega_p t} \mathrm{e}^{-t^2/\tau^2} \tag{2.31}$$

and

$$\Psi = \Psi_0 \mathrm{e}^{-i\omega_0 t} + \alpha(t) \Psi_1 \mathrm{e}^{-i\omega_1 t} \tag{2.32}$$

where all time dependence is shown explicitly. Assuming that initially the ground state Ψ_0 is occupied so $\alpha(t = -\infty) = 0$, then $\alpha(t)$ may be determined from Schrödinger's equation

$$i\hbar \frac{d\alpha}{dt} = \mathrm{e}^{i\omega_{10} t} H_{10}(t)$$

$$= H_{10}(0)e^{i(\omega_{10}-\omega_p)t}e^{-t^2/\tau^2} \tag{2.33}$$

Now integrating over all time

$$\begin{aligned}\alpha(t=\infty) &= \frac{H_{10}(0)\tau}{i\hbar}\int_{-\infty}^{+\infty} e^{-v^2}e^{-iv\Delta\tau}dv \\ &= \frac{H_{10}(0)\tau}{i\hbar}\sqrt{\pi}e^{-\Delta^2\tau^2/4}\end{aligned} \tag{2.34}$$

where $\Delta = \omega_p - \omega_{10}$. So the eventual occupation probability of the excited state Ψ_1 is given by

$$\begin{aligned}\rho_{11}(\infty) &= |\alpha(\infty)|^2 \\ &= \frac{\pi|H_{10}(0)|^2\tau^2}{\hbar^2}e^{-\Delta^2\tau^2/2}\end{aligned} \tag{2.35}$$

Also from equation (2.31) it follows that

$$\int_{-\infty}^{+\infty}|H_{10}(t)|^2dt = |H_{10}(0)|^2\tau\sqrt{\pi/2} \tag{2.36}$$

and by writing

$$\delta(\Delta) = \frac{\tau}{\sqrt{2\pi}}e^{-\Delta^2\tau^2/2} \tag{2.37}$$

then equation (2.35) may be expressed as

$$\rho_{11}(\infty) = \frac{2\pi}{\hbar^2}\int_{-\infty}^{+\infty}|H_{10}(t)|^2dt\,\delta(\Delta) \tag{2.38}$$

If the pulse width is assumed to be large then by noting that

$$\int_{-\infty}^{+\infty}\delta(\Delta)d\Delta = 1 \tag{2.39}$$

and

$$\delta(\Delta \neq 0) \rightarrow 0 \quad \text{as} \quad \tau \rightarrow \infty \tag{2.40}$$

it is clear that $\delta(\Delta)$ approximates to a delta function. In this regime Fermi's Golden rule is applicable so that equations (2.29) and (2.38) are equivalent. However, the result in equation (2.35) is directly applicable to ultrashort pulses and agrees with values calculated from Liouville's equation by numerical methods (see figure 2.4). In this regime $\delta(\Delta)$ no longer approximates to a delta function and now represents the spectral dispersion of the ultrashort pulse. Figure 2.4 shows that significant absorption of the pulse is avoided only if $|\Delta\tau| \gg 1$, that is if the detuning $\Delta = \omega_p - \omega_{10}$ is much greater than the spectral width of the pulse $\sim 1/\tau$.

Further the τ dependence of $\rho_{11}(\infty)$ provides some indication of the population of the excited state throughout the pulse. This is particularly apparent for a square pulse since if the pulse is turned on at $t = 0$ then the excitation produced up to time $t = \tau$ is exactly the same as that produced by a complete pulse of width τ. For such a pulse

$$\rho_{11}(\infty) = \frac{|H_{10}(0)|^2}{\hbar^2}\tau^2 \text{sinc}^2(\Delta\tau/2) \tag{2.41}$$

or alternatively

$$\rho_{11}(\infty) = \frac{2\pi}{\hbar^2}\int_{-\infty}^{+\infty} |H_{10}(t)|^2 dt\, \delta(\Delta) \tag{2.42}$$

where

$$\delta(\Delta) = \frac{\tau}{2\pi}\text{sinc}^2(\Delta\tau/2) \tag{2.43}$$

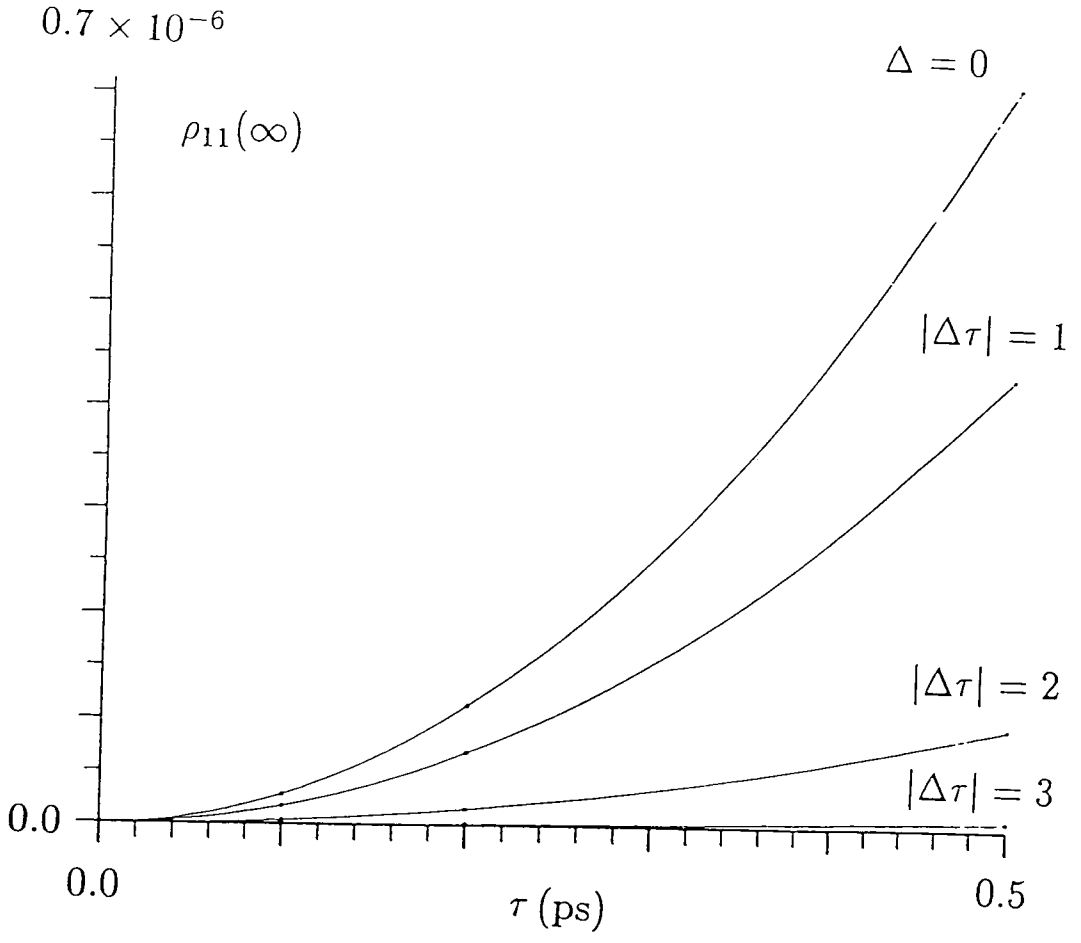

Figure 2.4. Relationship between the final occupation probability $\rho_{11}(\infty)$ of the excited state Ψ_1 and the pulse width τ, for various values of the detuning Δ. The continuous curves show values determined by equation (2.35) whilst the discrete points show values calculated numerically using Liouville's equation. A value of $H_{10}(0) = 10^{-25}$J is used throughout.

Now suppose that an ensemble of two-level systems, all initially in the ground state Ψ_0, are excited by the pulse. At the start of the pulse (cf. short pulses) the populations of the ground and excited states are determined by the τ^2 factor in equation (2.41) so that some of the systems are initially excited, but as the pulse continues (cf. longer pulses) the $\mathrm{sinc}^2(\Delta\tau/2)$ factor becomes more important and the number of excited systems starts to decrease. If the condition $|\Delta\tau| \gg 1$ is met then there are practically no systems in an excited state after the pulse has ended. The condition on $\Delta\tau$ is closely related to the uncertainty principle connecting energy and time, which allows non-conservation of energy on a sufficiently short timescale. The transiently generated excitations which exist only during the presence of the pulse are termed virtual excitations. In the semiconductor context of excitation across the band gap, the production of virtual excitations corresponds to the generation of virtual electrons in the conduction band and of virtual holes in the valence band.

CHAPTER THREE

Electromagnetic gauge theory

In this chapter the description of the electromagnetic interaction with the semiconductor system is considered in more detail. The electromagnetic fields may be described in terms of vector and scalar potentials and these are to some extent arbitrary. To specify the potentials exactly requires a particular choice of gauge, so the question of the choice of gauge is considered with particular attention paid to the two usual choices of gauge which give the so called **A.p** and the **E.r** interactions. It is shown that the expectation values of observables (which are the only physically meaningful quantities) are unaffected by the choice of gauge, although a particular choice of gauge may provide a more elegant method for obtaining the result. As an example of gauge invariance there is a discussion on the connection between the susceptibility calculations performed in the **A.p** and **E.r** gauges. Finally, an explicit expression is derived for the interaction Hamiltonian H_I in the electric dipole approximation for use in later chapters.

Section 3.1. Gauge theory and Schrödinger's equation.

The propagation of an electromagnetic wave through a material is described by Maxwell's equations

$$\nabla \times \mathbf{E} = -\frac{\partial \mathbf{B}}{\partial t} \tag{3.1}$$

$$\frac{1}{\mu_0}\nabla \times \mathbf{B} = \varepsilon_0 \frac{\partial \mathbf{E}}{\partial t} + \mathbf{J} \tag{3.2}$$

$$\varepsilon \nabla . \mathbf{E} = \rho \tag{3.3}$$

$$\nabla . \mathbf{B} = 0 \tag{3.4}$$

The electric and magnetic fields $\mathbf{E}$ and $\mathbf{B}$ may be described [1-3] in terms of a vector potential $\mathbf{A}$ and a scalar potential ϕ

$$\mathbf{E} = -\nabla\phi - \frac{\partial \mathbf{A}}{\partial t} \tag{3.5}$$

$$\mathbf{B} = \nabla \times \mathbf{A} \tag{3.6}$$

These descriptions contain an element of arbitrariness in that the vector and scalar potentials are not completely determined by the electromagnetic fields. The choice of particular functions $\mathbf{A}$ and ϕ constitutes a choice of gauge. Consider two gauges I and II related by the gauge transformation function $\Lambda(\mathbf{r}, t)$. Suppose that $\mathbf{A}$ and ϕ are the potentials in gauge I, then the potentials $\tilde{\mathbf{A}}$ and $\tilde{\phi}$ in gauge II are given by the relations

$$\tilde{\mathbf{A}} = \mathbf{A} + \nabla\Lambda \tag{3.7}$$

$$\tilde{\phi} = \phi - \frac{\partial \Lambda}{\partial t} \tag{3.8}$$

The transformation from one gauge to the other has no effect on the physically observable quantities which are the electric and magnetic fields. Thus

$$\begin{aligned}\mathbf{E} &= -\nabla\tilde{\phi} - \frac{\partial\tilde{\mathbf{A}}}{\partial t} \\ &= -\nabla\left(\phi - \frac{\partial\Lambda}{\partial t}\right) - \frac{\partial}{\partial t}\left(\mathbf{A} + \nabla\Lambda\right) \\ &= -\nabla\phi - \frac{\partial\mathbf{A}}{\partial t}\end{aligned} \tag{3.9}$$

and

$$\begin{aligned}\mathbf{B} &= \nabla \times \tilde{\mathbf{A}} \\ &= \nabla \times (\mathbf{A} + \nabla\Lambda) \\ &= \nabla \times \mathbf{A}\end{aligned} \tag{3.10}$$

since $\nabla \times \nabla\Lambda = \mathbf{0}$.

The transformation function Λ also defines the transformation of a quantum mechanical operator O in gauge I to the corresponding operator $\tilde{O}$ in gauge II through the relation [16,17]

$$\tilde{O} = UOU^{\dagger} \tag{3.11}$$

where

$$U = \exp\left(-q\Lambda/i\hbar\right) \tag{3.12}$$

and q is the charge on the particle described by the operators O and $\tilde{O}$. For an electron with charge $q = -e$, the velocity operator $\mathbf{v} = (\mathbf{p} + e\mathbf{A})/m$ in gauge I transforms to the operator $\tilde{\mathbf{v}} = (\mathbf{p} + e\tilde{\mathbf{A}})/m$ in gauge II [18-20].

Thus

$$\begin{aligned}
&\exp\left(e\Lambda/i\hbar\right)\left(\mathbf{p}+e\mathbf{A}\right)\exp\left(-e\Lambda/i\hbar\right)\\
&\quad=\mathbf{p}+e\mathbf{A}+\exp\left(e\Lambda/i\hbar\right)\left(-i\hbar\nabla\exp\left(-e\Lambda/i\hbar\right)\right)\\
&\quad=\mathbf{p}+e\tilde{\mathbf{A}}
\end{aligned}\tag{3.13}$$

Similarly the energy operator $O = i\hbar\frac{\partial}{\partial t}+e\phi$ in gauge I transforms to $\tilde{O} = i\hbar\frac{\partial}{\partial t}+e\tilde{\phi}$ in gauge II [18-20].

$$\begin{aligned}
&\exp\left(e\Lambda/i\hbar\right)\left(i\hbar\frac{\partial}{\partial t}+e\phi\right)\exp\left(-e\Lambda/i\hbar\right)\\
&\quad=i\hbar\frac{\partial}{\partial t}+e\phi+\exp\left(e\Lambda/i\hbar\right)\left(i\hbar\frac{\partial\left[\exp\left(-e\Lambda/i\hbar\right)\right]}{\partial t}\right)\\
&\quad=i\hbar\frac{\partial}{\partial t}+e\tilde{\phi}
\end{aligned}\tag{3.14}$$

The time dependent Schrödinger equation for an electron in a semiconductor subjected to an electromagnetic field described by the potentials $\mathbf{A}$ and ϕ is

$$H(\mathbf{A},\phi)\Psi = i\hbar\frac{\partial\Psi}{\partial t}\tag{3.15}$$

where

$$H(\mathbf{A},\phi) = \frac{1}{2m}\left(\mathbf{p}+e\mathbf{A}\right)^2+V-e\phi\tag{3.16}$$

and V is the potential energy of the unperturbed material system. The formulation of the Schrödinger equation should yield physically observable results which are not dependent on the choice of gauge. In gauge I the Schrödinger equation may be written as $S\Psi = 0$ where

$$S = \left[\frac{1}{2m}\left(\mathbf{p}+e\mathbf{A}\right)^2+V-\left(i\hbar\frac{\partial}{\partial t}+e\phi\right)\right]\tag{3.17}$$

and for gauge invariance the Schrödinger equation should be expressible in gauge II as $\tilde{S}\tilde{\Psi} = 0$ where

$$\tilde{S} = \left[\frac{1}{2m}\left(\mathbf{p} + e\tilde{\mathbf{A}}\right)^2 + V - \left(i\hbar\frac{\partial}{\partial t} + e\tilde{\phi}\right)\right] \tag{3.18}$$

Indeed equations (3.13) and (3.14) show that $\tilde{S} = USU^\dagger$ and it follows that the wavefunctions Ψ and $\tilde{\Psi}$ in the two gauges are related by

$$\tilde{\Psi} = U\Psi \tag{3.19}$$

where

$$U = \exp\left(e\Lambda/i\hbar\right) \tag{3.20}$$

Further, the expectation value of an operator $\tilde{O}$ in gauge II is given by

$$\langle\tilde{O}\rangle = \frac{\langle\tilde{\Psi}|\tilde{O}|\tilde{\Psi}\rangle}{\langle\tilde{\Psi}|\tilde{\Psi}\rangle} = \frac{\langle\Psi|U^\dagger\tilde{O}U|\Psi\rangle}{\langle\Psi|U^\dagger U|\Psi\rangle} = \frac{\langle\Psi|O|\Psi\rangle}{\langle\Psi|\Psi\rangle} = \langle O\rangle \tag{3.21}$$

and hence equals the expectation value of the operator O in gauge I. This shows that the expectation value of an operator is independent of gauge provided that the appropriate potentials (dependent on gauge) are used in the definition of the operator. Thus the operator $\tilde{O}$ should be the same function of $\tilde{\mathbf{A}}$ and $\tilde{\phi}$ as the operator O is of $\mathbf{A}$ and ϕ, as for example is the velocity operator discussed earlier.

Section 3.2. The use of gauges in perturbation theory.

The previous section discussed the application of gauge theory to the exact solution of the Schrödinger equation. This section shows how the results can be applied when calculating expectation values to some arbitrary order of perturbation theory [21]. The wavefunctions for the two gauges I and II discussed in section 3.1 may be expanded as perturbation series

$$\Psi = \Psi^{(0)} + \Psi^{(1)} + \Psi^{(2)} + \cdots \tag{3.22}$$

$$\tilde{\Psi} = \tilde{\Psi}^{(0)} + \tilde{\Psi}^{(1)} + \tilde{\Psi}^{(2)} + \cdots \tag{3.23}$$

where $\Psi^{(r)}$ and $\tilde{\Psi}^{(r)}$ have r^{th} order dependence on the electromagnetic perturbation. The exponential $U = \exp(e\Lambda/i\hbar)$ may be expanded as a power series

$$U = U^{(0)} + U^{(1)} + U^{(2)} + \cdots \tag{3.24}$$

to define the coefficients

$$U^{(r)} = \frac{1}{r!}\left(\frac{e\Lambda}{i\hbar}\right)^r \tag{3.25}$$

and from $\tilde{\Psi} = U\Psi$ in equation (3.19) it is reasonable to assume that the perturbative terms for the two wavefunctions are related by

$$\tilde{\Psi}^{(r)} = \sum_{s=0}^{r} U^{(r-s)}\Psi^{(s)} \tag{3.26}$$

In the exact solution

$$\tilde{S}\tilde{\Psi} = USU^{\dagger}U\Psi = U[S\Psi] \tag{3.27}$$

which implies that in the perturbative solution

$$[\tilde{S}\tilde{\Psi}]^{(r)} = \sum_{s=0}^{r} U^{(r-s)}[S\Psi]^{(s)} \tag{3.28}$$

for $r = 0, 1, 2, \ldots$ However, it remains to define the perturbative Schrödinger equations $[S\Psi]^{(r)} = 0$ and $[\tilde{S}\tilde{\Psi}]^{(r)} = 0$ for gauges I and II in a gauge invariant manner and to check that all definitions are consistent. So consider the Schrödinger equation $S\Psi = 0$ in gauge I and extract all terms from the left-hand side which have r^{th} order dependence on the electromagnetic perturbation to define $[S\Psi]^{(r)}$ as

$$[S\Psi]^{(r)} = \left[\frac{p^2}{2m} + V - i\hbar\frac{\partial}{\partial t}\right]\Psi^{(r)} + \left[\frac{e}{2m}(\mathbf{A}.\mathbf{p} + \mathbf{p}.\mathbf{A}) - e\phi\right]\Psi^{(r-1)} + \frac{e^2A^2}{2m}\Psi^{(r-2)} \tag{3.29}$$

Then $[S\Psi]^{(r)} = 0$ is the r^{th} order Schrödinger equation in gauge I. Similarly in gauge II $[\tilde{S}\tilde{\Psi}]^{(r)}$ may be defined as

$$[\tilde{S}\tilde{\Psi}]^{(r)} = \left[\frac{p^2}{2m} + V - i\hbar\frac{\partial}{\partial t}\right]\tilde{\Psi}^{(r)} + \left[\frac{e}{2m}(\tilde{\mathbf{A}}.\mathbf{p} + \mathbf{p}.\tilde{\mathbf{A}}) - e\tilde{\phi}\right]\tilde{\Psi}^{(r-1)} + \frac{e^2\tilde{A}^2}{2m}\tilde{\Psi}^{(r-2)} \tag{3.30}$$

so that $[\tilde{S}\tilde{\Psi}]^{(r)} = 0$ is the r^{th} order Schrödinger equation in gauge II. To show that these definitions are consistent, suppose that $\Psi^{(0)}, \Psi^{(1)}, \Psi^{(2)}, \ldots$ are solutions of the perturbative Schrödinger equations in gauge I

$$\begin{aligned} [S\Psi]^{(0)} &= 0 \\ [S\Psi]^{(1)} &= 0 \\ [S\Psi]^{(2)} &= 0 \\ &\vdots \end{aligned} \tag{3.31}$$

Then the wavefunctions $\tilde{\Psi}^{(0)}, \tilde{\Psi}^{(1)}, \tilde{\Psi}^{(2)}, \ldots$ which are defined by equation (3.26) should be solutions of the perturbative Schrödinger equations in gauge II

$$\begin{aligned} [\tilde{S}\tilde{\Psi}]^{(0)} &= 0 \\ [\tilde{S}\tilde{\Psi}]^{(1)} &= 0 \\ [\tilde{S}\tilde{\Psi}]^{(2)} &= 0 \\ &\vdots \end{aligned} \tag{3.32}$$

The basic approach is to assume that $[S\Psi]^{(r)} = 0$ for $r = 0, 1, 2, \ldots$ and to show that

$$[\tilde{S}\tilde{\Psi}]^{(r)} = \sum_{s=0}^{r} U^{(r-s)}[S\Psi]^{(s)} \tag{3.33}$$

and hence that $[\tilde{S}\tilde{\Psi}]^{(r)} = 0$. Firstly, it is neccessary to derive a few operator identities

$$\begin{aligned} \left[\frac{p^2}{2m}, U^{(r)}\right] &= \frac{1}{2m}\left[\mathbf{p}.(-i\hbar\nabla U^{(r)} + U^{(r)}\mathbf{p}) - U^{(r)}p^2\right] \\ &= \frac{1}{2m}\left[\mathbf{p}.(-i\hbar\nabla U^{(r)}) + (-i\hbar\nabla U^{(r)}).\mathbf{p}\right] \\ &= -\frac{e}{2m}\left[\mathbf{p}.(U^{(r-1)}\nabla\Lambda) + (U^{(r-1)}\nabla\Lambda).\mathbf{p}\right] \\ &= -\frac{e}{2m}(\mathbf{p}.\nabla\Lambda + \nabla\Lambda.\mathbf{p})U^{(r-1)} + \frac{e}{2m}\nabla\Lambda.(-i\hbar\nabla U^{(r-1)}) \\ &= -\frac{e}{2m}(\mathbf{p}.\nabla\Lambda + \nabla\Lambda.\mathbf{p})U^{(r-1)} - \frac{e^2}{2m}(\nabla\Lambda.\nabla\Lambda)U^{(r-2)} \end{aligned} \tag{3.34}$$

and

$$\begin{aligned} \left[\mathbf{A}.\mathbf{p} + \mathbf{p}.\mathbf{A}, U^{(r)}\right] &= \mathbf{A}.(-i\hbar\nabla U^{(r)}) + (-i\hbar\nabla U^{(r)}).\mathbf{A} \\ &= -e(\mathbf{A}.\nabla\Lambda + \nabla\Lambda.\mathbf{A})U^{(r-1)} \end{aligned} \tag{3.35}$$

and

$$\left[i\hbar\frac{\partial}{\partial t}, U^{(r)}\right] = e\frac{\partial\Lambda}{\partial t}U^{(r-1)} \tag{3.36}$$

Now consider

$$\begin{aligned}
&\sum_{s=0}^{r} U^{(r-s)}[S\Psi]^{(s)} \\
&= \sum_{s=0}^{r} U^{(r-s)}\left(\frac{p^2}{2m}+V\right)\Psi^{(s)} + \sum_{s=0}^{r-1} U^{(r-1-s)}\frac{e}{2m}(\mathbf{A}.\mathbf{p}+\mathbf{p}.\mathbf{A})\Psi^{(s)} + \sum_{s=0}^{r-2} U^{(r-2-s)}\frac{e^2A^2}{2m}\Psi^{(s)} \\
&\quad - \sum_{s=0}^{r} U^{(r-s)}i\hbar\frac{\partial\Psi^{(s)}}{\partial t} - \sum_{s=0}^{r-1} U^{(r-1-s)}e\phi\Psi^{(s)}
\end{aligned} \tag{3.37}$$

By using the operator identities (3.34), (3.35) and (3.36) this may be written as

$$\begin{aligned}
&\sum_{s=0}^{r} U^{(r-s)}[S\Psi]^{(s)} \\
&= \left(\frac{p^2}{2m}+V\right)\sum_{s=0}^{r} U^{(r-s)}\Psi^{(s)} + \frac{e}{2m}(\nabla\Lambda.\mathbf{p}+\mathbf{p}.\nabla\Lambda)\sum_{s=0}^{r-1} U^{(r-1-s)}\Psi^{(s)} + \frac{e^2}{2m}\nabla\Lambda.\nabla\Lambda\sum_{s=0}^{r-2} U^{(r-2-s)}\Psi^{(s)} \\
&\quad + \frac{e}{2m}(\mathbf{A}.\mathbf{p}+\mathbf{p}.\mathbf{A})\sum_{s=0}^{r-1} U^{(r-1-s)}\Psi^{(s)} + \frac{e^2}{2m}(\mathbf{A}.\nabla\Lambda+\nabla\Lambda.\mathbf{A})\sum_{s=0}^{r-2} U^{(r-2-s)}\Psi^{(s)} \\
&\quad + \frac{e^2A^2}{2m}\sum_{s=0}^{r-2} U^{(r-2-s)}\Psi^{(s)} \\
&\quad - i\hbar\frac{\partial}{\partial t}\sum_{s=0}^{r} U^{(r-s)}\Psi^{(s)} + e\frac{\partial\Lambda}{\partial t}\sum_{s=0}^{r-1} U^{(r-1-s)}\Psi^{(s)} \\
&\quad - e\phi\sum_{s=0}^{r-1} U^{(r-1-s)}\Psi^{(s)}
\end{aligned} \tag{3.38}$$

Finally, collecting terms in $\tilde{\Psi}^{(r)}$, $\tilde{\Psi}^{(r-1)}$ and $\tilde{\Psi}^{(r-2)}$ as defined by equation (3.26) and using the transformation relations (3.7) and (3.8) for the vector and scalar potentials gives

$$\begin{aligned}
&\sum_{s=0}^{r} U^{(r-s)}[S\Psi]^{(s)} \\
&\quad = \left(\frac{p^2}{2m}+V\right)\tilde{\Psi}^{(r)} + \frac{e}{2m}(\tilde{\mathbf{A}}.\mathbf{p}+\mathbf{p}.\tilde{\mathbf{A}})\tilde{\Psi}^{(r-1)} + \frac{e^2\tilde{A}^2}{2m}\tilde{\Psi}^{(r-2)} - i\hbar\frac{\partial\tilde{\Psi}^{(r)}}{\partial t} - e\tilde{\phi}\Psi^{(r-1)} \\
&\quad = [\tilde{S}\tilde{\Psi}]^{(r)}
\end{aligned} \tag{3.39}$$

Hence $[\tilde{S}\tilde{\Psi}]^{(r)} = 0$ and so $\tilde{\Psi}^{(r)}$ for $r = 0, 1, 2, \ldots$ as defined by equation (3.26) are indeed solutions of the perturbative Schrödinger equations (3.32) in gauge II.

Finally, it remains to show the equivalence of the r^{th} order expectation values $\langle O \rangle^{(r)}$ and $\langle \tilde{O} \rangle^{(r)}$ of an operator calculated in gauges I and II. So define

$$\begin{aligned} \langle O \rangle^{(r)} &= \left[\frac{\langle \Psi | O | \Psi \rangle}{\langle \Psi | \Psi \rangle} \right]^{(r)} \\ &= f\left(N^{(0)}(O), \ldots, N^{(r)}(O), N^{(0)}(1), \ldots, N^{(r)}(1) \right) \end{aligned} \tag{3.40}$$

where $N^{(s)}(\theta) = \langle \Psi | \theta | \Psi \rangle^{(s)}$ is the sum of all s^{th} order terms from $\langle \Psi | \theta | \Psi \rangle$. The function f represents a binomial expansion of the denominator and the arguments of f with $\theta = O$ derive from the numerator whilst those with $\theta = 1$ derive from the denominator. The term $N^{(s)}(\theta)$ is expanded as

$$N^{(s)}(\theta) = \sum_{l=0}^{s} \langle \Psi^{(s-l)} | \, [\theta | \Psi \rangle]^{(l)} \tag{3.41}$$

whilst the expansion of $[\theta | \Psi \rangle]^{(l)}$ depends on the explicit form of the operator θ. For θ equal to the total operator S in the Schrödinger equation the expansion is given by equation (3.29). Now in gauge II the r^{th} order expectation value is

$$\begin{aligned} \langle \tilde{O} \rangle^{(r)} &= \left[\frac{\langle \tilde{\Psi} | \tilde{O} | \tilde{\Psi} \rangle}{\langle \tilde{\Psi} | \tilde{\Psi} \rangle} \right]^{(r)} \\ &= f\left(\tilde{N}^{(0)}(\tilde{O}), \ldots, \tilde{N}^{(r)}(\tilde{O}), \tilde{N}^{(0)}(1), \ldots, \tilde{N}^{(r)}(1) \right) \end{aligned} \tag{3.42}$$

where $\tilde{N}^{(s)}(\tilde{\theta})$ is defined in an analogous manner to $N^{(s)}(\theta)$. Because the same function f appears in gauges I and II it follows that $\langle O \rangle^{(r)}$ and $\langle \tilde{O} \rangle^{(r)}$ are equivalent if $N^{(s)}(\theta) = \tilde{N}^{(s)}(\tilde{\theta})$. So assume that

$$\left[\tilde{\theta} | \tilde{\Psi} \rangle \right]^{(l)} = \sum_{n=0}^{l} U^{(l-n)} \, [\theta | \Psi \rangle]^{(n)} \tag{3.43}$$

This has just been demonstrated for the operators S and $\tilde{S}$ (see equation (3.33)) and also holds for the operators of interest here, such as the velocity operator. Hence

$$\begin{aligned}
\tilde{N}^{(s)}(\tilde{\theta}) &= \langle\tilde{\Psi}|\tilde{\theta}|\tilde{\Psi}\rangle^{(s)} \\
&= \sum_{l=0}^{s}\langle\tilde{\Psi}^{(s-l)}|\left[\tilde{\theta}|\tilde{\Psi}\rangle\right]^{(l)} \\
&= \sum_{l=0}^{s}\sum_{m=0}^{s-l}\sum_{n=0}^{l}\langle\Psi^{(m)}|\overline{U}^{(s-l-m)}U^{(l-n)}\left[\theta|\Psi\rangle\right]^{(n)} \\
&= \sum_{n=0}^{s}\sum_{v=0}^{s-n}\sum_{w=0}^{v}\langle\Psi^{(s-n-v)}|\overline{U}^{(v-w)}U^{(w)}\left[\theta|\Psi\rangle\right]^{(n)} \\
&= \sum_{n=0}^{s}\sum_{v=0}^{s-n}\langle\Psi^{(s-n-v)}|\delta_{v0}\left[\theta|\Psi\rangle\right]^{(n)} \\
&= \sum_{n=0}^{s}\langle\Psi^{(s-n)}|\left[\theta|\Psi\rangle\right]^{(n)} \\
&= \langle\Psi|\theta|\Psi\rangle^{(s)} \\
&= N^{(s)}(\theta)
\end{aligned} \tag{3.44}$$

Thus $N^{(s)}(\theta) = \tilde{N}^{(s)}(\tilde{\theta})$ and $\langle O\rangle^{(r)} = \langle\tilde{O}\rangle^{(r)}$ so that the expectation values are independent of gauge to any order of perturbation theory.

Section 3.3. The A.p and E.r gauges.

In this section the general results of the previous section are exemplified with the aid of an example of practical importance, namely that of the connection between calculations performed in two particular gauges I and II which give the so called **A.p** and **E.r** interactions [22,23]. Consider a plane electromagnetic wave propagating in the z-direction

$$\mathbf{E} = E(\omega)\left[\mathrm{e}^{i(kz-\omega t)} + \mathrm{e}^{-i(kz-\omega t)}\right]\mathbf{e}_x \tag{3.45}$$

$$\mathbf{B} = B(\omega)\left[\mathrm{e}^{i(kz-\omega t)} + \mathrm{e}^{-i(kz-\omega t)}\right]\mathbf{e}_y \tag{3.46}$$

where $E(\omega) = (\omega/k)B(\omega)$. Suppose that the wave propagates in the plane of a semiconductor quantum well with the electric field vector oriented in the quantisation direction $\mathbf{e}_x$ of the quantum well. It is assumed that the electronic states $\{\Psi_l\}$ are bound in the x-direction so that matrix elements of the position operator x are defined and the standard relation [8,9]

$$\langle\Psi_m|p^x|\Psi_l\rangle = im\omega_{ml}\langle\Psi_m|x|\Psi_l\rangle \tag{3.47}$$

is applicable. Also suppose that initially the system is in the electronic state Ψ_s and is subsequently perturbed by the electromagnetic wave. The fields can be described by the gauge

$$\phi = 0 \tag{3.48}$$

$$\mathbf{A} = \frac{E(\omega)}{i\omega}\left[\mathrm{e}^{i(kz-\omega t)} - \mathrm{e}^{-i(kz-\omega t)}\right]\mathbf{e}_x \tag{3.49}$$

The first order Schrödinger equation in this gauge is

$$H_0\Psi^{(1)} + \frac{e}{m}\mathbf{A}.\mathbf{p}\Psi^{(0)} = i\hbar\frac{\partial\Psi^{(1)}}{\partial t} \tag{3.50}$$

where the electromagnetic interaction is provided by the $(e/m)\mathbf{A}.\mathbf{p}$ term, so that gauge I is commonly called the $\mathbf{A}.\mathbf{p}$ gauge. The zero order wavefunction is

$$\Psi^{(0)}(t) = \mathrm{e}^{-i\omega_s t}\Psi_s \tag{3.51}$$

and the first order wavefunction may be expanded over the orthonormal basis set of time independent states $\{\Psi_l\}$ as

$$\Psi^{(1)}(t) = \sum_l a_l^{(1)}(t)\Psi_l \tag{3.52}$$

Substituting into the first order Schrödinger equation (3.50) gives

$$i\hbar\frac{d}{dt}\left(a_l^{(1)}\mathrm{e}^{i\omega_l t}\right) = \frac{eE(\omega)}{im\omega}\left[\mathrm{e}^{i(\omega_{ls}-\omega)t}\sum_m p_{lm}^x \mathrm{e}_{ms}^{ikz} - \mathrm{e}^{i(\omega_{ls}+\omega)t}\sum_m p_{lm}^x \mathrm{e}_{ms}^{-ikz}\right] \tag{3.53}$$

so that by integration

$$a_l^{(1)} = -\frac{eE(\omega)}{i\hbar m\omega}\left[\frac{\mathrm{e}^{-i(\omega_s+\omega)t}}{\omega_{ls}-\omega}\sum_m p_{lm}^x \mathrm{e}_{ms}^{ikz} - \frac{\mathrm{e}^{-i(\omega_s-\omega)t}}{\omega_{ls}+\omega}\sum_m p_{lm}^x \mathrm{e}_{ms}^{-ikz}\right] \tag{3.54}$$

The first order current may be calculated as

$$\begin{aligned}
\mathbf{J}^{(1)} &= -\frac{e}{m}\langle \mathbf{p} + e\mathbf{A}\rangle^{(1)} \\
&= -\frac{e}{m}\left[\frac{\langle\Psi|\mathbf{p}+e\mathbf{A}|\Psi\rangle}{\langle\Psi|\Psi\rangle}\right]^{(1)} \\
&= -\frac{e}{m}\Big[\langle\Psi^{(1)}|\mathbf{p}|\Psi^{(0)}\rangle + \langle\Psi^{(0)}|\mathbf{p}|\Psi^{(1)}\rangle + \langle\Psi^{(0)}|e\mathbf{A}|\Psi^{(0)}\rangle \\
&\quad - \langle\Psi^{(0)}|\mathbf{p}|\Psi^{(0)}\rangle\left(\langle\Psi^{(1)}|\Psi^{(0)}\rangle + \langle\Psi^{(0)}|\Psi^{(1)}\rangle\right)\Big] \\
&= -\frac{e}{m}\sum_l\left(\overline{a}_l^{(1)}\mathbf{p}_{ls}\mathrm{e}^{-i\omega_s t} + \mathrm{e}^{i\omega_s t}\mathbf{p}_{sl}a_l^{(1)}\right) - \frac{e^2}{m}\mathbf{A}_{ss}
\end{aligned} \tag{3.55}$$

Now considering just the component at frequency ω gives

$$\mathbf{J}^{(1)}(\omega) = \frac{e^2 E(\omega)}{i\hbar m^2 \omega} \sum_l \left[\frac{1}{\omega_{ls}+\omega} \sum_m \mathrm{e}^{ikz}_{sm} p^x_{ml} \mathbf{p}_{ls} + \frac{1}{\omega_{ls}-\omega} \sum_m \mathbf{p}_{sl} p^x_{lm} \mathrm{e}^{ikz}_{ms} \right] - \frac{e^2 E(\omega)}{im\omega} \mathrm{e}^{ikz}_{ss} \mathbf{e}_x \tag{3.56}$$

and the time integral of the current provides the polarisation

$$\mathbf{P}^{(1)}_I(\omega) = \frac{e^2 E(\omega)}{\hbar m^2 \omega^2} \sum_l \left[\frac{1}{\omega_{ls}+\omega} \sum_m \mathrm{e}^{ikz}_{sm} p^x_{ml} \mathbf{p}_{ls} + \frac{1}{\omega_{ls}-\omega} \sum_m \mathbf{p}_{sl} p^x_{lm} \mathrm{e}^{ikz}_{ms} \right] - \frac{e^2 E(\omega)}{m\omega^2} \mathrm{e}^{ikz}_{ss} \mathbf{e}_x \tag{3.57}$$

With the polarisation in gauge I determined, suppose that gauge II is defined by the transformation function $\Lambda = -\mathbf{A}.\mathbf{r}$. In gauge II the dominant electromagnetic interaction term is provided by $-e\tilde{\phi} = e\mathbf{E}.\mathbf{r}$ so that gauge II is commonly called the **E.r** gauge. The scalar and vector potentials for the plane electromagnetic wave of equations (3.45) and (3.46) are given in gauge II by

$$\tilde{\phi} = -xE(\omega) \left[\mathrm{e}^{i(kz-\omega t)} + \mathrm{e}^{-i(kz-\omega t)} \right] \tag{3.58}$$

$$\tilde{\mathbf{A}} = -\frac{kx}{\omega} E(\omega) \left[\mathrm{e}^{i(kz-\omega t)} + \mathrm{e}^{-i(kz-\omega t)} \right] \mathbf{e}_z \tag{3.59}$$

and the first order Schrödinger equation in this gauge is

$$H_0 \tilde{\Psi}^{(1)} - e\tilde{\phi}\tilde{\Psi}^{(0)} + \frac{e}{m} \tilde{\mathbf{A}}.\mathbf{p} \tilde{\Psi}^{(0)} + \frac{e}{2m} \tilde{\Psi}^{(0)} \mathbf{p}.\tilde{\mathbf{A}} = i\hbar \frac{\partial \tilde{\Psi}^{(1)}}{\partial t} \tag{3.60}$$

The zero order wavefunction is unchanged from equation (3.51). The first order wavefunction may again be expanded over the basis set $\{\Psi_l\}$ as

$$\tilde{\Psi}^{(1)} = \sum_l \tilde{a}^{(1)}_l \Psi_l \tag{3.61}$$

and the coefficients determined by substitution into the Schrödinger equation (3.60)

$$\tilde{a}_l^{(1)} = -\frac{eE(\omega)}{\hbar}\left[\frac{\mathrm{e}^{-i(\omega_s+\omega)t}}{\omega_{ls}-\omega}\sum_m x_{lm}\mathrm{e}_{ms}^{ikz} + \frac{\mathrm{e}^{-i(\omega_s-\omega)t}}{\omega_{ls}+\omega}\sum_m x_{lm}\mathrm{e}_{ms}^{-ikz}\right]$$
$$+\frac{ekE(\omega)}{\hbar m\omega}\left[\frac{\mathrm{e}^{-i(\omega_s+\omega)t}}{\omega_{ls}-\omega}\sum_{m,n} x_{lm}\mathrm{e}_{mn}^{ikz}p_{ns}^z + \frac{\mathrm{e}^{-i(\omega_s-\omega)t}}{\omega_{ls}+\omega}\sum_{m,n} x_{lm}\mathrm{e}_{mn}^{-ikz}p_{ns}^z\right]$$
$$+\frac{ek^2E(\omega)}{2m\omega}\left[\frac{\mathrm{e}^{-i(\omega_s+\omega)t}}{\omega_{ls}-\omega}\sum_m x_{lm}\mathrm{e}_{ms}^{ikz} - \frac{\mathrm{e}^{-i(\omega_s-\omega)t}}{\omega_{ls}+\omega}\sum_m x_{lm}\mathrm{e}_{ms}^{-ikz}\right] \qquad (3.62)$$

As in the first gauge the polarisation may be obtained from the time integral of the current

$$\mathbf{P}_{II}^{(1)}(\omega) = -\frac{e^2E(\omega)}{i\hbar m\omega}\sum_l\left[\frac{1}{\omega_{ls}+\omega}\sum_m \mathrm{e}_{sm}^{ikz}x_{ml}\mathrm{p}_{ls} + \frac{1}{\omega_{ls}-\omega}\sum_m \mathrm{p}_{sl}x_{lm}\mathrm{e}_{ms}^{ikz}\right]$$
$$+\frac{e^2kE(\omega)}{i\hbar m^2\omega^2}\sum_l\left[\frac{1}{\omega_{ls}+\omega}\sum_{m,n} p_{sn}^z\mathrm{e}_{nm}^{ikz}x_{ml}\mathrm{p}_{ls} + \frac{1}{\omega_{ls}-\omega}\sum_{m,n}\mathrm{p}_{sl}x_{lm}\mathrm{e}_{mn}^{ikz}p_{ns}^z\right]$$
$$-\frac{e^2k^2E(\omega)}{2im^2\omega^2}\sum_l\left[\frac{1}{\omega_{ls}+\omega}\sum_m \mathrm{e}_{sm}^{ikz}x_{ml}\mathrm{p}_{ls} - \frac{1}{\omega_{ls}-\omega}\sum_m \mathrm{p}_{sl}x_{lm}\mathrm{e}_{ms}^{ikz}\right]$$
$$-\frac{e^2kE(\omega)}{im\omega^2}\sum_m x_{sm}\mathrm{e}_{ms}^{ikz}\mathbf{e}_z \qquad (3.63)$$

From the general discussion given in section 3.2 the two expressions (3.57) and (3.63) for the polarisation should be equivalent, but this can be demonstrated explicitly. Consider the expression (3.57) for the polarisation derived in gauge I and substitute for p_{ml}^x and p_{lm}^x by means of the standard relation $p_{ml}^x = im\omega_{ml}x_{ml}$ of equation (3.47) before employing the relations

$$\frac{\omega_{ml}}{\omega(\omega_{ls}+\omega)} = \frac{1}{\omega_{ls}+\omega} - \frac{\omega_{sm}}{\omega(\omega_{ls}+\omega)} - \frac{1}{\omega} \qquad (3.64)$$

and

$$\frac{\omega_{lm}}{\omega(\omega_{ls}-\omega)} = \frac{1}{\omega_{ls}-\omega} - \frac{\omega_{ms}}{\omega(\omega_{ls}-\omega)} + \frac{1}{\omega} \qquad (3.65)$$

to obtain

$$\begin{aligned}\mathbf{P}_I^{(1)}(\omega) = &-\frac{e^2E(\omega)}{i\hbar m\omega}\sum_l\left[\frac{1}{\omega_{ls}+\omega}\sum_m \mathrm{e}^{ikz}_{sm}x_{ml}\mathrm{p}_{ls}+\frac{1}{\omega_{ls}-\omega}\sum_m \mathrm{p}_{sl}x_{lm}\mathrm{e}^{ikz}_{ms}\right]\\ &+\frac{e^2E(\omega)}{i\hbar m\omega^2}\sum_l\left[\frac{1}{\omega_{ls}+\omega}\sum_m \omega_{sm}\mathrm{e}^{ikz}_{sm}x_{ml}\mathrm{p}_{ls}+\frac{1}{\omega_{ls}-\omega}\sum_m \mathrm{p}_{sl}x_{lm}\mathrm{e}^{ikz}_{ms}\omega_{ms}\right]\\ &+\frac{e^2E(\omega)}{i\hbar m\omega^2}\sum_{l,m}\left(\mathrm{e}^{ikz}_{sm}x_{ml}\mathrm{p}_{ls}-\mathrm{p}_{sl}x_{lm}\mathrm{e}^{ikz}_{ms}\right)\\ &-\frac{e^2E(\omega)}{m\omega^2}\mathrm{e}^{ikz}_{ss}\mathbf{e}_x \end{aligned} \tag{3.66}$$

Now consideration of $[H_0, \exp(\pm ikz)]$ yields the relations

$$\omega_{sm}\mathrm{e}^{ikz}_{sm} = \frac{k}{m}\sum_n p^z_{sn}\mathrm{e}^{ikz}_{nm} - \frac{\hbar k^2}{2m}\mathrm{e}^{ikz}_{sm} \tag{3.67}$$

and

$$\omega_{ms}\mathrm{e}^{ikz}_{ms} = \frac{k}{m}\sum_n \mathrm{e}^{ikz}_{mn}p^z_{ns} + \frac{\hbar k^2}{2m}\mathrm{e}^{ikz}_{ms} \tag{3.68}$$

which may be substituted into the expression (3.66) for $\mathbf{P}_I^{(1)}(\omega)$ to obtain

$$\begin{aligned}\mathbf{P}_I^{(1)}(\omega) = &-\frac{e^2E(\omega)}{i\hbar m\omega}\sum_l\left[\frac{1}{\omega_{ls}+\omega}\sum_m \mathrm{e}^{ikz}_{sm}x_{ml}\mathrm{p}_{ls}+\frac{1}{\omega_{ls}-\omega}\sum_m \mathrm{p}_{sl}x_{lm}\mathrm{e}^{ikz}_{ms}\right]\\ &+\frac{e^2kE(\omega)}{i\hbar m^2\omega^2}\sum_l\left[\frac{1}{\omega_{ls}+\omega}\sum_{m,n} p^z_{sn}\mathrm{e}^{ikz}_{nm}x_{ml}\mathrm{p}_{ls}+\frac{1}{\omega_{ls}-\omega}\sum_{m,n} \mathrm{p}_{sl}x_{lm}\mathrm{e}^{ikz}_{mn}p^z_{ns}\right]\\ &-\frac{e^2k^2E(\omega)}{2im^2\omega^2}\sum_l\left[\frac{1}{\omega_{ls}+\omega}\sum_m \mathrm{e}^{ikz}_{sm}x_{ml}\mathrm{p}_{ls}-\frac{1}{\omega_{ls}-\omega}\sum_m \mathrm{p}_{sl}x_{lm}\mathrm{e}^{ikz}_{ms}\right]\\ &+\frac{e^2E(\omega)}{i\hbar m\omega^2}\left[\mathrm{e}^{ikz}x,\mathrm{p}\right]_{ss}-\frac{e^2E(\omega)}{m\omega^2}\mathrm{e}^{ikz}_{ss}\mathbf{e}_x \end{aligned} \tag{3.69}$$

Finally expanding the commutator

$$\frac{1}{i\hbar}\left[\mathrm{e}^{ikz}x,\mathrm{p}\right]_{ss} = \mathrm{e}^{ikz}_{ss}\mathbf{e}_x + ik\sum_m x_{sm}\mathrm{e}^{ikz}_{ms}\mathbf{e}_z \tag{3.70}$$

and comparing equation (3.69) with equation (3.63) shows that $\mathbf{P}_I^{(1)}(\omega) = \mathbf{P}_{II}^{(1)}(\omega)$ so that the value calculated for the first order polarisation is independent of the gauge.

Now Ehrenfest's theorem [8,9] states that for a bound system the time derivative of the expectation value of the position operator $\mathbf{r}$ equals the expectation value of the velocity operator $\mathbf{v}$, that is

$$\frac{\partial}{\partial t}\left[\frac{\langle\Psi|\mathbf{r}|\Psi\rangle}{\langle\Psi|\Psi\rangle}\right] = \frac{\langle\Psi|\mathbf{v}|\Psi\rangle}{\langle\Psi|\Psi\rangle} \tag{3.71}$$

Thus for the quantum well system considered above the polarisation in the x-direction may be calculated directly as

$$\hat{P} = -e\langle x\rangle \tag{3.72}$$

and Ehrenfest's theorem guarantees that this gives the same result as obtaining the polarisation through time integration of the current since

$$P = \int J dt = -e\int \langle v\rangle dt = -e\langle x\rangle = \hat{P} \tag{3.73}$$

This will be demonstrated for the example problem shortly, but first it is shown that the first order polarisations calculated from equation (3.72) are equivalent in the two gauges I and II. Thus taking the wavefunction coefficients $a_l^{(1)}$ in gauge I from equation (3.54) the polarisation in the x-direction is given by

$$\hat{P}_I^{(1)}(\omega) = \frac{e^2E(\omega)}{i\hbar m\omega}\sum_l\left[\frac{1}{\omega_{ls}+\omega}\sum_m \mathrm{e}_{sm}^{ikz}p_{ml}^x x_{ls} + \frac{1}{\omega_{ls}-\omega}\sum_m x_{sl}p_{lm}^x \mathrm{e}_{ms}^{ikz}\right] \tag{3.74}$$

Similarly taking the wavefunction coefficients $\tilde{a}_l^{(1)}$ in gauge II from equation (3.62) the polarisation is given by

$$\hat{P}_{II}^{(1)}(\omega) = \frac{e^2E(\omega)}{\hbar}\sum_l\left[\frac{1}{\omega_{ls}+\omega}\sum_m \mathrm{e}_{sm}^{ikz}x_{ml}x_{ls} + \frac{1}{\omega_{ls}-\omega}\sum_m x_{sl}x_{lm}\mathrm{e}_{ms}^{ikz}\right]$$

$$- \frac{e^2 kE(\omega)}{\hbar m\omega} \sum_l \left[\frac{1}{\omega_{ls}+\omega} \sum_{m,n} p^z_{sn} \mathrm{e}^{ikz}_{nm} x_{ml} x_{ls} + \frac{1}{\omega_{ls}-\omega} \sum_{m,n} x_{sl} x_{lm} \mathrm{e}^{ikz}_{mn} p^z_{ns} \right]$$
$$+ \frac{e^2 k^2 E(\omega)}{2m\omega} \sum_l \left[\frac{1}{\omega_{ls}+\omega} \sum_m \mathrm{e}^{ikz}_{sm} x_{ml} x_{ls} - \frac{1}{\omega_{ls}-\omega} \sum_m x_{sl} x_{lm} \mathrm{e}^{ikz}_{ms} \right] \quad (3.75)$$

Now applying the standard relation $p^x_{ml} = im\omega_{ml} x_{ml}$ of equation (3.47) to substitute for p^x_{ml} and p^z_{lm} in the expression (3.74) for $\hat{P}^{(1)}_I(\omega)$ and using the relations (3.64) and (3.65) gives

$$\hat{P}^{(1)}_I(\omega) = \frac{e^2 E(\omega)}{\hbar} \sum_l \left[\frac{1}{\omega_{ls}+\omega} \sum_m \mathrm{e}^{ikz}_{sm} x_{ml} x_{ls} + \frac{1}{\omega_{ls}-\omega} \sum_m x_{sl} x_{lm} \mathrm{e}^{ikz}_{ms} \right]$$
$$- \frac{e^2 E(\omega)}{\hbar\omega} \sum_l \left[\frac{1}{\omega_{ls}+\omega} \sum_m \omega_{sm} \mathrm{e}^{ikz}_{sm} x_{ml} x_{ls} + \frac{1}{\omega_{ls}-\omega} \sum_m x_{sl} x_{lm} \mathrm{e}^{ikz}_{ms} \omega_{ms} \right]$$
$$- \frac{e^2 E(\omega)}{\hbar\omega} \sum_{l,m} \left(\mathrm{e}^{ikz}_{sm} x_{ml} x_{ls} - x_{sl} x_{lm} \mathrm{e}^{ikz}_{ms} \right) \quad (3.76)$$

and then using the relations (3.67) and (3.68) gives

$$\hat{P}^{(1)}_I(\omega) = \frac{e^2 E(\omega)}{\hbar} \sum_l \left[\frac{1}{\omega_{ls}+\omega} \sum_m \mathrm{e}^{ikz}_{sm} x_{ml} x_{ls} + \frac{1}{\omega_{ls}-\omega} \sum_m x_{sl} x_{lm} \mathrm{e}^{ikz}_{ms} \right]$$
$$- \frac{e^2 kE(\omega)}{\hbar m\omega} \sum_l \left[\frac{1}{\omega_{ls}+\omega} \sum_{m,n} p^z_{sn} \mathrm{e}^{ikz}_{nm} x_{ml} x_{ls} + \frac{1}{\omega_{ls}-\omega} \sum_{m,n} x_{sl} x_{lm} \mathrm{e}^{ikz}_{mn} p^z_{ns} \right]$$
$$+ \frac{e^2 k^2 E(\omega)}{2m\omega} \sum_l \left[\frac{1}{\omega_{ls}+\omega} \sum_m \mathrm{e}^{ikz}_{sm} x_{ml} x_{ls} - \frac{1}{\omega_{ls}-\omega} \sum_m x_{sl} x_{lm} \mathrm{e}^{ikz}_{ms} \right]$$
$$- \frac{e^2 E(\omega)}{\hbar\omega} \left[\mathrm{e}^{ikz} x, x \right]_{ss} \quad (3.77)$$

and since the commutator $[\exp(ikz)x, x] = 0$ then comparison with equation (3.75) shows that $\hat{P}^{(1)}_I(\omega) = \hat{P}^{(1)}_{II}(\omega)$.

Earlier it was shown that the calculation of polarisation by time integration of the current yields identical results in gauges I and II, so that $P^{(1)}_I = P^{(1)}_{II}$. Also the values obtained in the two gauges by direct calculation of the polarisation are

equivalent, so that $\hat{P}_I^{(1)} = \hat{P}_{II}^{(1)}$. It remains to show that $P_I^{(1)} = \hat{P}_I^{(1)}$ so that all four methods of calculating the polarisation produce the same result. So consider $\hat{P}_I^{(1)}$ from equation (3.74) and use the relations

$$\frac{1}{\omega_{ls}+\omega} = \frac{-\omega_{ls}}{\omega(\omega_{ls}+\omega)} + \frac{1}{\omega} \tag{3.78}$$

and

$$\frac{1}{\omega_{ls}-\omega} = \frac{-\omega_{sl}}{\omega(\omega_{ls}-\omega)} - \frac{1}{\omega} \tag{3.79}$$

to obtain

$$\begin{aligned}\hat{P}_I^{(1)}(\omega) = &-\frac{e^2E(\omega)}{i\hbar m\omega^2}\sum_l\left[\frac{1}{\omega_{ls}+\omega}\sum_m \mathrm{e}^{ikz}_{sm}p^x_{ml}x_{ls}\omega_{ls} + \frac{1}{\omega_{ls}-\omega}\sum_m \omega_{sl}x_{sl}p^x_{lm}\mathrm{e}^{ikz}_{ms}\right] \\ &+ \frac{e^2E(\omega)}{i\hbar m\omega^2}\sum_{l,m}\left(\mathrm{e}^{ikz}_{sm}p^x_{ml}x_{ls} - x_{sl}p^x_{lm}\mathrm{e}^{ikz}_{ms}\right)\end{aligned} \tag{3.80}$$

and then the standard relation $p^x_{ls} = im\omega_{ls}x_{ls}$ of equation (3.47) shows that

$$\begin{aligned}\hat{P}_I^{(1)}(\omega) = &\frac{e^2E(\omega)}{\hbar m^2\omega^2}\sum_l\left[\frac{1}{\omega_{ls}+\omega}\sum_m \mathrm{e}^{ikz}_{sm}p^x_{ml}p^x_{ls} + \frac{1}{\omega_{ls}-\omega}\sum_m p^x_{sl}p^x_{lm}\mathrm{e}^{ikz}_{ms}\right] \\ &+ \frac{e^2E(\omega)}{i\hbar m\omega^2}\left[\mathrm{e}^{ikz}p^x, x\right]_{ss}\end{aligned} \tag{3.81}$$

and the commutator is

$$\frac{1}{i\hbar}\left[\mathrm{e}^{ikz}p^x, x\right]_{ss} = -\mathrm{e}^{ikz}_{ss} \tag{3.82}$$

so comparing equations (3.81) and (3.57) shows that $P_I^{(1)} = \hat{P}_I^{(1)}$ as required, and all four methods of calculating the polarisation are equivalent.

Section 3.4. The electric dipole approximation.

The electric dipole approximation [4,24] neglects the z-dependence of the electromagnetic wave defined in equations (3.45) and (3.46) so that $\exp(ikz) = 1$. The magnetic field $\mathbf{B}$ is neglected and the electric field

$$\mathbf{E} = E(\omega)\left[\mathrm{e}^{-i\omega t} + \mathrm{e}^{i\omega t}\right]\mathbf{e}_x \tag{3.83}$$

polarises the quantum well system in the x-direction. The first order polarisation in gauge I may be approximated using $P_I^{(1)}$ whilst the first order polarisation in gauge II may be approximated using $\hat{P}_{II}^{(1)}$. Thus from equation (3.57)

$$P_I^{(1)}(\omega) \simeq \frac{e^2 E(\omega)}{\hbar m^2 \omega^2} \sum_l \left[\frac{p_{sl}^x p_{ls}^x}{\omega_{ls} + \omega} + \frac{p_{sl}^x p_{ls}^x}{\omega_{ls} - \omega}\right] - \frac{e^2 E(\omega)}{m\omega^2} \tag{3.84}$$

Also using the relations (3.67) and (3.68) then equation (3.75) gives

$$\begin{aligned}\hat{P}_{II}^{(1)}(\omega) &= \frac{e^2 E(\omega)}{\hbar} \sum_l \left[\frac{1}{\omega_{ls}+\omega} \sum_m \mathrm{e}_{sm}^{ikz} x_{ml} x_{ls} \left(1 - \frac{\omega_{sm}}{\omega}\right) + \frac{1}{\omega_{ls}-\omega} \sum_m x_{sl} x_{lm} \mathrm{e}_{ms}^{ikz} \left(1 - \frac{\omega_{ms}}{\omega}\right)\right] \\ &\simeq \frac{e^2 E(\omega)}{\hbar} \sum_l \left[\frac{x_{sl} x_{ls}}{\omega_{ls} + \omega} + \frac{x_{sl} x_{ls}}{\omega_{ls} - \omega}\right]\end{aligned} \tag{3.85}$$

By application of the sum rule [8,9]

$$\sum_{l \neq s} \frac{|p_{ls}^x|^2}{\omega_{ls}} = \frac{\hbar m}{2} \tag{3.86}$$

to the last term in equation (3.84) the polarisation in the first gauge may be approximated by

$$\begin{aligned}P_I^{(1)}(\omega) &\simeq \frac{e^2 E(\omega)}{\hbar m^2 \omega^2} \sum_l \left[\frac{1}{\omega_{ls}+\omega} + \frac{1}{\omega_{ls}-\omega}\right] |p_{ls}^x|^2 - \frac{2e^2 E(\omega)}{\hbar m^2 \omega^2} \sum_{l \neq s} \frac{|p_{ls}^x|^2}{\omega_{ls}} \\ &= \frac{e^2 E(\omega)}{\hbar m^2} \sum_l \left[\frac{1}{\omega_{ls} + \omega} + \frac{1}{\omega_{ls} - \omega}\right] \frac{|p_{ls}^x|^2}{\omega_{ls}^2}\end{aligned} \tag{3.87}$$

so that the two gauges produce identical results. However, if a two-level approximation is made directly from equations (3.84) and (3.85) to obtain the susceptibilities

$$\chi_I^{(1)}(\omega) = \frac{e^2}{\varepsilon_0 \hbar m^2 \omega^2} \left[\frac{1}{\omega_{10} + \omega} + \frac{1}{\omega_{10} - \omega} \right] |p_{10}^x|^2 - \frac{e^2}{\varepsilon_0 m \omega^2} \tag{3.88}$$

and

$$\chi_{II}^{(1)}(\omega) = \frac{e^2}{\varepsilon_0 \hbar} \left[\frac{1}{\omega_{10} + \omega} + \frac{1}{\omega_{10} - \omega} \right] |x_{10}|^2 \tag{3.89}$$

then the first result produces a $1/\omega^2$ dependence for small frequencies whilst the second result does not. Further, near resonance ($\omega \simeq \omega_{10}$) the last term in equation (3.88) may be neglected to obtain the dubious result $\chi_I^{(1)}(\omega) = (\omega_{10}/\omega)^2 \chi_{II}^{(1)}(\omega)$. As the equivalence of equations (3.85) and (3.87) indicates, these inconsistencies are not a direct consequence of using different gauges but result from the two-level approximation.

or

$$\tilde{H}_I = \frac{e}{2m}\left(\tilde{\mathbf{A}}.\mathbf{p} + \mathbf{p}.\tilde{\mathbf{A}}\right) + \frac{e^2\tilde{A}^2}{2m} - e\tilde{\phi} \tag{3.96}$$

The potentials for the first gauge are given by equations (3.48) and (3.49) (so that $\mathbf{p}.\mathbf{A} = \mathbf{A}.\mathbf{p}$) whilst the potentials for the second gauge are given by equations (3.58) and (3.59). In the electric dipole approximation the vector potential $\mathbf{A}$ in the first gauge becomes a function of time only so that in the second gauge $\tilde{\phi} = -\mathbf{E}.\mathbf{r}$ and $\tilde{\mathbf{A}} = \mathbf{0}$. Further, because the term $e^2A^2/2m$ is a function of time only, it commutes with the density matrix operator and so may be neglected in the calculations. Hence the interaction Hamiltonians for the two gauges are taken as

$$H_I = \frac{e}{m}\mathbf{A}.\mathbf{p} \tag{3.97}$$

and

$$\tilde{H}_I = e\mathbf{E}.\mathbf{r} \tag{3.98}$$

in the Schrödinger picture, whilst in the interaction picture these become

$$H_I = \exp(-H_0t/i\hbar)\left(\frac{e}{m}\mathbf{A}.\mathbf{p}\right)\exp(H_0t/i\hbar) \tag{3.99}$$

and

$$\tilde{H}_I = \exp(-H_0t/i\hbar)\,(e\mathbf{E}.\mathbf{r})\exp(H_0t/i\hbar) \tag{3.100}$$

It should be noted that equations (3.97) and (3.99) must be used when extended states are involved and that equations (3.98) and (3.100) are appropriate for use with bound state systems only.

CHAPTER FOUR

Off-resonance phenomena

In this chapter the response of a semiconductor system to an ultrashort optical pulse is considered for the case of excitation slightly off-resonance with the allowed transitions, that is with a photon energy just below the bandgap energy. At moderate illumination levels this results in the generation of virtual carriers whilst at very high intensities it is possible to produce real carriers by an effect analogous to the Landau-Zener transitions found in atomic systems. The usefulness of operating in the virtual regime is apparent for ultrafast switching devices where device recovery time is not limited by the recombination rate for electron-hole pairs. A proposal for enhancing the effectiveness of the nonlinear response in this regime by tailoring the conduction bandstructure of a quantum well device has recently been put forward by Morrison and Jaros [25-29], and the viability of this proposal is examined in the final section of the chapter.

Section 4.1. Model of a two-band semiconductor system.

The model used here of a typical semiconductor quantum well employs a simplified bandstructure as depicted in figure 4.1. In each of the valence and conduction bands only a single subband is considered and these are labelled $n = 0$ and $n = 1$ respectively. In subband n at a parallel wavevector $\mathbf{k}$ the Bloch function $\Psi_{n\mathbf{k}}$ is a solution of the Schrödinger equation

$$H_0 \Psi_{n\mathbf{k}} = E_n(\mathbf{k}) \Psi_{n\mathbf{k}} \tag{4.1}$$

where H_0 is the Hamiltonian of the unperturbed system. It is assumed that the in-plane dispersion of the energy $E_n(\mathbf{k})$ with electron wavevector $\mathbf{k}$ is parabolic,

$$E_n(\mathbf{k}) = E_n(0) + \frac{\hbar k^2}{2m_n^*} \tag{4.2}$$

where m_n^* is the electron effective mass for the subband. In chapter six a more realistic bandstructure will be considered but the present model allows consideration of the essential physical processes. The response of the material system to optical excitation can be described using the Liouville equation for the density matrix operator ρ as discussed in chapter two. The usual approximation that the optical interactions do not change electron wavevector (because the photons have very small wavevectors in comparison) is adopted and the differential equations for the density matrix are consequently assumed to decouple at each particular value of electron wavevector. It is thus possible to consider the optical interaction at each value of $\mathbf{k}$ separately, and so for a given value of $\mathbf{k}$ the Liouville equation

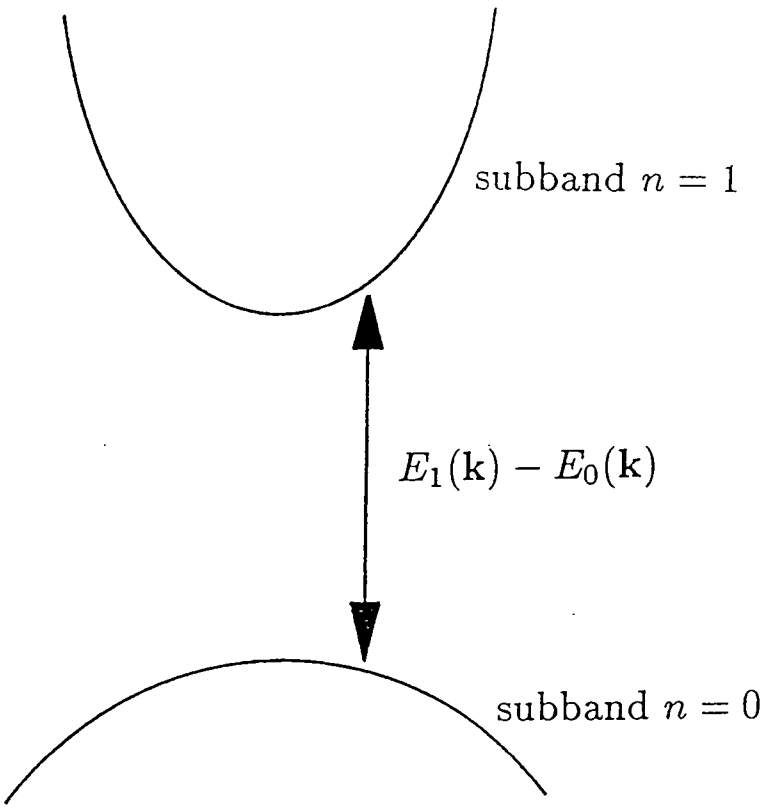

Figure 4.1. In-plane bandstructure of a semiconductor quantum well with one valence subband ($n = 0$) and one conduction subband ($n = 1$).

in the interaction picture may be written as

$$i\hbar\frac{d\rho_{nm}^{(r)}}{dt} = \left[H_I, \rho_I^{(r-1)}\right]_{nm} \tag{4.3}$$

where $\rho_{nm}^{(r)}$ is the r^{th} order perturbative term in the density matrix element between states Ψ_{nk} and Ψ_{mk}. The interaction Hamiltonian is taken from equation (3.99) or (3.100) and has matrix elements

$$H_{nm} = \frac{e}{m}\mathbf{A}.\mathbf{p}_{nm}\exp(i\omega_{nm}t) \tag{4.4}$$

or

$$\tilde{H}_{nm} = e\mathbf{E}.\mathbf{r}_{nm}\exp(i\omega_{nm}t) \tag{4.5}$$

dependent on gauge and the energy separation between states is $\hbar\omega_{nm} = E_n(\mathbf{k}) - E_m(\mathbf{k})$. The bandstructure influences the optical response in a number of ways. Firstly, the energy dispersion within a subband results in variation of the detuning $\Delta = \omega_p - \omega_{nm}$ where ω_p is the photon frequency. Secondly, the matrix elements $\mathbf{p}_{nm}$ and $\mathbf{r}_{nm}$ are dependent on the semiconductor wavefunctions which in turn depend on the wavevector $\mathbf{k}$. However, this variation of the matrix elements is neglected in this chapter. Finally, the density of electronic states $g(\mathbf{k})$ determines the relative influence of the interactions throughout the Brillouin zone.

The optical perturbation is taken to be an ultrafast pulse with a gaussian envelope

$$\mathbf{E}(t) = \mathbf{E}_0\cos\omega_p t\exp(-t^2/\tau^2) \tag{4.6}$$

which represents a plane-polarised light beam whose orientation is determined by the vector $\mathbf{E_0}$ and whose centre frequency is ω_p. It is pulsed with time constant τ and thus has a frequency spectrum distributed about ω_p with bandwidth of order $1/\tau$. The pulse duration is made sufficiently short that all thermal processes may be neglected and so the decoupling of the Liouville equation assumed in equation (4.3) is indeed valid. The pulse time constant is taken as $\tau \sim$ 100fs and for optical excitation below the bandgap energy, the thermal scattering typically occurs on the picosecond timescale. The photon energy E_p is set below the bandgap energy E_g and the curvature of the subbands further increases the detuning as $\mathbf{k}$ moves away from the Brillouin zone centre. For $E_g - E_p \gg \hbar/\tau$ this ensures operation in the virtual excitation regime with practically no photogeneration of real carriers.

At each value of $\mathbf{k}$, the response of the subsystem is examined in terms of the electron occupation of the two states Ψ_0 and Ψ_1 and of the electronic polarisation produced by the mixing of these states through interaction with the electromagnetic field. The electron occupation varies on the timescale of the pulse envelope whilst the polarisation follows the more rapidly oscillating electric field vector. The electron occupation probability for the valence state Ψ_0 is given by ρ_{00} and that for the conduction state Ψ_1 is given by ρ_{11}. The polarisation may be calculated from the off-diagonal density matrix elements ρ_{01} and ρ_{10}. The linear response is a polarisation of the initial electron population. There is also a transient generation of electron-hole pairs and the nonlinear response arises from a polarisation of this

photogenerated population. These phenomena are discussed at some length in the following three sections.

Section 4.2. Physical description of the optical interaction.

Suppose that initially the valence state of the subsystem is occupied, so that the subsystem wavefunction is given by $\Psi(t_0) = \Psi_0$. The effect of the electromagnetic interaction is to mix in some of the conduction state so that

$$\Psi(t) = \Psi_0 + \alpha(t)\Psi_1 \tag{4.7}$$

where $\alpha(t)$ is small and may be calculated by elementary perturbation theory [8,9]. As discussed in chapter two, this mixing of states results in a polarisation of the subsystem when the dipole matrix element between the states is non-zero. Hence the linear response is a polarisation which arises from the introduction of an admixture of the conduction state to the initial valence state wavefunction as depicted in figure 4.2a. The system is now prepared to make an upward transition from the valence state to the conduction state by a further interaction with the electromagnetic field.

Alternatively suppose that the system is somehow arranged with the electron initially occupying the conduction state so that $\Psi(t_0) = \Psi_1$. The effect of the electromagnetic interaction is now to mix in some of the valence state so that

$$\Psi(t) = \Psi_1 - \alpha(t)\Psi_0 \tag{4.8}$$

In this case the response is a polarisation which prepares for a downward transition from the initial conduction state population to the valence state. This is depicted in figure 4.2b. Note that the polarisation induced when the electron is initially in

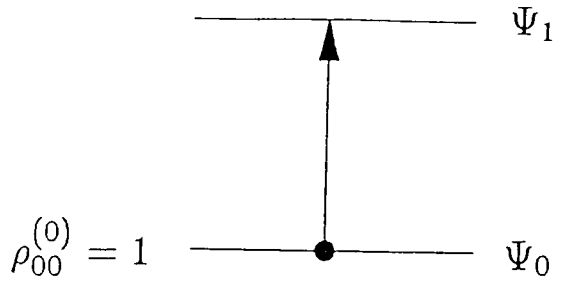

Figure 4.2a. Polarisation of the initial valence state population resulting in an induced dipole moment p.

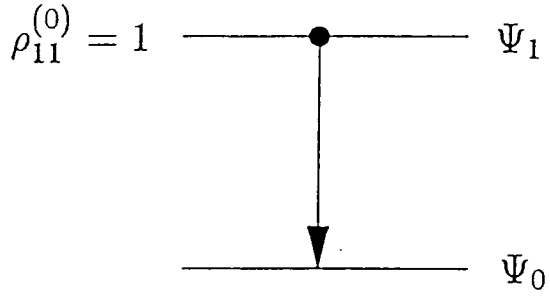

Figure 4.2b. Polarisation of the initial conduction state population resulting in an induced dipole moment $-p$.

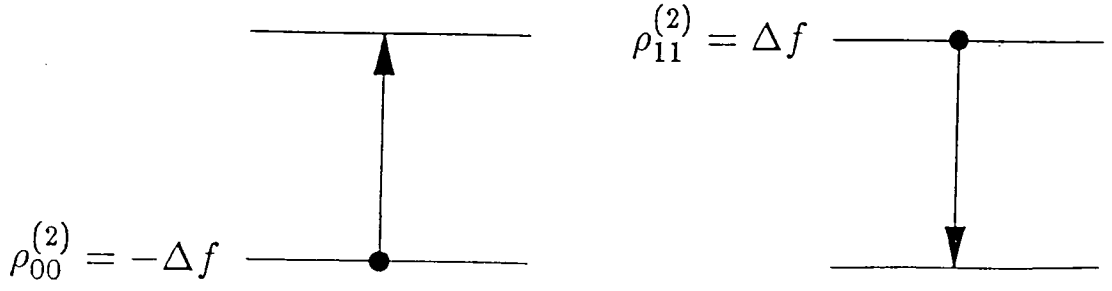

Figure 4.2c. Polarisation of the photogenerated populations resulting in a change in induced dipole moment $-2p\Delta f$.

the valence state is in antiphase with the polarisation induced when the electron is initially in the conduction state. Thus if a dipole moment p is induced in the former case, then a dipole moment $-p$ is induced in the latter case.

Now returning to the case where all electrons are initially in the valence subband, the optical pulse produces a transient change in the electron population of the states in each two-level subsystem, decreasing the valence state population by Δf and increasing the conduction state population by Δf. This results in two equal contributions to the nonlinear polarisation depicted in figure 4.2c. Firstly the reduced valence state population decreases the number of possible upward transitions, and secondly the optically generated conduction state population makes downward transitions possible. Thus the dipole moment induced by polarisation of the photogenerated electron-hole pairs is $-2p\Delta f$ and the nonlinear polarisation is in opposition to the linear polarisation.

The generation of virtual carriers as the conduction subband is transiently populated with electrons is depicted in figure 4.3 for a typical case (bandgap energy $E_g = 1.5\text{eV}$, photon energy $E_p = 0.9E_g$, combined effective mass $m^* = 0.045m$, maximum electronic wavevector $k_{\max} = 0.05\text{Å}^{-1}$, gaussian pulse time constant $\tau = 100\text{fs}$). A corresponding transient population of holes appears in the valence subband. The figure shows the time evolution of the virtual carrier population $\rho_{11}(k)g(k)$ which has been weighted by the density of states function $g(k) \sim k$. It is assumed that the bandstructure is isotropic so that the response is dependent only

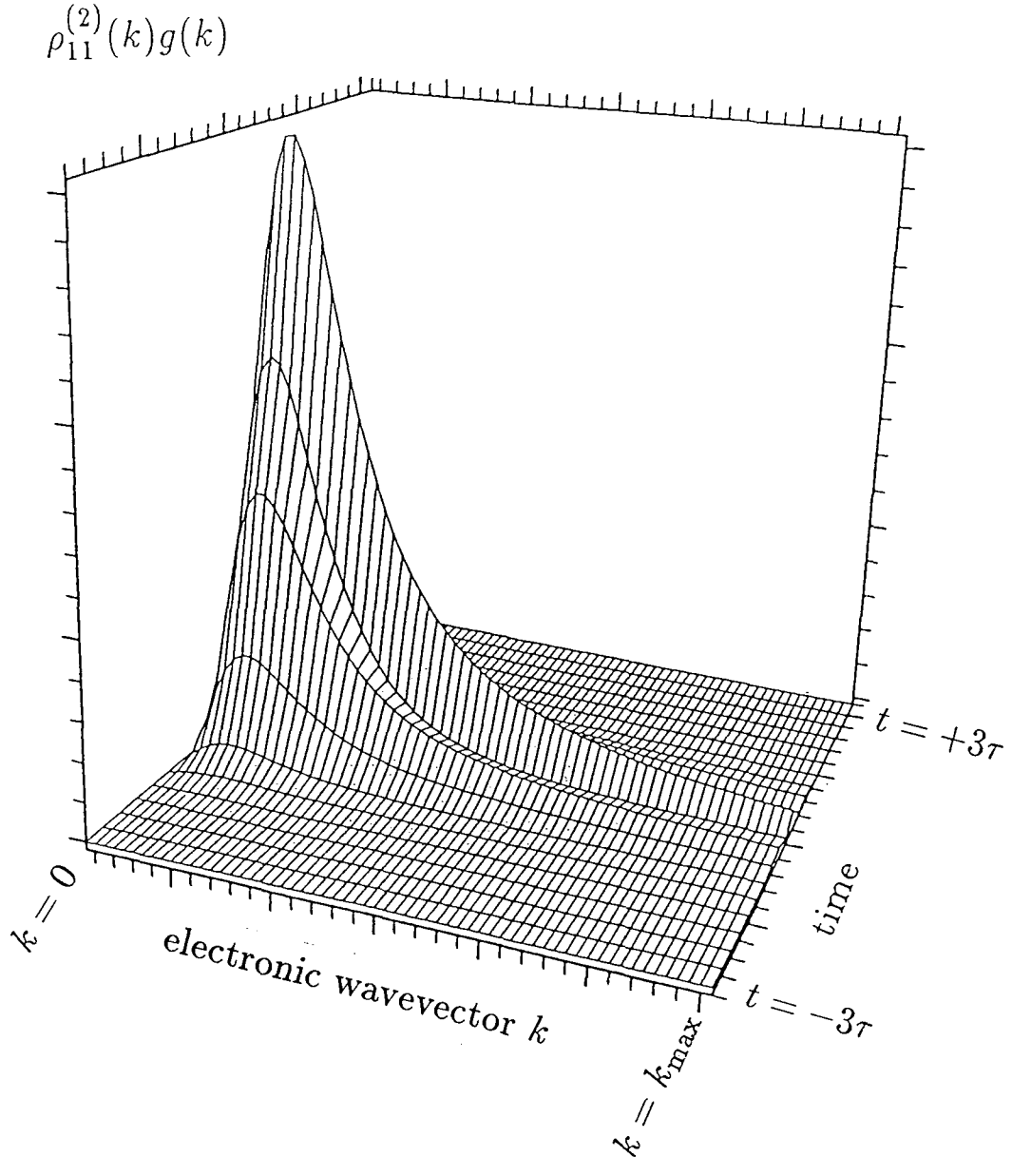

Figure 4.3. Transient generation of virtual electrons throughout the conduction subband as a function of time. The carriers are produced through excitation by a gaussian light pulse of time constant $\tau = 100$fs and centre frequency $\omega_p = 0.9\omega_g$ detuned below the bandgap ($E_g = 1.5$eV). The value of $k_{\max}$ is 0.05Å^{-1}.

on the magnitude k of the wavevector. As a function of k the form of the response is determined by the increasing detuning at large k which reduces the response, and by the density of states which tends to zero at the Brillouin zone centre. The real part of the frequency spectrum for the nonlinear polarisation is shown in figure 4.4. The polarisation is calculated as $P_k^{(3)} = -d_k(\rho_{10}^{(3)}(k) + \rho_{01}^{(3)}(k))g(k)$ where d_k is the dipole matrix element at electronic wavevector k and $\rho_{10}^{(3)}$ and $\rho_{01}^{(3)}$ are third order density matrix elements discussed further in section 4.3. The Fourier transform of P_k provides the frequency spectrum about $\omega = \omega_p$. The imaginary part of the frequency spectrum is not shown as the pulse detuning is sufficiently large to ensure no significant excitation of real carriers. The spectrum is distributed around the optical centre frequency ω_p with a spread of order $1/\tau$, and the response is again weighted with the density of states function. The figure shows the relative contributions due to polarisation of carriers throughout the Brillouin zone and the shape is again determined by increasing detuning at large k and by decreasing density of states at small k.

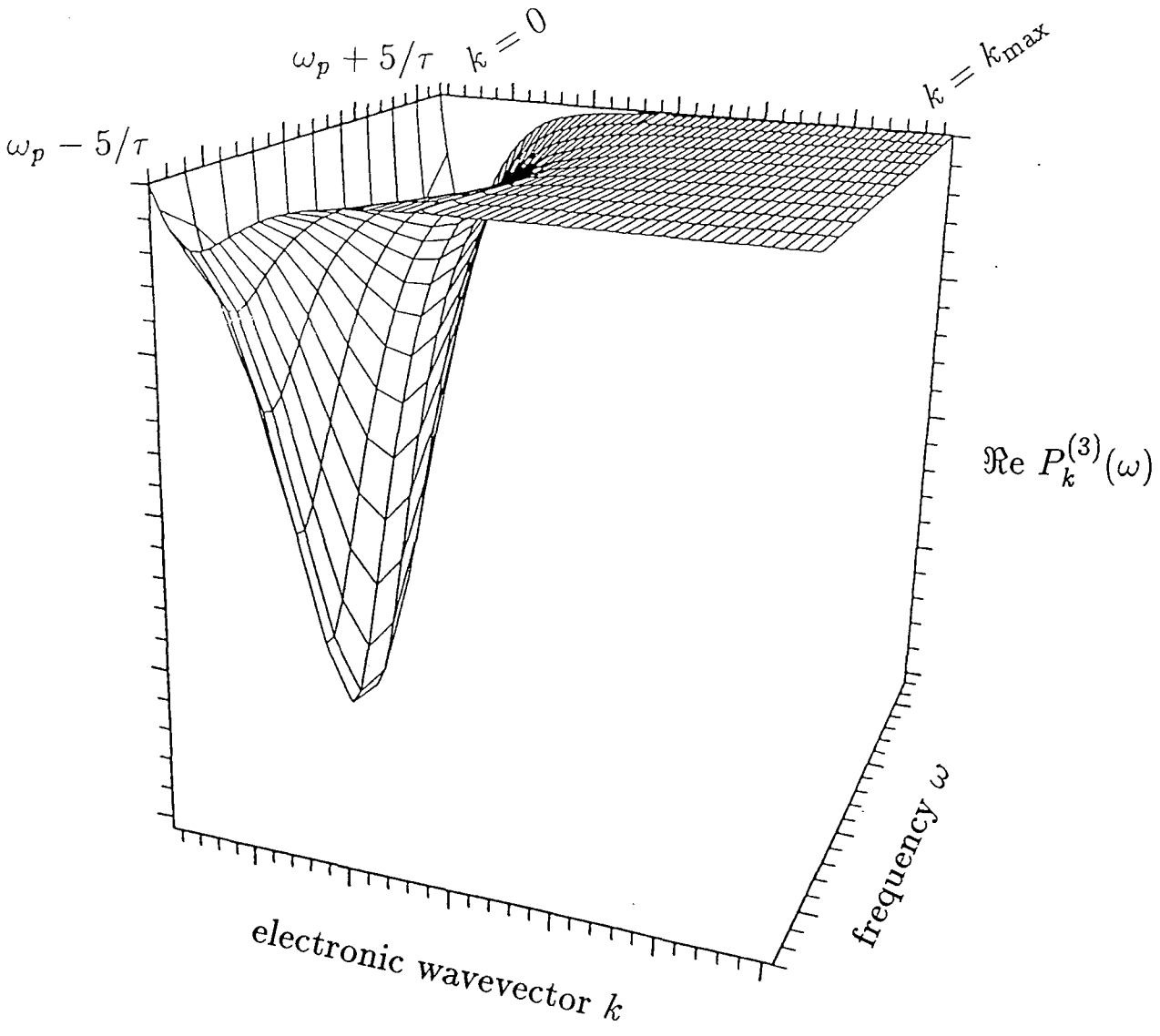

Figure 4.4. Frequency domain response of the quantum well showing the nonlinear polarisation of the two-band system subject to excitation by a gaussian light pulse of time constant $\tau = 100$fs and centre frequency $\omega_p = 0.9\omega_g$ detuned below the bandgap ($E_g = 1.5$eV). The relative contribution to the polarisation from different points in the Brillouin zone is depicted for electronic wavevectors up to $k_{max} = 0.05\text{Å}^{-1}$.

Section 4.3. Feynman diagram description of the optical interaction.

The linear and nonlinear responses of the system are now examined using a more mathematical approach. The maximally resonant terms can easily be selected with the help of double Feynman diagrams as described in chapter two. They are identified by considering only resonant transitions at each step of the perturbation calculation. It is assumed that all electrons are initially in the valence subband and that there is no phase coherence between states, so $\rho_{00}^{(0)} = 1$ and the other zero order density matrix elements $\rho_{01}^{(0)}$, $\rho_{10}^{(0)}$ and $\rho_{11}^{(0)}$ are zero. The linear response is a polarisation of the equilibrium population which introduces an admixture of the conduction state to the initial valence state wavefunction. The mixing of the two states is described by the first order density matrix elements $\rho_{10}^{(1)}$ and $\rho_{01}^{(1)}$ for which the Feynman diagrams are shown in figures 4.5a and 4.5b respectively. The resonant response for $\rho_{10}^{(1)}$ results from the positive frequency term whilst the resonant response for $\rho_{01}^{(1)}$ results from the negative frequency term. This is illustrated in the figure by the direction of the arrow for the photon involved in the interaction. From the density matrix elements the linear polarisation can be calculated directly by means of the trace operation

$$\begin{aligned} \mathbf{P}_{linear}(t) &= -e \int Trace(\mathbf{r}\rho^{(1)}) g(\mathbf{k}) d\mathbf{k} \\ &= -e \int (\mathbf{r}_{01}\rho_{10}^{(1)} + \mathbf{r}_{10}\rho_{01}^{(1)}) g(\mathbf{k}) d\mathbf{k} \end{aligned} \tag{4.9}$$

where $g(\mathbf{k})$ is the density of states function. The matrix elements may be written

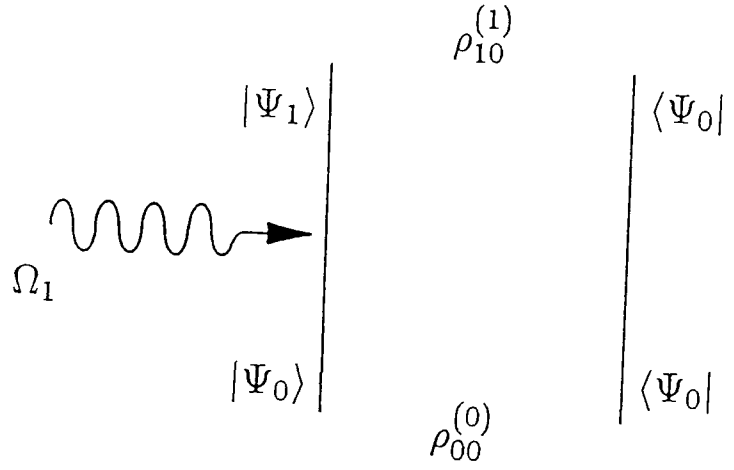

Figure 4.5a. Feynman diagram for the calculation of the first order density matrix element $\rho_{10}^{(1)}$.

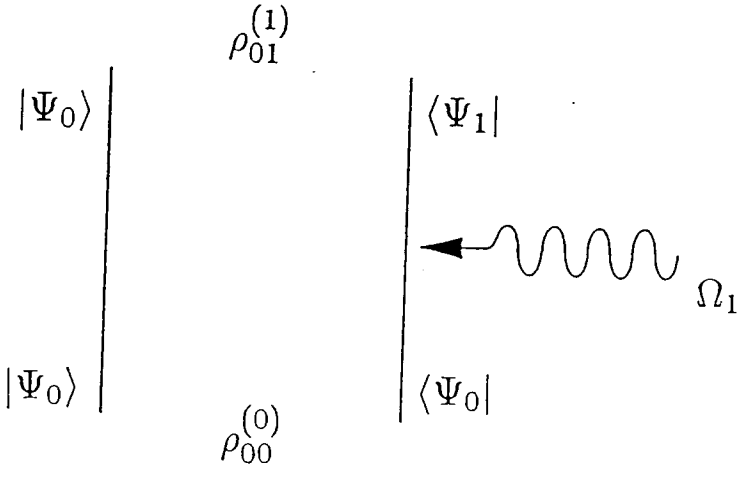

Figure 4.5b. Feynman diagram for the calculation of the first order density matrix element $\rho_{01}^{(1)}$.

directly from the diagrams in figure 4.5 as

$$\rho_{10}^{(1)}(t) = \overline{\rho_{01}^{(1)}}(t) = \frac{1}{i\hbar}\int_{t_0}^{t} H_{10}(t_1)\rho_{00}^{(0)}dt_1 \exp(-i\omega_{10}t) \tag{4.10}$$

where H_{10} is given by equation (4.4) or (4.5) and the bar denotes complex conjugation. Alternatively the linear current can be calculated as

$$\begin{aligned}\mathbf{J}_{linear}(t) &= -\frac{e}{m}\int Trace(\mathbf{p}\rho^{(1)})g(\mathbf{k})d\mathbf{k} \\ &= -\frac{e}{m}\int(\mathbf{p}_{01}\rho_{10}^{(1)} + \mathbf{p}_{10}\rho_{01}^{(1)})g(\mathbf{k})d\mathbf{k}\end{aligned} \tag{4.11}$$

where the plasma term is neglected as it provides only a non-resonant contribution. The linear polarisation may then be obtained as a time integral of the linear current.

Now consider the nonlinear terms, starting with those second order terms which describe the photogeneration of virtual carriers. Figure 4.6a shows the diagrams which relate to the generation of holes in the valence subband whilst figure 4.6b shows the diagrams for generation of electrons in the conduction subband. The density matrix elements $\rho_{00}^{(2)}$ and $\rho_{11}^{(2)}$ are given by the expressions

$$\begin{aligned}\rho_{00}^{(2)}(t) = -\rho_{11}^{(2)}(t) &= \frac{1}{(i\hbar)^2}\int_{t_0}^{t} H_{01}(t_2)\int_{t_0}^{t_2} H_{10}(t_1)\rho_{00}^{(0)}dt_1dt_2 \\ &+ \frac{1}{(i\hbar)^2}\int_{t_0}^{t} H_{10}(t_2)\int_{t_0}^{t_2} H_{01}(t_1)\rho_{00}^{(0)}dt_1dt_2\end{aligned} \tag{4.12}$$

Figure 4.7 shows the nonlinear response due to the polarisation of these carriers. Note the similarity of figures 4.7a and 4.7b to figure 4.5 which is attributable to the linear response being a polarisation of the equilibrium population whilst the

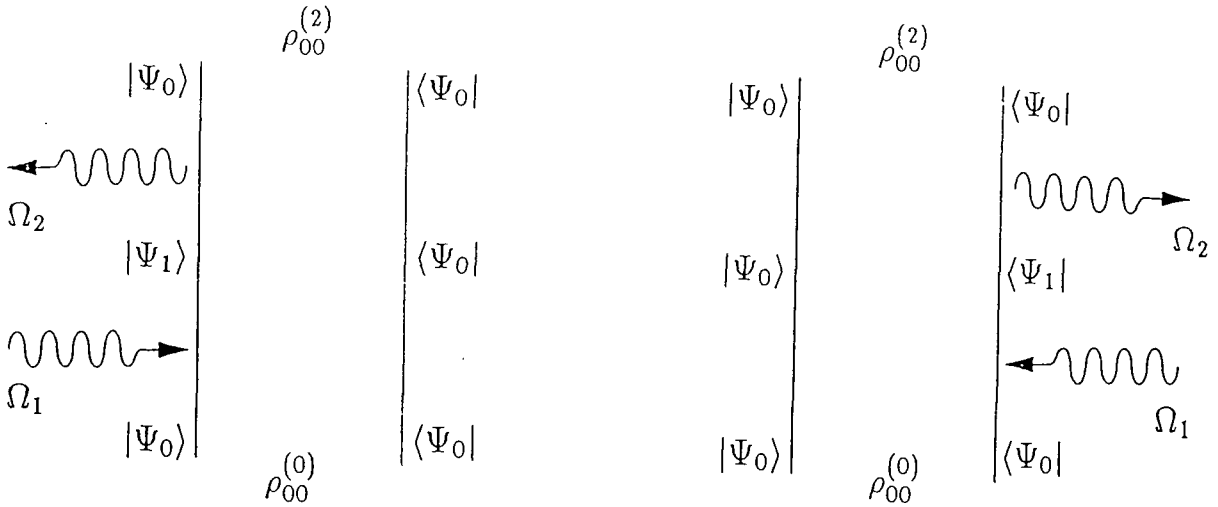

Figure 4.6a. Feynman diagrams for the calculation of the second order density matrix element $\rho_{00}^{(2)}$.

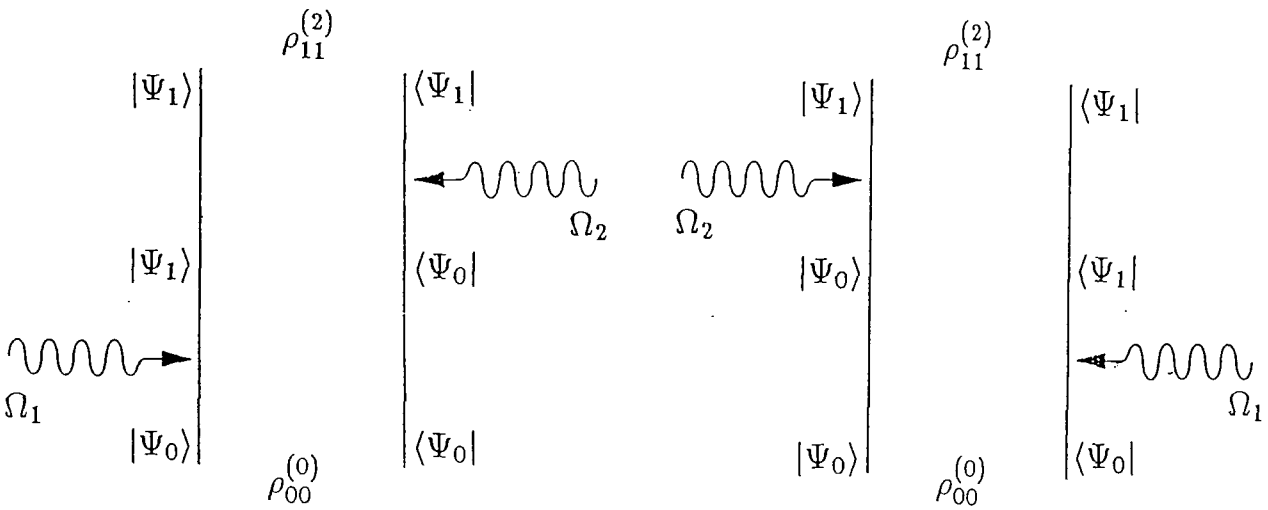

Figure 4.6b. Feynman diagrams for the calculation of the second order density matrix element $\rho_{11}^{(2)}$.

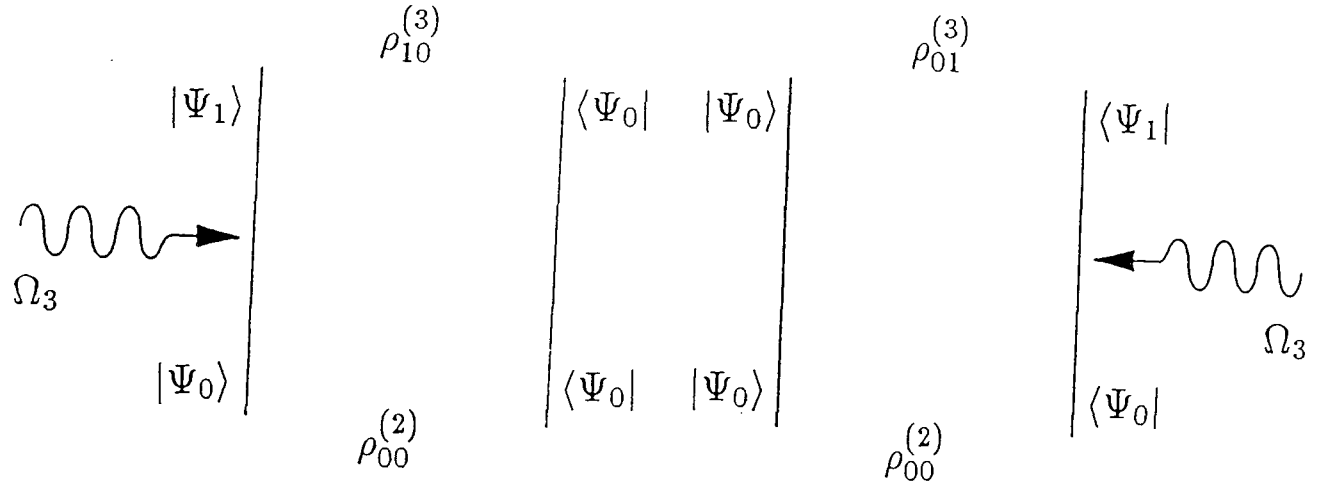

Figure 4.7a. Feynman diagrams for the calculation of the contribution to the third order density matrix elements $\rho_{10}^{(3)}$ and $\rho_{01}^{(3)}$ due to polarisation of photogenerated holes in the valence band.

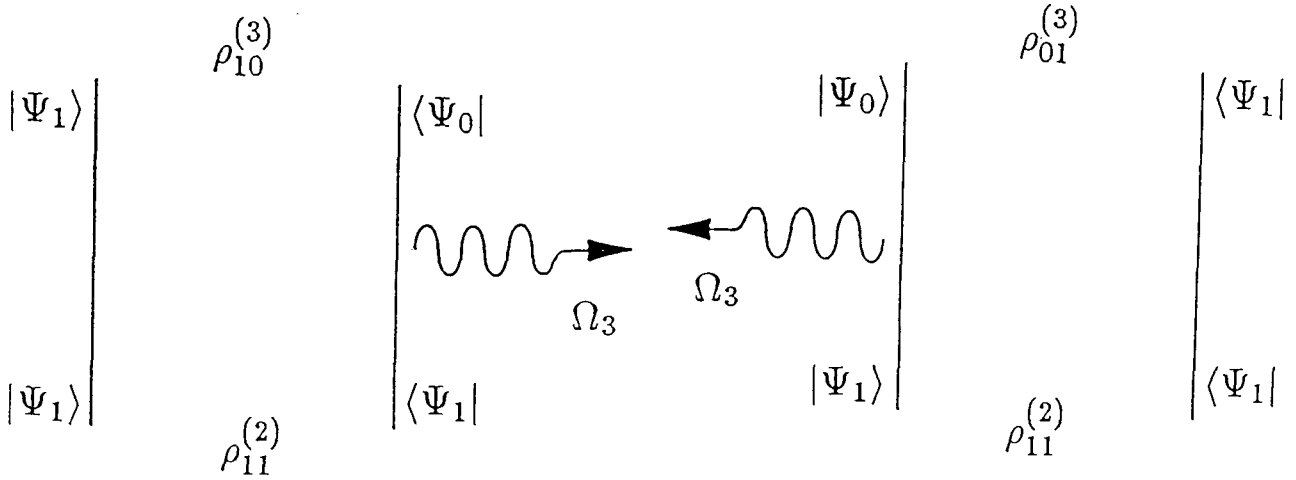

Figure 4.7b. Feynman diagrams for the calculation of the contribution to the third order density matrix elements $\rho_{10}^{(3)}$ and $\rho_{01}^{(3)}$ due to polarisation of photogenerated electrons in the conduction band.

nonlinear response is a polarisation of the photogenerated population. These diagrams give a nonlinear response in opposition to the linear response either because $\rho_{00}^{(2)}$ is **negative** after removal of electrons from the valence subband (figure 4.7a), or because the polarisation prepares for a **downward** transition from the conduction subband to the valence subband (figure 4.7b). The third-order nonlinear polarisation is given by

$$\mathbf{P}_{nonlinear}(t) = -e \int (\mathbf{r}_{01}\rho_{10}^{(3)} + \mathbf{r}_{10}\rho_{01}^{(3)}) g(\mathbf{k}) d\mathbf{k} \tag{4.13}$$

or may be obtained from time integration of the nonlinear current

$$\mathbf{J}_{nonlinear}(t) = -\frac{e}{m} \int (\mathbf{p}_{01}\rho_{10}^{(3)} + \mathbf{p}_{10}\rho_{01}^{(3)}) g(\mathbf{k}) d\mathbf{k} \tag{4.14}$$

The third-order matrix elements are

$$\rho_{10}^{(3)}(t) = \overline{\rho_{01}^{(3)}}(t) = \frac{2}{i\hbar} \int_{t_0}^{t} H_{10}(t_3)\rho_{00}^{(2)}(t_3) dt_3 \exp(-i\omega_{10}t) \tag{4.15}$$

which may be written directly from figure 4.7.

Section 4.4. Optical Stark shift description of the optical interaction.

An alternative point of view is provided by the concept of dressed states [30,31]. Instead of considering the electromagnetic interaction as producing a change in the occupancy of the 'bare' electronic states Ψ_0 and Ψ_1, it can be regarded as producing a set of 'dressed' states of the quantum well. These are states of the combined system of semiconductor and electromagnetic radiation, whose electronic parts are mixtures of the bare states. The shift in transition energy when bare states are replaced by dressed states is termed the optical Stark shift [31-36]. The energy shift provides an alternative (but equivalent) description of the nonlinear polarisation to that provided by the state filling mechanism described in the previous sections. The connection between the two descriptions is further discussed by Burt [37].

The dressed states may be assigned a 'quasi-energy' which depends on the magnitude of the optical electric field. With zero applied electric field the energy levels E_0 and E_1 are replicated at energy steps determined by the photon energy E_p to form a pair of energy ladders $E_0 + nE_p$ and $E_1 + nE_p$ for $n = 0, \pm 1, \pm 2, \ldots$ shown in figure 4.8a. When the energy separation $E_g = E_1 - E_0$ is near to the photon energy, this brings pairs of energy levels (one from each ladder) into close proximity. As the magnitude of the applied electric field is increased from zero, this proximity of energy levels results in a splitting of the levels and produces the Stark shift illustrated in figure 4.8b. To calculate these energy shifts [38-40], suppose that the Hamiltonian $H_S = H_0 + H_I$ of the interacting system is periodic

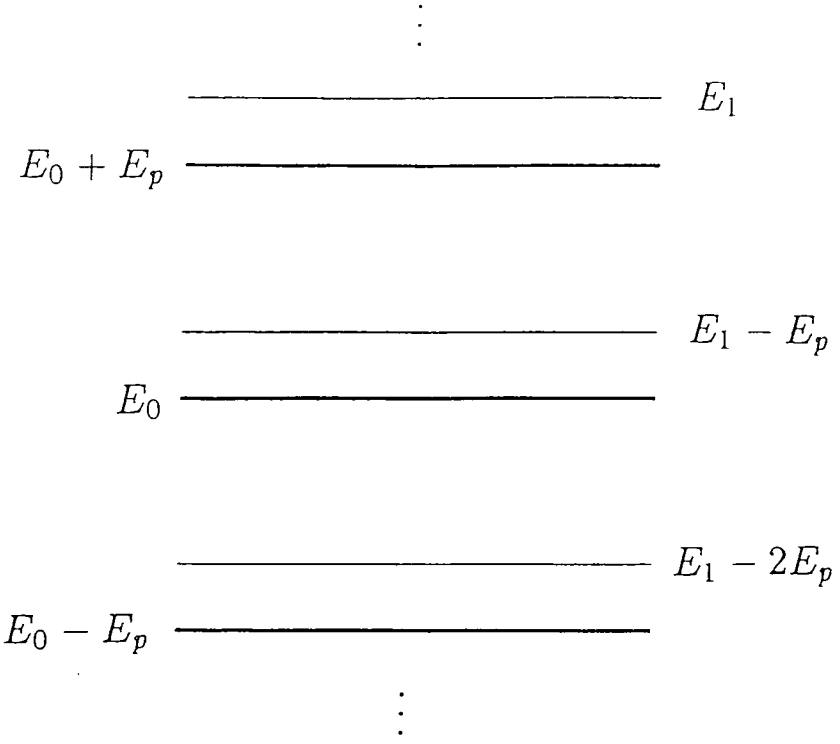

Figure 4.8a. Energy ladders $E_0 + nE_p$ and $E_1 + nE_p$ showing quasi-energies of the dressed states at zero electric field.

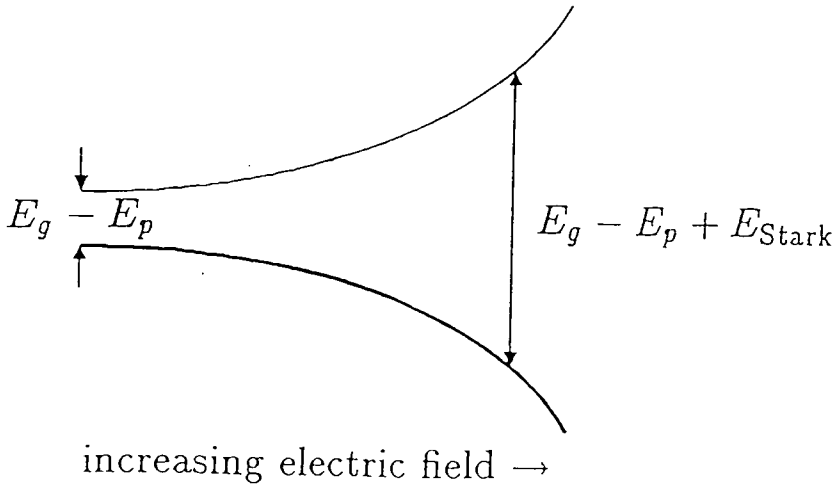

Figure 4.8b. Splitting of a pair of adjacent quasi-energy levels as the electric field is increased from zero.

in time with period $T = 2\pi/\omega_p$ but otherwise does not vary in time (i.e. there is no pulse envelope). Then the matrix elements of H_S over the basis of time-independent states $\{\Psi_n\}$ defined in equation (4.1) are $H_{nm} = \langle\Psi_n|H_S|\Psi_m\rangle$ and these may be expanded as a Fourier series

$$H_{nm} = \sum_r H_{nm}^{(r)} \mathrm{e}^{ir\omega_p t} \tag{4.16}$$

Further, the theorem of Floquet states that an eigenvector Ψ of H_S may be written as

$$\Psi = \mathrm{e}^{-iqt}\Phi \tag{4.17}$$

where Φ is periodic in time with period $T = 2\pi/\omega_p$ and q is a constant determined uniquely modulo ω_p. This is closely related to the theorem of Bloch where the periodicity occurs in space rather than in time. Hence, expanding Φ as a Fourier series

$$\langle\Psi_n|\Psi\rangle = \sum_r \Phi_n^{(r)} \mathrm{e}^{ir\omega_p t}\mathrm{e}^{-iqt} \tag{4.18}$$

and equating coefficients of $\exp(ir\omega_p t)$ in the time-dependent Schrödinger equation

$$H_S\Psi = i\hbar\frac{\partial\Psi}{\partial t} \tag{4.19}$$

gives

$$\sum_{s,m}\left[H_{nm}^{(r-s)} + r\hbar\omega_p\delta_{rs}\delta_{nm}\right]\Phi_m^{(s)} = \hbar q\Phi_n^{(r)} \tag{4.20}$$

which may be written as

$$\sum_{(sm)} M_{(rn)(sm)}\hat{\Phi}_{(sm)} = E_q\hat{\Phi}_{(rn)} \tag{4.21}$$

so that E_q is the eigenvalue of the eigenvector $\hat{\Phi}$, and is known as the quasi-energy of the Floquet state. For the two-level system the matrix M may be written as

$$M = \begin{bmatrix} \ddots & & & \vdots & & & & \\ & E_0 - E_p & 0 & 0 & H_{01} & 0 & 0 & \\ & 0 & E_1 - E_p & H_{10} & 0 & 0 & 0 & \\ & 0 & H_{01} & E_0 & 0 & 0 & H_{01} & \\ \cdots & H_{10} & 0 & 0 & E_1 & H_{10} & 0 & \cdots \\ & 0 & 0 & 0 & H_{01} & E_0 + E_p & 0 & \\ & 0 & 0 & H_{10} & 0 & 0 & E_1 + E_p & \\ & & & \vdots & & & & \ddots \end{bmatrix} \tag{4.22}$$

where $H_{10} = \overline{H_{01}} = \langle \Psi_1 | H_I(\pm\omega_p) | \Psi_0 \rangle$ are the frequency components of the interaction terms. Now referring to figure 4.8 and concentrating on the interaction of a single pair of levels in close proximity, the matrix M may be truncated to

$$M = \begin{bmatrix} E_1 - E_p & H_{10} \\ H_{01} & E_0 \end{bmatrix} \tag{4.23}$$

and the eigenvalue problem $\det(M - E_q I) = 0$ solved to obtain

$$E_q = E_0 - \frac{\Delta}{2} \pm \left[\left(\frac{\Delta}{2} \right)^2 + |H_{10}|^2 \right]^{1/2} \tag{4.24}$$

where $\Delta = E_p - E_g$ is the detuning and $\Delta < 0$ in this case. For zero field $|H_{10}| = 0$ and $E_q = E_0$ or $E_q = E_0 - \Delta$ which are the unshifted energy levels. And for low fields with $|H_{10}| \ll |\Delta|$ then

$$E_q = E_0 + \frac{|H_{10}|^2}{\Delta} \tag{4.25}$$

or

$$E_q = E_0 - \Delta - \frac{|H_{10}|^2}{\Delta} \tag{4.26}$$

so that the energy levels split as shown in figure 4.8b and the Stark shift is

$$E_{\text{Stark}} = \frac{2|H_{10}|^2}{E_g - E_p} \tag{4.27}$$

Now returning to the case of pulsed illumination, if the pulse envelope does not vary too rapidly (such that $\hbar/\tau \ll E_g - E_p$) then the response is adiabatic and the quasi-energies calculated for the continuous-wave case are valid. Figure 4.9 shows how the curve of quasi-energies is traced out as the pulse amplitude increases and then is retraced as the pulse amplitude decreases back from its maximum to zero. There is a similar adiabatic evolution of the dressed wavefunctions as the illumination is pulsed on and off. Initially the dressed state comprises just the ground electronic state, but as the dressed state evolves a contribution of the excited electronic state is introduced during the pulse, and then finally after the pulse is ended the dressed state returns to its original composition with just the ground electronic state present. This provides an alternative way to view the processes described in section 4.2, where mixing of the bare electronic states here corresponds to variation of the electronic components of the adiabatically changing dressed state.

However, this approach also allows consideration of effects which occur for very high illumination levels. As the amplitude of the electric field is increased it is necessary to return to the large matrix M of equation (4.21) and solve the eigenvalue problem $\det(M - E_q I) = 0$ numerically. The results for an example three-level system are shown in figure 4.10a where $\omega_{10} = 10\omega_{21} = 1.1\omega_p = 10^{15}\mathrm{s}^{-1}$ and the matrix elements of the interaction Hamiltonian are related by $H_{10} = H_{20} = 10H_{21}$. From the figure it is clear that the quasi-energies are periodic in

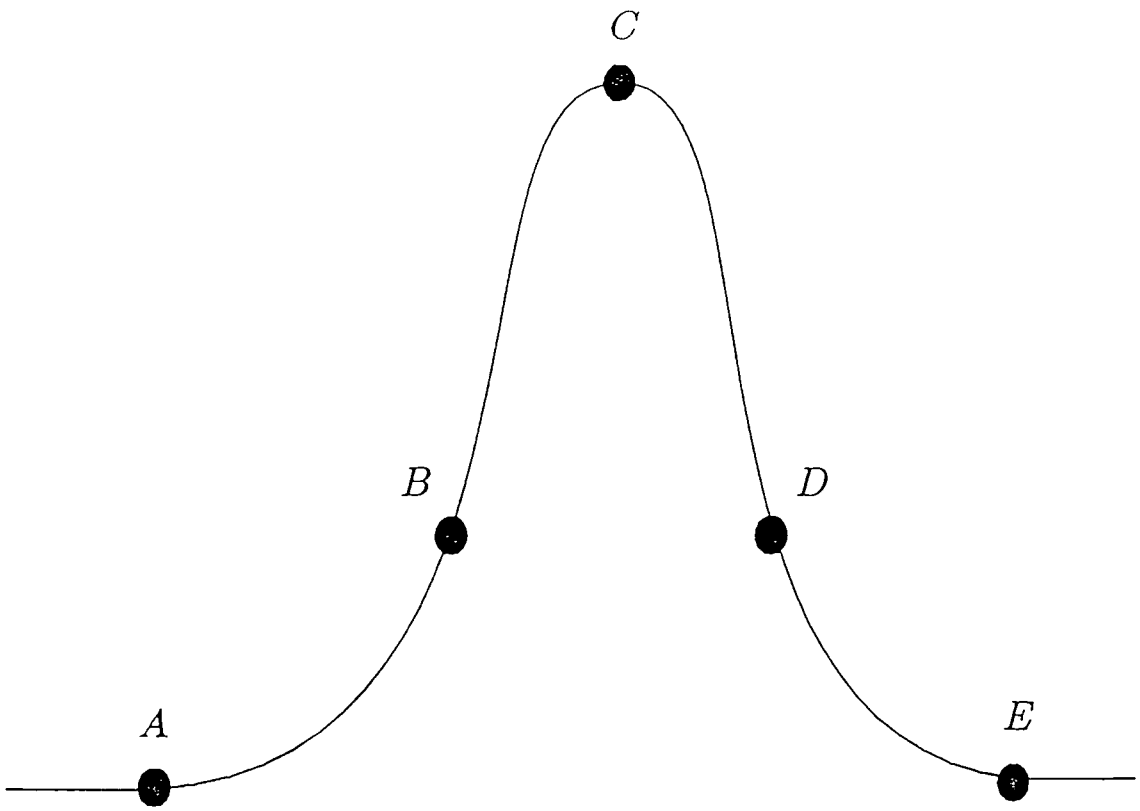

Figure 4.9a. Variation in time of the electric field amplitude as the light is pulsed on and off.

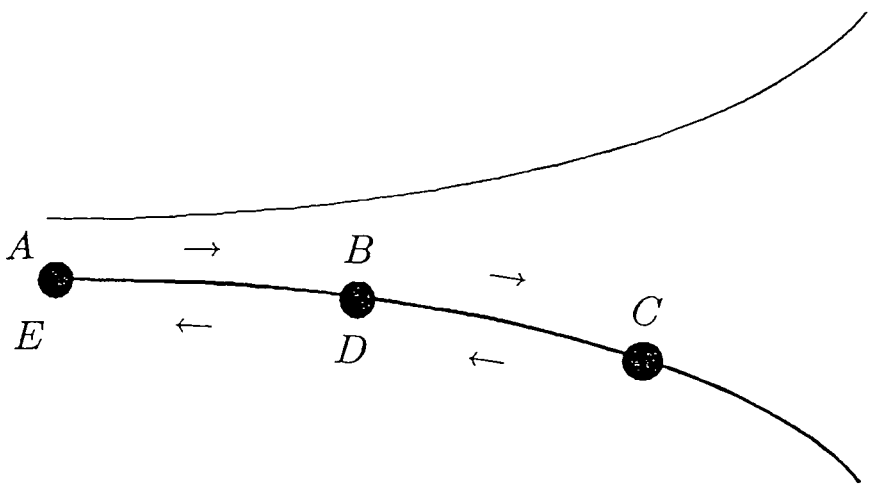

Figure 4.9b. Variation in time of the quasi-energy of the dressed state of the system (points A-E correspond to figure 9a).

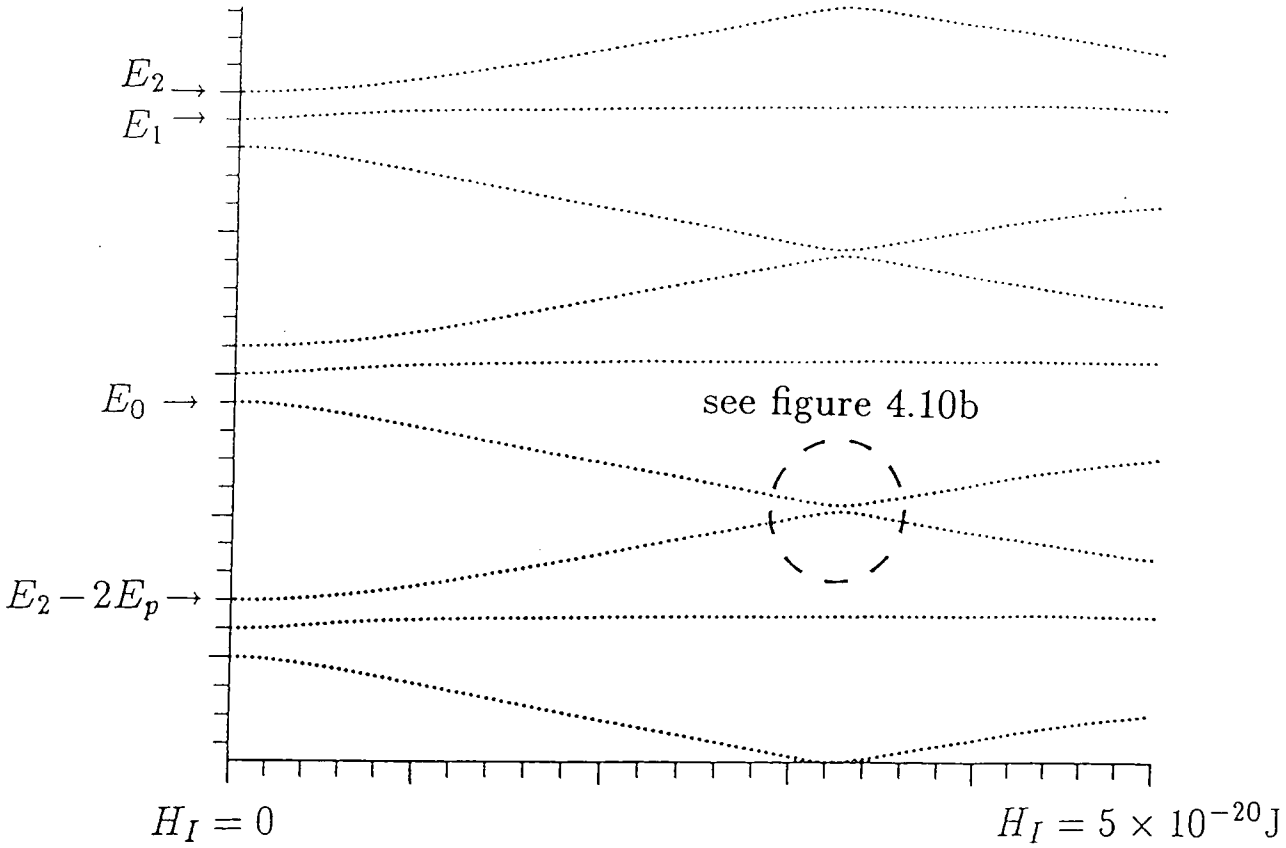

Figure 4.10a. Quasi-energy plot for three-level system with $\omega_{10} = 10\omega_{21} = 10^{15}\mathrm{s}^{-1}$ and $\omega_p = 0.9\,\omega_{10}$ for a range of values of the interaction Hamiltonian $H_I = H_{10} = H_{20} = 10H_{21}$.

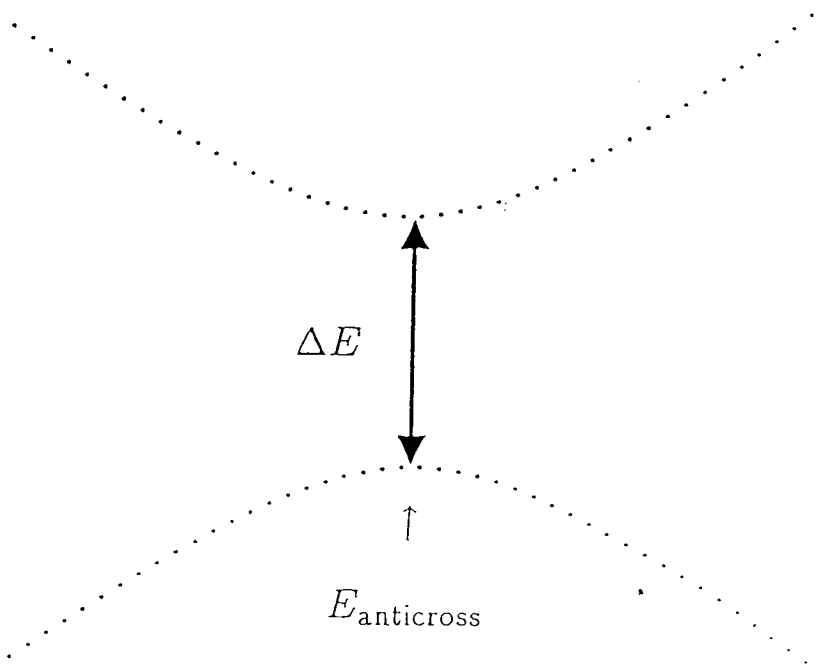

Figure 4.10b. Magnified view of anticrossing region taken from figure 4.10a.

energy with period equal to the photon energy E_p. Also for larger electric fields the quasi-energy curves anticross at certain values of the electric field $E_{\text{anticross}}$ as shown in figure 4.10b. In this case the anticrossing occurs between quasi-energy curves which for zero optical interaction relate to the ground state Ψ_0 and to the second excited state Ψ_2. If the amplitude of the pulse is varied slowly through one of these anticrossing regions then the adiabatic approximation still holds [41-45]. Indeed it continues to hold as long as $\hbar/\tau \ll \Delta E$ where ΔE is the energy gap between the two quasi-energy curves shown in figure 4.10b. The reponse at low fields is just a special case where $\Delta E = E_g - E_p$ is the difference between the excitation energy of the material system and the photon energy. However, if the electric field amplitude varies rapidly through the anticrossing region then the wavefunction continues as a mixture of the two dressed states which correspond to the two anticrossing quasi-energy curves [41-45]. There is a similar effect when the electric field amplitude decreases back through the anticrossing region, at which point the (Berry) phases of the two parts depend on the behaviour of the amplitude in the intervening period. When the electric field amplitude finally returns to zero the wavefunction has consequently been split into two parts. One of these parts corresponds to the ground state (as for the virtual carrier case) but the other part corresponds to an excited state. Hence there is some probability of making a transition from the ground state to an excited state even though the photon energy is less than the energy gap between the two states. Figure 4.11 depicts

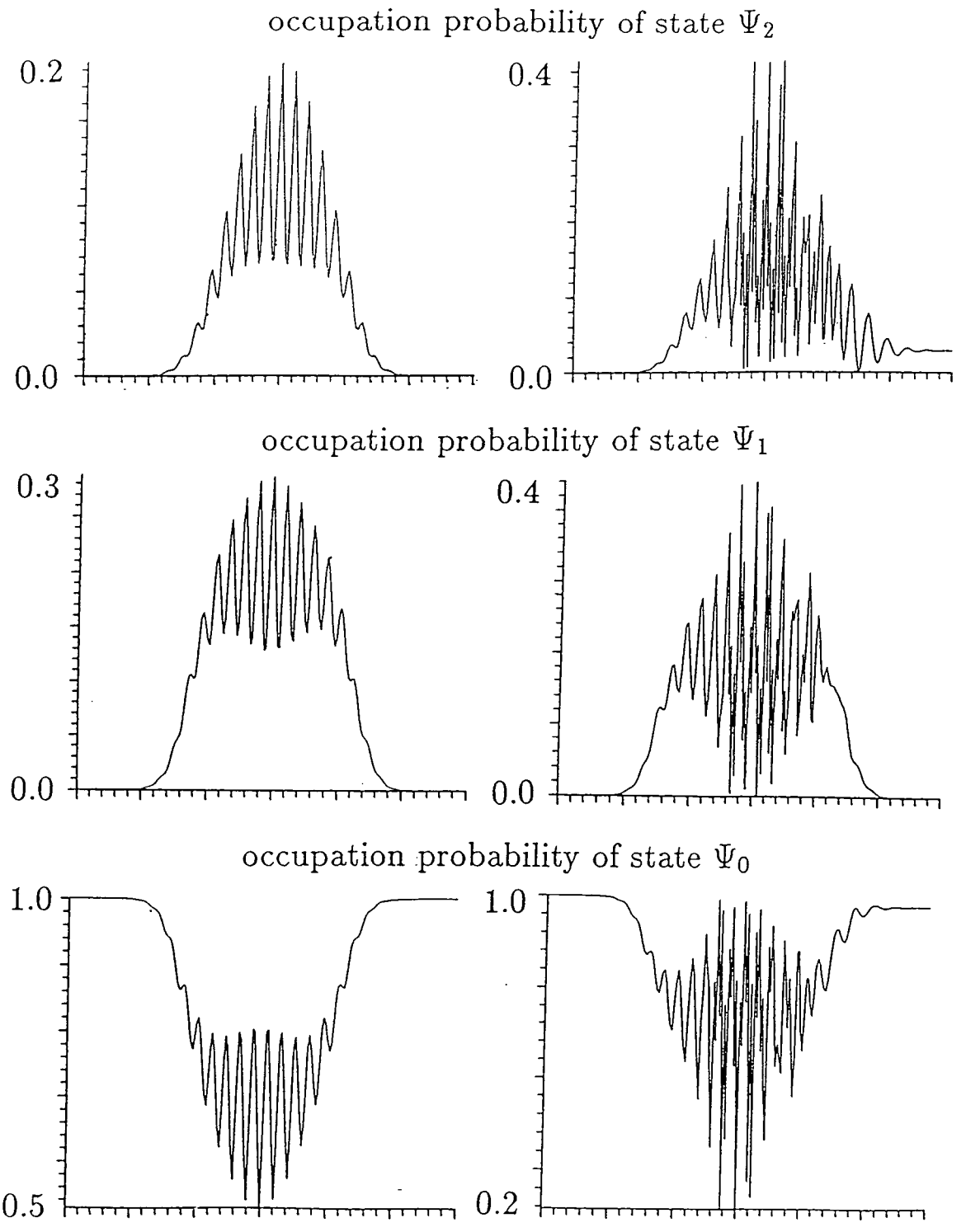

Figure 4.11. Occupation probabilities ρ_{00}, ρ_{11} and ρ_{22} of the three-level system as a function of time showing the two cases $E_{\max} < E_{\text{anticross}}$ (left) and $E_{\max} > E_{\text{anticross}}$ (right).

the response of the example system of figure 4.10 to an optical pulse with peak electric field $E_{\max}$ and rapidly changing envelope. The figure shows the occupation probabilities of the three states Ψ_0, Ψ_1 and Ψ_2 as they vary in time subject to the optical excitation for the two cases $E_{\max} < E_{\text{anticross}}$ and $E_{\max} > E_{\text{anticross}}$. The critical value $E_{\text{anticross}}$ is defined as the electric field amplitude at which the anticrossing occurs in figure 4.10. As noted above the anticrossing occurs between quasi-energy curves which at zero optical interaction correspond to the states Ψ_0 and Ψ_2, so that in the case $E_{\max} > E_{\text{anticross}}$ there is a residual occupation of the excited state Ψ_2 (and not Ψ_1).

Section 4.5. Enhancement of optical nonlinearity.

It has recently been suggested [25-29] that the bandstructure of a quantum well may be engineered to provide a second conduction subband which will contribute resonantly to the nonlinear susceptibility and consequently enhance the nonlinear response. So suppose that as for the two subband system the energy dispersion of the subbands is given by

$$E_n(\mathbf{k}) = E_n(0) + \frac{\hbar^2 k^2}{2m_n^*} \tag{4.28}$$

for $n = 0, 1, 2$. The proposal is to ensure that the principal energy gap $E_2(0) - E_1(0)$ between the upper and lower conduction subbands is equal to the principal energy gap $E_1(0) - E_0(0)$ between the lower conduction subband and valence subband. As with the two band system it is possible to consider each point in the Brillouin zone separately and restrict attention to the subsystem of three states, one from each subband, at a given value of electronic wavevector $\mathbf{k}$. However, due to the curvature of the bands, the energy separations of the two states are equal only at the Brillouin zone centre.

Suppose that the subsystem is somehow arranged with the electron placed in the lower conduction state. The presence of the upper conduction state allows polarisation of the system in preparation for an upward transition between the conduction states as shown in figure 4.12a, and results in an induced dipole moment p'. Thus the introduction of the upper conduction state permits an extra contribution to the **nonlinear** response because the optically generated popula-

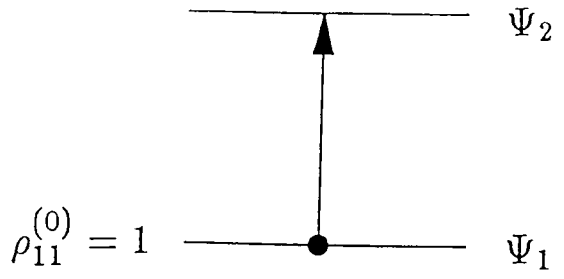

Figure 4.12a. Polarisation of the initial lower conduction state population across the transition between conduction subbands resulting in an induced dipole moment p'.

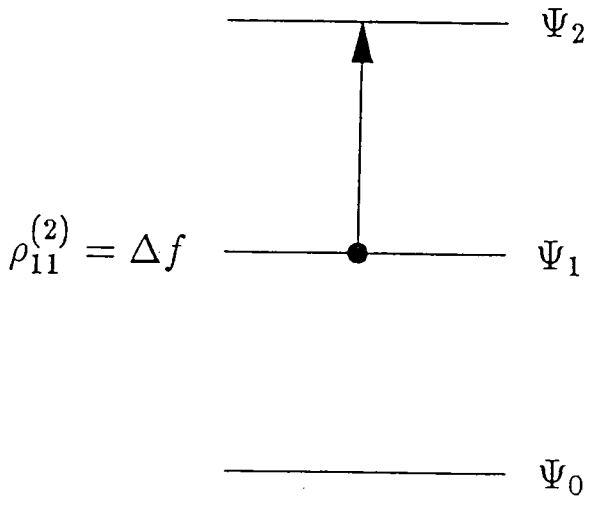

Figure 4.12b. Polarisation of the photogenerated population across the transition between conduction subbands resulting in a change in induced dipole moment $p'\Delta f$.

tion in the lower conduction state may be polarised in preparation for an upward transition to the upper conduction state, as depicted in figure 4.12b. This leads to a simple physical picture for the nonlinear response. As previously discussed there is the reduction in polarisation across the lower transition due to the production of electron-hole pairs, but this is opposed by polarisation of the optically generated population across the upper transition and the presence of the third level actually reduces the nonlinear response from $-2p\Delta f$ to $-(2p-p')\Delta f$.

The relevant Feynman diagrams are shown in figure 4.13. They result in a nonlinear response which is very like the linear response in figure 4.5 except that it arises from polarisation of the photogenerated population across the upper transition instead of polarisation of the equilibrium population across the lower transition. The additional nonlinear polarisation corresponding to these diagrams is

$$\mathbf{P}_{\text{nonlinear}}(t) = -e\int(\mathbf{r}_{12}\rho_{21}^{(3)} + \mathbf{r}_{21}\rho_{12}^{(3)})g(\mathbf{k})d\mathbf{k} \tag{4.29}$$

or may be calculated from the nonlinear current

$$\mathbf{J}_{\text{nonlinear}}(t) = -\frac{e}{m}\int(\mathbf{p}_{12}\rho_{21}^{(3)} + \mathbf{p}_{21}\rho_{12}^{(3)})g(\mathbf{k})d\mathbf{k} \tag{4.30}$$

where

$$\rho_{21}^{(3)}(t) = \overline{\rho_{12}^{(3)}}(t) = \frac{1}{i\hbar}\int_{t_0}^{t} H_{21}(t_3)\rho_{11}^{(2)}(t_3)dt_3\exp(-i\omega_{21}t) \tag{4.31}$$

and $\rho_{11}^{(2)}(t)$ is given by equation (4.12).

As well as providing an additional way to polarise the photogenerated carriers

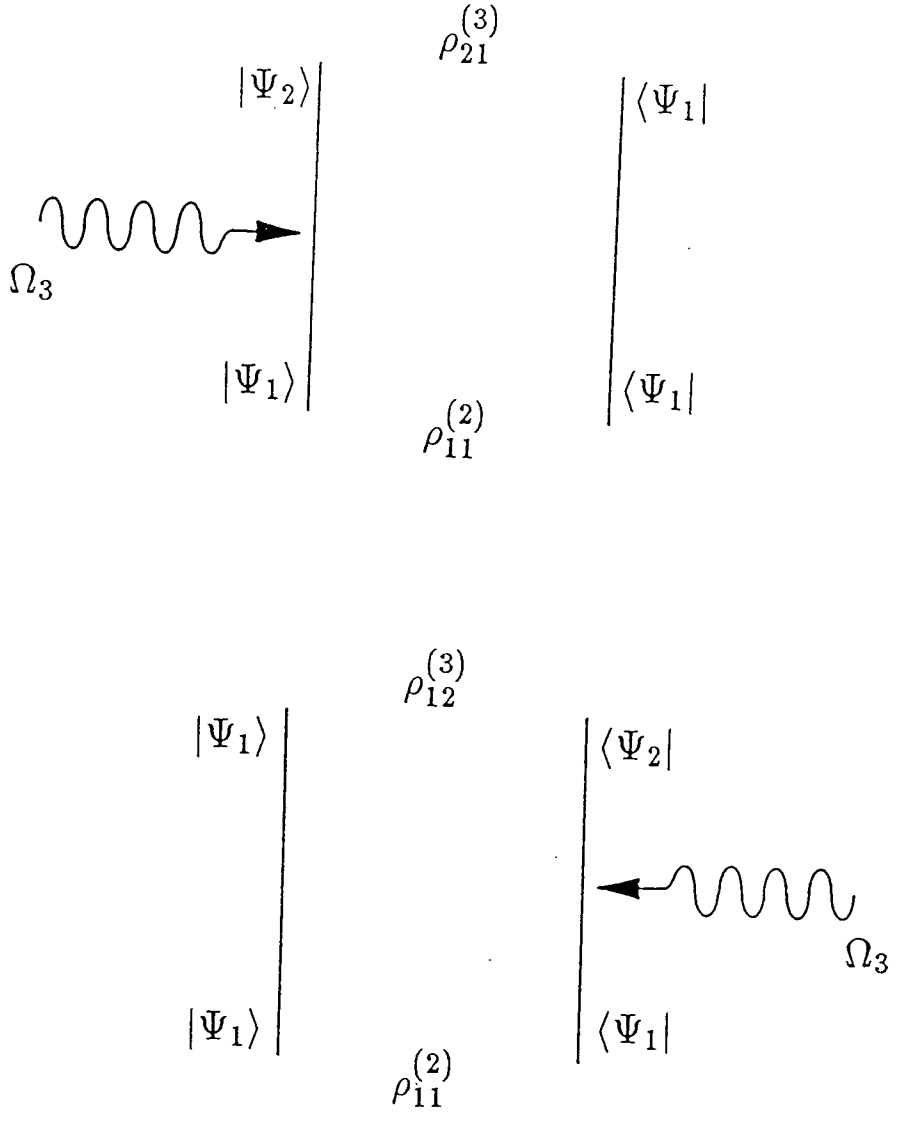

Figure 4.13. Feynman diagrams for the calculation of the contribution to the third order density matrix elements $\rho_{21}^{(3)}$ and $\rho_{12}^{(3)}$ due to polarisation of the photogenerated population $\rho_{11}^{(2)}$ across the transition between conduction subbands.

in the lower conduction state, the presence of the upper conduction state also permits second-order mixing to occur. The linear response of the system consists of a polarisation (shown in figure 4.14a) which prepares for an upward transition from the valence state to the lower conduction state. However, instead of making this transition the system can move from participation in a one-photon interaction to participation in a two-photon interaction as shown in figure 4.14b. In the linear case the electromagnetic field introduces an admixture of the lower conduction state via a one-photon interaction, whereas in the nonlinear case the electromagnetic field introduces an admixture of the upper conduction state via a two-photon interaction. The existence of the lower conduction state makes this two-photon process possible (by providing allowed transitions) and its midway position enhances the interaction. The two-photon process prepares for the movement of an electron directly from the valence state to the upper conduction state by the process of two-photon absorption. This should be contrasted with the fourth-order term derived from figure 4.12b where the electron is moved from the valence state to the upper conduction state via the lower conduction state in a series of two one-photon absorptions. The nonlinear polarisation which results from the second-order mixing consists of two terms shown in figures 4.15a and 4.15b. The corresponding nonlinear polarisation is given directly by

$$\mathbf{P}_{nonlinear}(t) = -e \int (\mathbf{r}_{01}\rho_{10}^{(3)} + \mathbf{r}_{10}\rho_{01}^{(3)} + \mathbf{r}_{12}\rho_{21}^{(3)} + \mathbf{r}_{21}\rho_{12}^{(3)}) g(\mathbf{k}) d\mathbf{k} \qquad (4.32)$$

or it may be calculated from the nonlinear current.

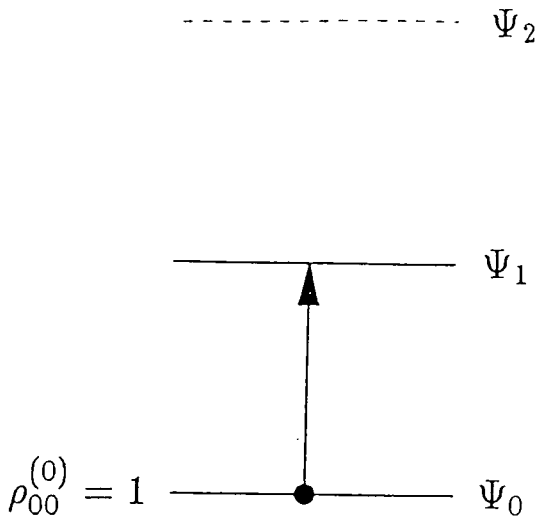

Figure 4.14a. One-photon interaction which introduces an admixture of the lower conduction state to the initial valence state wavefunction.

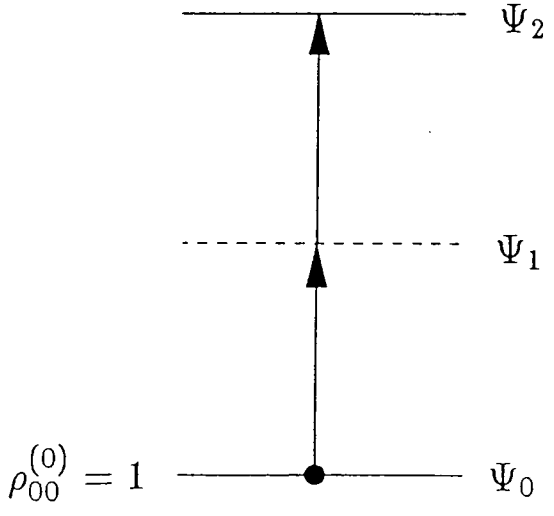

Figure 4.14b. Two-photon interaction which introduces an admixture of the upper conduction state to the initial valence state wavefunction.

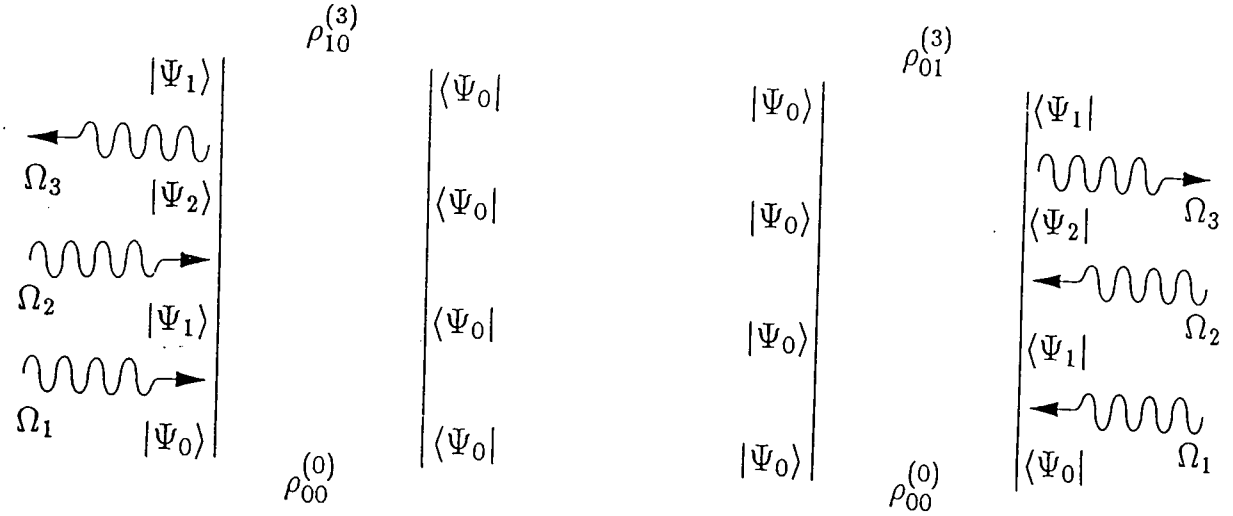

Figure 4.15a. Feynman diagrams for the calculation of the contribution to the third order density matrix elements $\rho_{10}^{(3)}$ and $\rho_{01}^{(3)}$ due to second-order mixing.

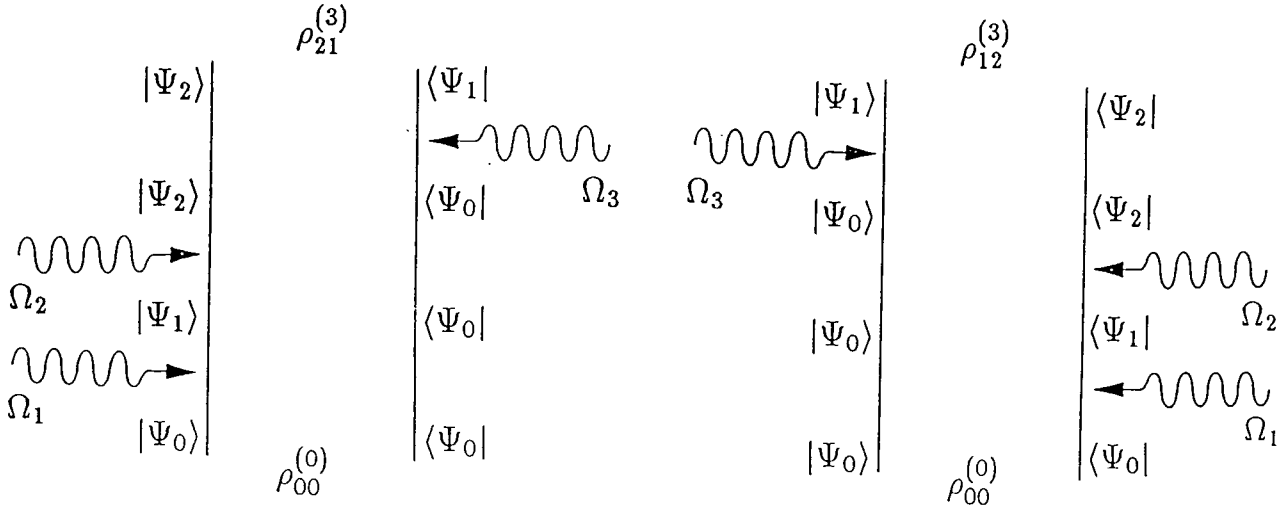

Figure 4.15b. Feynman diagrams for the calculation of the contribution to the third order density matrix elements $\rho_{21}^{(3)}$ and $\rho_{12}^{(3)}$ due to second-order mixing.

The nonlinear current is

$$\mathbf{J}_{nonlinear}(t) = -\frac{e}{m}\int (\mathbf{p}_{01}\rho_{10}^{(3)} + \mathbf{p}_{10}\rho_{01}^{(3)} + \mathbf{p}_{12}\rho_{21}^{(3)} + \mathbf{p}_{21}\rho_{12}^{(3)})g(\mathbf{k})d\mathbf{k} \tag{4.33}$$

and in equations (4.32) and (4.33) the density matrix elements are

$$\rho_{10}^{(3)}(t) = \overline{\rho_{01}^{(3)}}(t) = \frac{1}{(i\hbar)^3}\int_{t_0}^{t} H_{12}(t_3)\int_{t_0}^{t_3} H_{21}(t_2)\int_{t_0}^{t_2} H_{10}(t_1)\rho_{00}^{(0)}dt_1dt_2dt_3\exp(-i\omega_{10}t) \tag{4.34}$$

and

$$\rho_{21}^{(3)}(t) = \overline{\rho_{12}^{(3)}}(t) = -\frac{1}{(i\hbar)^3}\int_{t_0}^{t} H_{01}(t_3)\int_{t_0}^{t_3} H_{21}(t_2)\int_{t_0}^{t_2} H_{10}(t_1)\rho_{00}^{(0)}dt_1dt_2dt_3\exp(-i\omega_{21}t) \tag{4.35}$$

The contributions from equations (4.34) and (4.35) tend to cancel so that the second-order mixing makes only a small contribution to the nonlinear polarisation. Indeed for $\omega_{21} = \omega_{10}$ (as at the Brillouin zone centre) the two contributions cancel exactly regardless of the dipole matrix elements for the two transitions. The nonlinear polarisation is separated into the three terms corresponding to equations (4.13), (4.29) and (4.32). The real part of the frequency spectrum for each of these terms is shown in figures 4.16a-4.16c respectively where it has been assumed that the electromagnetic interaction terms for the two transitions are equal. The electron effective masses are taken to be $m_0^* = -0.5m$ and $m_1^* = m_2^* = 0.05m$, the pulse time constant is $\tau = 100$fs and the transition frequencies are $\omega_{21} = \omega_{10} = 1.1\,\omega_p = 10^{15}\mathrm{s}^{-1}$. Figure 4.16a shows the only nonlinear polarisation present without the upper conduction subband, figure 4.16b shows

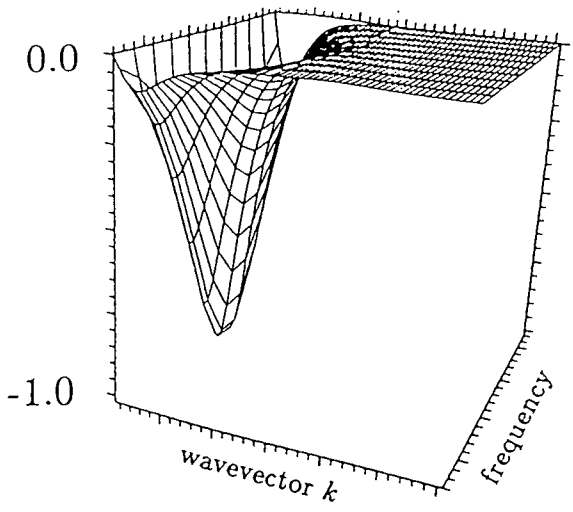

Figure 4.16a. Frequency domain response showing nonlinear polarisation of virtual carriers across the lower transition.

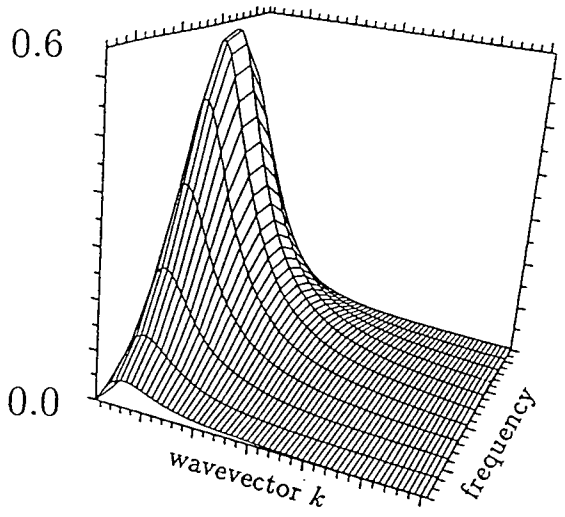

Figure 4.16b. Frequency domain response showing nonlinear polarisation of virtual carriers across the upper transition.

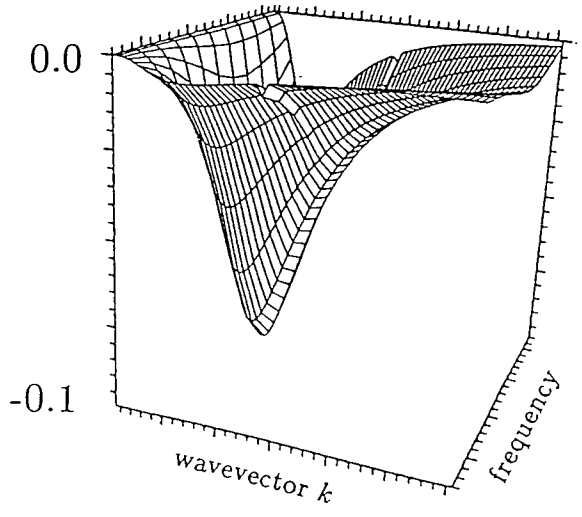

Figure 4.16c. Frequency domain response showing nonlinear polarisation due to second-order mixing.

polarisation of the virtual carriers across the upper transition, and figure 4.16c shows the nonlinear polarisation arising from second-order mixing. The results are given in units normalised so that the peak response in the two band case is -1.0 units. Although the introduction of the upper conduction subband produces additional contributions to the nonlinear polarisation, figure 4.16 clearly shows that for a plane-polarised electric field it does not enhance the nonlinear properties of the device. As noted above the contribution due to second-order mixing is small despite variation in the detuning energy across the Brillouin zone, and the polarisation of the virtual carriers across the upper transition serves only to oppose the nonlinear polarisation already present.

However, it may be possible to utilise the additional flexibility provided by the third band by, for example, the use of unequal energy separations at the Brillouin zone centre. If second-order mixing is ignored the following results (derived in chapter five) for the low-intensity adiabatic response are applicable here

$$\rho_{11}^{(2)} = -\rho_{00}^{(2)} = \frac{1}{2} - \frac{1}{2}\left[1 + \left(\frac{\beta_{10}}{\Delta_{10}}\right)^2\right]^{-1/2} \simeq \left(\frac{\beta_{10}}{2\Delta_{10}}\right)^2 \tag{4.36}$$

$$\rho_{22}^{(2)} = 0 \tag{4.37}$$

$$\rho_{10}^{(3)} = \left(\frac{\beta_{10}}{2\Delta_{10}}\right)(\rho_{00}^{(2)} - \rho_{11}^{(2)})\exp(-i\omega_p t) = -2\left(\frac{\beta_{10}}{2\Delta_{10}}\right)\rho_{11}^{(2)}\exp(-i\omega_p t) \tag{4.38}$$

$$\rho_{21}^{(3)} = \left(\frac{\beta_{21}}{2\Delta_{21}}\right)(\rho_{11}^{(2)} - \rho_{22}^{(2)})\exp(-i\omega_p t) = \left(\frac{\beta_{21}}{2\Delta_{21}}\right)\rho_{11}^{(2)}\exp(-i\omega_p t) \tag{4.39}$$

where $\Delta_{nm} = \omega_p - \omega_{nm}$ and

$$\beta_{nm} = (e/\hbar)\mathbf{E}_0.\mathbf{r}_{nm}\exp(-t^2/\tau^2) \tag{4.40}$$

or

$$\beta_{nm} = (e/\hbar m)\mathbf{A}_0.\mathbf{p}_{nm}\exp(-t^2/\tau^2) \tag{4.41}$$

is the Rabi frequency. Hence making Δ_{21} positive (whilst keeping Δ_{10} negative) should provide an enhancement of the nonlinear response, certainly for a three-level system. In a quantum well, where there is energy dispersion, the problem is absorption, but it may be possible to make Δ_{10} negative, Δ_{21} positive and still avoid absorption provided that $\omega_{20} > 2\omega_p$.

Alternatively, a number of light beams oriented in different directions may be employed and several studies have been performed for this situation by Jaros and co-workers [26,29,95-96]. In these studies the influence of the bandstructure on the optical matrix elements is important and chapter six briefly considers such effects.

CHAPTER FIVE

On-resonance phenomena

In this chapter on-resonance optical phenomena are considered with particular emphasis on modelling the optical response of semiconductor laser amplifiers. Recent experimental investigations [46-53] have indicated that such devices are capable of providing a large nonlinear refractive index and if suitably biased they can also provide recovery times on the order of picoseconds. The model must include a description of on-resonance excitation where the photon energy coincides with an allowed transition of the semiconductor material. The assumptions made in previous chapters which allowed a perturbative approach to be adopted are not applicable here and it is necessary to return to the exact Liouville equation and make a different set of simplifying assumptions. The first section of the chapter introduces the formalism required to describe resonant transitions in a two-level system. The bandstructure of the semiconductor material is modelled as a collection of two-level systems. Next follows a consideration of thermal effects as these can no longer be neglected when illumination occurs in the absorption band of a semiconductor. Finally, the newly discussed techniques are applied to a description of the laser amplifier and a comparison is made with experimental results.

The laser amplifier possesses a nonlinear response which is generally greater than that provided by the off-resonance mechanism of virtual carriers, and despite relatively long recovery times it is nonetheless of considerable practical interest for the design of fast all-optical switching devices.

Section 5.1. The Bloch equations and Rabi frequency.

In this section the Liouville equation is taken as the starting point for the derivation of the Bloch equations [4] which describe the state occupation probability and electronic polarisation of a two-level system subject to on-resonance optical excitation. The Liouville equation in the Schrödinger picture is

$$i\hbar\frac{d\rho_S}{dt} = [H_0 + H_I, \rho_S] \tag{5.1}$$

where H_0 is the unperturbed Hamiltonian and H_I describes the optical interaction. The various components may be written explicitly as

$$i\hbar\frac{d\rho_{10}}{dt} = \rho_{10}\hbar\omega_{10} + H_{10}(\rho_{00} - \rho_{11}) \tag{5.2}$$

$$i\hbar\frac{d\rho_{01}}{dt} = \rho_{01}\hbar\omega_{01} + H_{01}(\rho_{11} - \rho_{00}) \tag{5.3}$$

$$i\hbar\frac{d\rho_{00}}{dt} = H_{01}\rho_{10} - \rho_{01}H_{10} \tag{5.4}$$

$$i\hbar\frac{d\rho_{11}}{dt} = H_{10}\rho_{01} - \rho_{10}H_{01} \tag{5.5}$$

where the subscripts refer to the states Ψ_0 and Ψ_1 which are separated in energy by $\hbar\omega_{10}$ and which have H_{10} as the optical interaction matrix element. Suppose that $H_{01} = H_{10} = H_{\text{env}}\cos\omega_p t$ (for a pulsed interaction $H_{\text{env}}(t)$ describes the variation of the pulse envelope) and define $\beta = H_{\text{env}}/\hbar$ and $\Delta = \omega_p - \omega_{10}$. Also introduce two new real functions u and v such that

$$\rho_{10} = \frac{1}{2}(u + iv)\exp(-i\omega_p t) \tag{5.6}$$

so that using $\rho_{10} = \overline{\rho_{01}}$ the functions u and v may be expressed as

$$u = \rho_{10}e^{i\omega_p t} + \rho_{01}e^{-i\omega_p t} \tag{5.7}$$

$$iv = \rho_{10}e^{i\omega_p t} - \rho_{01}e^{-i\omega_p t} \tag{5.8}$$

Also note the relation

$$i(\rho_{10} - \rho_{01}) = u \sin \omega_p t - v \cos \omega_p t \tag{5.9}$$

Now take $f_0 = 1 - \rho_{00}$ and $f_1 = \rho_{11}$ so that f_0 measures hole occupancy in the ground state Ψ_0 and f_1 measures electron occupancy in the excited state Ψ_1. Then differentiating equations (5.7) and (5.8) and substituting from equations (5.2) and (5.3) gives

$$\frac{du}{dt} = -\Delta v + \beta \sin 2\omega_p t\,(1 - f_0 - f_1) \tag{5.10}$$

$$\frac{dv}{dt} = \Delta u - \beta\,(1 + \cos 2\omega_p t)\,(1 - f_0 - f_1) \tag{5.11}$$

Also equations (5.4) and (5.5) may be rewritten using equation (5.9) as

$$\frac{df_0}{dt} = \frac{df_1}{dt} = -\frac{\beta v}{2}\,(1 + \cos 2\omega_p t) + \frac{\beta u}{2} \sin 2\omega_p t \tag{5.12}$$

The terms in $\sin 2\omega_p t$ and $\cos 2\omega_p t$ result in rapid oscillations of u, v and f_0, f_1 but for excitation near resonance ($\omega_p \simeq \omega_{10}$) the magnitude of the oscillations is negligibly small and the terms containing $\sin 2\omega_p t$ and $\cos 2\omega_p t$ may be dropped from the equations. This is the rotating frame approximation [4] and is equivalent to the omission of non-resonant terms in the solution of the Liouville equation as discussed in chapter two. The equations (5.10) to (5.12) become

$$\frac{du}{dt} = -\Delta v \tag{5.13}$$

$$\frac{dv}{dt} = \Delta u - \beta\,(1 - f_0 - f_1) \tag{5.14}$$

$$\frac{df_0}{dt} = \frac{df_1}{dt} = -\frac{\beta v}{2} \tag{5.15}$$

which are amenable to the inclusion of thermal scattering effects as discussed in the next section. As expected the equations predict that the optical excitation generates equal numbers of electrons and holes since $f_0 = f_1$. Further if the substitution $w = 1 - f_0 - f_1$ is made then the Bloch equations

$$\frac{du}{dt} = -\Delta v \tag{5.16}$$

$$\frac{dv}{dt} = \Delta u - \beta w \tag{5.17}$$

$$\frac{dw}{dt} = \beta v \tag{5.18}$$

are obtained and these may be written in a particularly compact form by employing vector notation. Hence defining $\mathbf{r}_{\text{Bloch}} = (u, v, w)$ and $\Omega = (\beta, 0, \Delta)$ the equations (5.16) to (5.18) become

$$\frac{d\mathbf{r}_{\text{Bloch}}}{dt} = \Omega \times \mathbf{r}_{\text{Bloch}} \tag{5.19}$$

The Bloch vector $\mathbf{r}_{\text{Bloch}}$ rotates about the axis specified by the vector Ω (in a manner analogous to magnetic spin precession). The magnitude of $\mathbf{r}_{\text{Bloch}}$ is constant since

$$\begin{aligned} \frac{d|\mathbf{r}_{\text{Bloch}}|^2}{dt} &= 2\mathbf{r}_{\text{Bloch}} \cdot \frac{d\mathbf{r}_{\text{Bloch}}}{dt} \\ &= 2\mathbf{r}_{\text{Bloch}} \cdot (\Omega \times \mathbf{r}_{\text{Bloch}}) \\ &= 0 \end{aligned} \tag{5.20}$$

The frequency of rotation is given by the magnitude of the vector Ω and is called the Rabi frequency [4]. Since $\Omega = (\beta, 0, \Delta)$ it follows that for exact resonance ($\Delta = 0$)

the Rabi frequency is given by β whilst for $\Delta \neq 0$ it is given by $\left(\beta^2 + \Delta^2\right)^{1/2}$. As the vector $\mathbf{r}_{\text{Bloch}}$ rotates about Ω there is a periodic variation in the coordinate $w = \rho_{00} - \rho_{11}$ and this describes the continual movement of electrons between the ground and excited states. This phenomenon is illustrated in figure 5.1 which shows the time variation of the occupation probabilities of the two states for a particular case. The ground state Ψ_0 is initially occupied but an on-resonance optical pulse excites the electrons back and forth between the two states Ψ_0 and Ψ_1 so that Rabi oscillations are clearly visible. The interaction Hamiltonian has a gaussian envelope H_{env} with time constant $\tau = 100$fs and peak value $H_{\text{env}}(\text{peak}) = 10^{-20}$J at time $t = 0$. Note that the frequency of the Rabi oscillations is lower during the time when the pulse is rising and falling, whilst near the pulse maximum at $t = 0$ the Rabi oscillations become more rapid. The final occupancies of the states depend on the integral of the Rabi frequency $\beta(t)$ over the whole of the pulse duration.

Although it is primarily applicable to the study of on-resonance phenomena, the formalism developed here may also be applied to the virtual carrier regime considered in the previous chapter. Suppose that the system is initially in the ground state with $f_0 = f_1 = 0$ (w=1) and that there is no phase coherence between states so that equations (5.7) and (5.8) give $u = v = 0$. Then for a pulsed interaction with the photon energy detuned below the energy gap ($\Delta < 0$), the vectors Ω and $\mathbf{r}_{\text{Bloch}}$ are initially collinear with $\Omega = (0, 0, \Delta)$ and $\mathbf{r}_{\text{Bloch}} =$

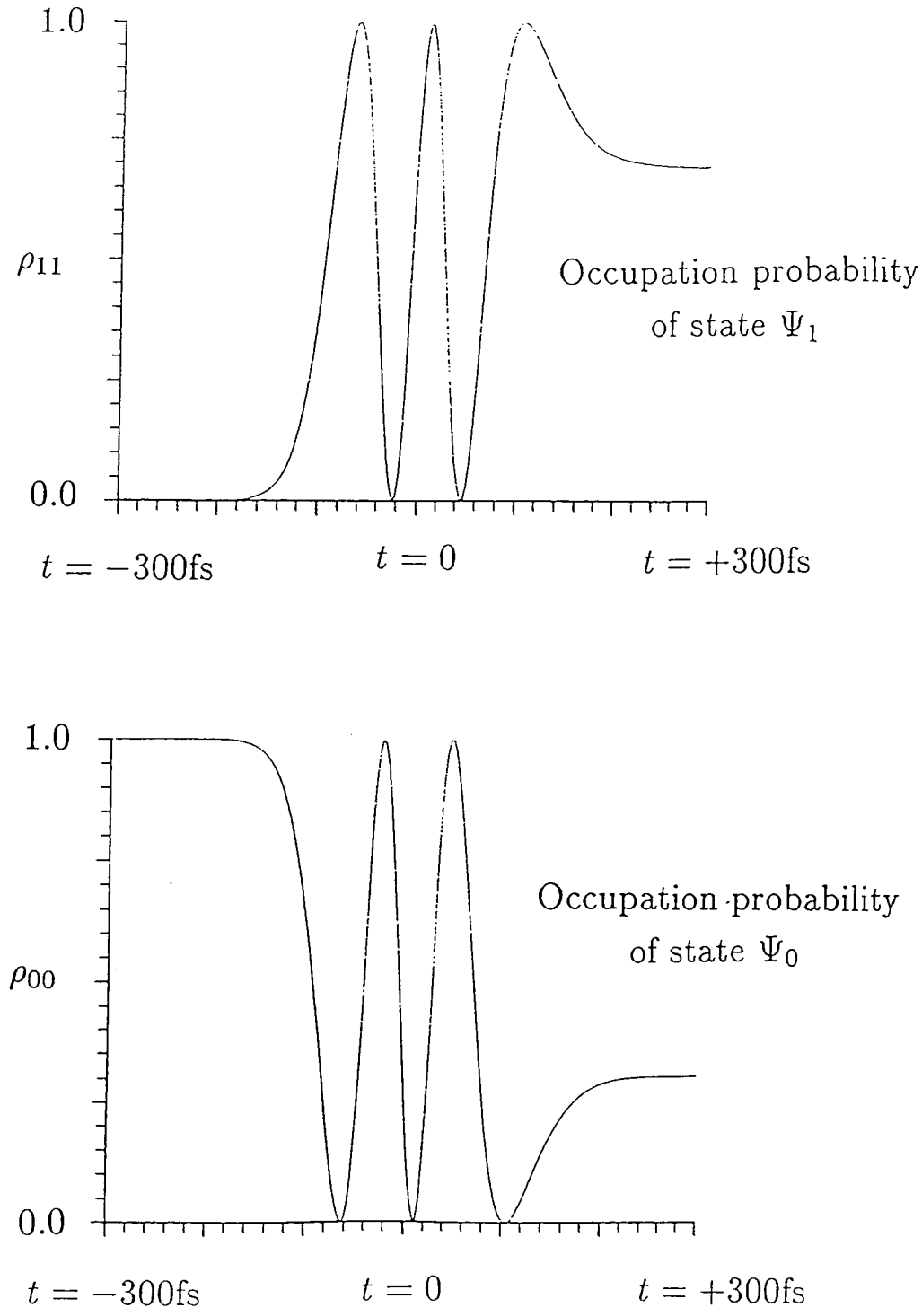

Figure 5.1. Occupation probabilities of the two states Ψ_0 (bottom) and Ψ_1 (top) plotted against time t. The ground state Ψ_0 is initially occupied and the system is subject to a pulsed excitation with gaussian envelope H_{env} having time constant $\tau = 100$fs and a peak value of 10^{-20}J at time $t = 0$.

$(0,0,1)$. If the pulse amplitude increases sufficiently slowly then the Bloch vector is able to follow the motion of $\Omega = (\beta, 0, \Delta)$ and the two vectors remain collinear (although with $\Delta < 0$ they point in opposite directions). This is known as the adiabatic following regime [54-55]. Also $\mathbf{r}_{\text{Bloch}}$ initially has unit magnitude and equation (5.20) shows that thenceforth it has constant magnitude. Hence

$$\mathbf{r}_{\text{Bloch}} = \left(\beta^2 + \Delta^2\right)^{-1/2} (-\beta, 0, -\Delta) \tag{5.21}$$

From equations (5.21) and (5.6) it follows that

$$\begin{aligned} f_0 = f_1 &= \frac{1}{2} - \frac{w}{2} \\ &= \frac{1}{2} - \frac{1}{2}\left[1 + \left(\frac{\beta}{\Delta}\right)^2\right]^{-1/2} \end{aligned} \tag{5.22}$$

and

$$\rho_{10} = \frac{u}{2} \mathrm{e}^{-i\omega_p t} = \frac{\beta}{2\Delta} \left(\rho_{00} - \rho_{11}\right) \mathrm{e}^{-i\omega_p t} \tag{5.23}$$

which may be used to derive the low intensity results with $(\beta/\Delta) \ll 1$ that were presented at the end of chapter four.

Section 5.2. Thermal effects in the relaxation approximation.

In the previous chapter the effect of thermal interactions on the optical response of the system was neglected because the thermal scattering rates of virtual carriers were assumed to be slow in comparison with the pulse width. However, when considering illumination by a light beam where the photon energy lies in the absorption band of the semiconductor, it is no longer possible to the neglect the thermal effects due to carrier-carrier and carrier-phonon scattering. These processes occur on a timescale of approximately 10 femtoseconds to picoseconds [56-57] which is comparable with the shortest pulse widths currently available. Thus it is necessary to find some way to include the effects of the scattering processes within the Liouville-Bloch formalism. The relaxation approximation [58-63] provides a simple method for inclusion of these effects, whereby the density matrix elements are allowed to relax to equilibrium values at rates determined by a number of phenomenological time constants.

In the semiconductor model the two states Ψ_0 and Ψ_1 of section 5.1 are assumed to correspond to the valence and conduction states at a particular electronic wavevector $\mathbf{k}$ in a two-band model. The off-diagonal matrix elements ρ_{10} and ρ_{01} (and hence u and v) decay due to dephasing, that is the phase coherence between the states Ψ_0 and Ψ_1 is destroyed by thermal interactions at a rate $\Gamma(dephasing)$. The density matrix elements ρ_{00} and ρ_{11} (or equivalently f_0 and f_1) are affected by thermal processes which act to redistribute the carriers within a band so as to

form various quasi-Fermi distributions. In addition electron-hole recombination removes carriers from the bands (and current injection replaces them). Hence in the relaxation approximation the Bloch equations (5.13) to (5.15) can be written as

$$\frac{du}{dt} = -\Delta v - \Gamma(dephasing)u \tag{5.24}$$

$$\frac{dv}{dt} = \Delta u - \beta\,(1 - f_0 - f_1) - \Gamma(dephasing)v \tag{5.25}$$

$$\begin{aligned}\frac{df_0}{dt} = &-\frac{\beta v}{2} - \Gamma(hole - hole)\,(f_0 - f_0(hole - hole)) \\ &- \Gamma(electron - hole)\,(f_0 - f_0(electron - hole)) \\ &- \Gamma(hole - phonon)\,(f_0 - f_0(hole - phonon)) \\ &- \Gamma(recombination)\,(f_0 - f_0(recombination))\end{aligned} \tag{5.26}$$

$$\begin{aligned}\frac{df_1}{dt} = &-\frac{\beta v}{2} - \Gamma(electron - electron)\,(f_1 - f_1(electron - electron)) \\ &- \Gamma(electron - hole)\,(f_1 - f_1(electron - hole)) \\ &- \Gamma(electron - phonon)\,(f_1 - f_1(electron - phonon)) \\ &- \Gamma(recombination)\,(f_1 - f_1(recombination))\end{aligned} \tag{5.27}$$

In addition to the dephasing effects, there are four thermal relaxation processes. Firstly, there is carrier-carrier scattering within each band at a rate $\Gamma(carrier - carrier)$ to a distribution $f_i(carrier - carrier)$ which is a quasi-Fermi distribution determined by the number of carriers in the band and their total energy. Secondly, there is electron-hole scattering between the carriers in the two bands at the rate $\Gamma(electron - hole)$ to quasi-Fermi distributions $f_i(electron - hole)$ which again are

determined by the number of carriers in each band but now by the combined energy of both types of carrier. These two scattering processes are assumed to be elastic so that in each case the total energy of the carriers involved is a conserved quantity. Thirdly, there is carrier-phonon scattering as the carriers equilibrate their temperature T with that of the lattice T_0, thus relaxing to a distribution $f_i(carrier-phonon)$ at a rate $\Gamma(carrier-phonon)$. The quasi-Fermi distributions $f_i(carrier-phonon)$ are determined by the number of carriers in each band but the total energy of the carriers changes and is eventually set by the lattice temperature T_0. Finally, recombination between the two bands restores the equlibrium distributions $f_i(recombination)$ at a rate $\Gamma(recombination)$. These quasi-Fermi distributions are determined by the lattice temperature T_0 and by the number of carriers pumped into the bands by some external mechanism such as injected electrical current.

To calculate the distribution

$$f_i(carrier-phonon)(k) = \frac{1}{1 + A\exp(E(k)/k_B T_0)} \tag{5.28}$$

requires determination of the constant $A = \exp(-E_F/k_B T_0)$ where E_F is the quasi-Fermi energy of the distribution and k_B is Boltzmann's constant. A parabolic band model is assumed so that $E(k) = \hbar^2 k^2/2m^*$ with m^* the effective mass of the band. The number of carriers n in each band is not altered by the carrier-phonon scattering and so may be calculated from

$$n = \int_0^\infty f_i(k)g(k)dk \tag{5.29}$$

where $g(k)$ is the density of states function including spin. For a quantum well $g(k)$ is given by

$$g(k) = \frac{2}{(2\pi)^2} 2\pi k \tag{5.30}$$

and for the bulk by

$$g(k) = \frac{2}{(2\pi)^3} 4\pi k^2 \tag{5.31}$$

The number of carriers n may then be used to find A by inverting the integral relation

$$\begin{aligned} n &= \int_0^\infty f_i(carrier - phonon)(k) g(k) dk \\ &= \left\{ \begin{array}{l} K_{\mathrm{QW}}^{-1} I_1 \text{ for QW} \\ K_{\mathrm{Bulk}}^{-1} I_2 \text{ for Bulk} \end{array} \right] \end{aligned} \tag{5.32}$$

where the constants K are

$$K_{\mathrm{QW}} = \frac{\pi \hbar^2}{m^* k_B T_0} \tag{5.33}$$

and

$$K_{\mathrm{Bulk}} = \frac{2\pi^2 \hbar^3}{(2m^* k_B T_0)^{3/2}} \tag{5.34}$$

The integral I_r is defined as

$$I_r = \int_0^\infty \frac{2x^r dx}{1 + A \exp(x^2)} \tag{5.35}$$

In the case of a quantum well the inversion may be achieved through the relation $nK_{\mathrm{QW}} = \log(1 + 1/A)$ but for the bulk the inversion is most easily performed numerically.

Now to find the distribution

$$f_i(carrier-carrier)(k) = \frac{1}{1+A\exp(E(k)/k_BT)} \tag{5.36}$$

requires determination of the two constants A (related to the quasi-Fermi energy) and T (the carrier temperature). The number of carriers n in each band is again given by equation (5.29) and the conservation of this quantity yields the relations

$$\begin{aligned} n &= \int_0^\infty f_i(carrier-carrier)(k)g(k)dk \\ &= \left\{ \begin{array}{c} K_{\mathrm{QW}}^{-1}\hat{T}I_1 \text{ for QW} \\ K_{\mathrm{Bulk}}^{-1}\hat{T}^{3/2}I_2 \text{ for Bulk} \end{array} \right] \end{aligned} \tag{5.37}$$

where $\hat{T} = T/T_0$ is the carrier temperature normalised to the lattice temperature T_0. As before, in the quantum well case the relation may be written as $nK_{\mathrm{QW}} = \hat{T}\log(1+1/A)$ which is easily inverted. Further, since the carrier-carrier scattering is elastic the total energy of carriers in each band is also conserved and may be calculated (in units of k_BT_0) as

$$E = \int_0^\infty f_i(k)E_B(k)g(k)dk \tag{5.38}$$

where $E_B(k) = \hbar^2k^2/2m^*k_BT_0$. The relations

$$\begin{aligned} E &= \int_0^\infty f_i(carrier-carrier)(k)E_B(k)g(k)dk \\ &= \left\{ \begin{array}{c} K_{\mathrm{QW}}^{-1}\hat{T}^2I_3 \text{ for QW} \\ K_{\mathrm{Bulk}}^{-1}\hat{T}^{5/2}I_4 \text{ for Bulk} \end{array} \right] \end{aligned} \tag{5.39}$$

may be solved numerically to find $\hat{T}$ by substituting for A from equation (5.37) and then finally A may be calculated from equation (5.37) using the appropriate value

of $\hat{T}$. The case of electron-hole scattering may be treated in a similar fashion except that the total energy of both electrons and holes together is conserved. Thus a common value of $\hat{T}$ may be found which is applicable to both valence and conduction bands and from which the individual quasi-Fermi energies can be calculated.

Finally, the distribution

$$f_i(recombination) = \frac{1}{1 + A\exp(E(k)/k_B T_0)} \tag{5.40}$$

is entirely determined by the number of carriers n that is established by the competing forces of recombination and current injection. The integral relation

$$n = \int_0^\infty f_i(recombination)(k)g(k)dk \tag{5.41}$$

may be inverted to calculate A.

Section 5.3. Application to laser amplifiers.

Recent experimental investigations [46-53] have studied the ultrafast optical response of semiconductor laser amplifiers. The results show a large nonlinear refractive index ($\Delta n \sim 10^{-4}$) and if the device is biased for unity gain (transparency) the recovery time is on the order of picoseconds. This sort of response would be particularly useful in the design of fast all-optical switching devices based on semiconductors. The basic experiment is to send pump and probe pulses through the laser amplifier with orthogonal polarisations (so that there is little direct optical coupling from the intense pump beam to the much weaker probe beam) and to vary the time delay between the pump and probe beams. The measurements use a novel time division interferometry technique [64,65] which employs a third reference pulse to determine the phase shift of the probe pulse. The pulses are sufficiently short (around 100-500 fs) that it is possible to resolve the temporal changes in absorption coefficient and refractive index experienced by the probe beam due to the carrier dynamics of the semiconductor material.

The formalism developed in the previous two sections is now used to model the experiments described above in an attempt to understand some of the results observed. The Bloch equations with relaxation terms included may be used to first calculate the effects of the pump beam on the carrier population in the valence and conduction bands. The probe beam is then assumed to be sufficiently weak that it has no further effect on the carrier populations, but simply produces a linear

polarisation of the particular carrier distribution generated by the pump pulse. The polarisation due to the probe is assumed to have a gaussian envelope like the incident field and an amplitude P_0 corresponding to the electric field amplitude E_0 of the probe. The standard linear relation connnecting P_0 and E_0 is $P_0 = \varepsilon_0 \chi E_0$ where ε_0 is the permittivity of free space and χ is the complex susceptibility. The relative permittivity is $\varepsilon_r = 1 + \chi$ and from this may be calculated the refractive index $n = Re\sqrt{\varepsilon_r}$ and the intensity absorption coefficient $\alpha = (2\omega_p/c) Im\sqrt{\varepsilon_r}$ where c is the speed of light. The electric field of both the pump and probe pulses has the form

$$E = E_0 \cos \omega_p t \, \mathrm{e}^{-t^2/\tau^2} \tag{5.42}$$

although the pump field amplitude E_0 is greater and the pump pulse envelope is displaced in time relative to that of the probe pulse. As a rapid dephasing rate will be used in the model, the polarisation induced by the probe is assumed to have a similar form

$$P = P_0 \cos(\omega_p t + \theta) \, \mathrm{e}^{-t^2/\tau^2} \tag{5.43}$$

where θ determines the phase of the polarisation relative to the electric field of the probe beam. The value of θ depends on the time delay between the pump and probe pulses. The Bloch equations (5.24) to (5.27) are solved to find the populations f_0 and f_1 induced by the pump field and then are re-solved for the probe field using the values of f_0 and f_1 calculated for the pump field in order to find values of u and v appropriate to the probe field. The Brillouin zone is

divided into discrete regions (spherical shells for the bulk and circular rings for the quantum well) with steps Δk in the magnitude of the wavevector between regions, and values u_k and v_k are calculated for each region. The total polarisation is then

$$P(t) = \sum_k P_k(t) g(k) \Delta k \tag{5.44}$$

where

$$P_k(t) = -d_k \left(u_k \cos \omega_p t + v_k \sin \omega_p t \right) \tag{5.45}$$

and d_k is the dipole matrix element at a given wavevector $\mathbf{k}$. In the case of a quantum well d_k must be divided by the well width in order to obtain $P(t)$ as a dipole moment per unit volume. The Fourier transform of the polarisation is calculated as

$$\begin{aligned} P(\omega_p) &= \frac{1}{2\pi} \sum_t P(t) \mathrm{e}^{i\omega_p t} \Delta t \\ &\simeq -\sum_{k,t} \frac{d_k}{4\pi} \left(u_k + i v_k \right) g(k) \Delta k \Delta t \end{aligned} \tag{5.46}$$

Finally from equation (5.43) $P_0 = (4\sqrt{\pi}/\tau) P(\omega_p)$ so that

$$P_0 = -\sum_{k,t} \frac{d_k}{\tau \sqrt{\pi}} \left(u_k + i v_k \right) g(k) \Delta k \Delta t \tag{5.47}$$

From this expression the values of the refractive index and absorption coefficient experienced by the probe pulse may be predicted. The results for a variety of situations comparing bulk and quantum well laser amplifiers are presented below.

For both the bulk and quantum well studies the energy gap at the Brillouin zone centre is taken as $E_g = 1.5\mathrm{eV}$, and the effective masses for the valence and

conduction bands are taken as $m_0^* = 0.5$ and $m_1^* = 0.05$ respectively. The dipole matrix element d_k is assumed independent of k with a value of $d_k = 10^{-28}$Cm corresponding to an electronic displacement of about 10Å. In the case of the quantum well this is divided by the well width of 100Å. The pump beam has a gaussian envelope of time constant $\tau = 100$fs and the peak value of the pump beam electric field is $E_0 = 10^7$V/m. The probe beam is much weaker ($E_0 \sim 10^3$V/m) and is displaced in time relative to the pump beam in the range 1ps ahead of the pump to 5ps after the pump. Experimental observations [56,57] have indicated that rapid dephasing occurs and a value of $\Gamma(dephasing) = 10^{14}\text{s}^{-1}$ is used in the model. For the sake of simplicity, the carrier-carrier scattering is limited to just the electron-hole scattering as this is the only one of the three carrier-carrier processes discussed in section 5.2 to include both electrons and holes. A scattering rate of $\Gamma(electron-hole) = 10^{13}\text{s}^{-1}$ is chosen. The electron-electron and hole-hole scatterings are ignored and further calculations are required to determine their influence on the optical response. The carrier-phonon scattering rate in each band is taken as $\Gamma(carrier-phonon) = 10^{12}\text{s}^{-1}$. All calculations are performed with a lattice temperature $T_0 = 300$K. In the numerical calculations, the discretization in reciprocal space and in time uses steps of $\Delta k = 4.5 \times 10^6\text{m}^{-1}$ and $\Delta t = 1$fs respectively.

For the pump photon energy equal to the bandgap energy ($E_p = E_g$), the model predicts that the laser amplifier achieves transparency (i.e. the injected

carrier density is unchanged after the pump pulse) when the bulk carrier density is around $N_{\mathrm{Bulk}} = 6 \times 10^{24}\mathrm{m}^{-3}$ whilst for the 100Å quantum well device the model predicts that transparency is achieved with an injected carrier density of around $N_{\mathrm{QW}} = 2.5 \times 10^{16}\mathrm{m}^{-2}$. These values agree with the typical values seen in actual devices. The distribution of holes $f_0(k)$ and of electrons $f_1(k)$ corresponding to these injected carrier concentrations are depicted in figure 5.2 which shows that the electrons are to be found nearer to the Brillouin zone centre due to the higher curvature of the conduction band. Figure 5.2 also shows the function $f_0 + f_1$ which determines whether absorption or stimulated emission occurs at a particular value of electronic wavevector k. This function appears in equation (5.25) and as expected results in stimulated emission when $f_0 + f_1 > 1$ and in absorption when $f_0 + f_1 < 1$. Hence carriers (holes in the valence band and electrons in the conduction band) are removed near the Brillouin zone centre where the pump beam stimulates recombination and are generated further out in the zone ($k > 0.05$Å) where $f_0 + f_1 < 1$. The changes in the bulk carrier densities relative to the initial values obtained from figure 5.2 are shown in figures 5.3 and 5.4 for holes and electrons respectively. The quantum well model provides qualitatively similar results. It is possible to see the recombination-generation response described above (particularly in figure 5.4 which depicts electrons) but within 0.5ps the distribution is smoothed by the carrier-carrier scattering to a quasi-Fermi distribution at temperature T. Over the next 5ps the carrier-phonon scattering equilibrates the carrier

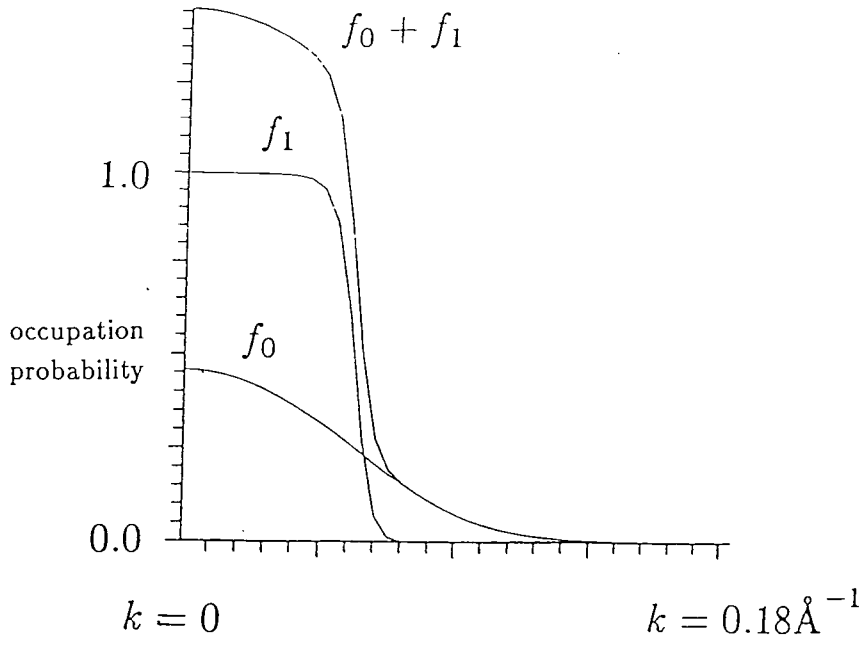

Figure 5.2a. Transparency carrier distributions plotted against wavevector k showing holes in the valence band f_0 and electrons in the conduction band f_1 for the bulk.

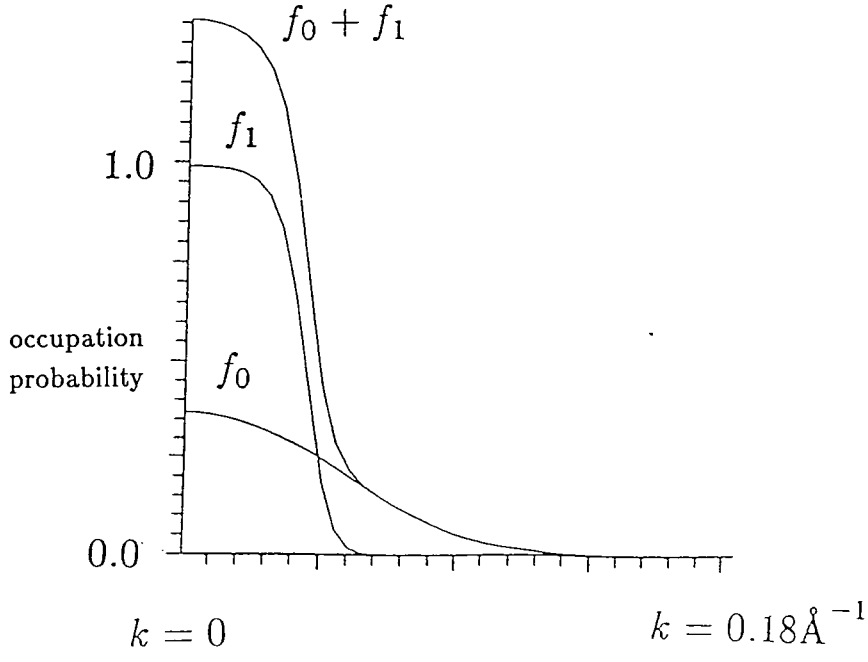

Figure 5.2b. Transparency carrier distributions plotted against wavevector k showing holes in the valence band f_0 and electrons in the conduction band f_1 for the quantum well.

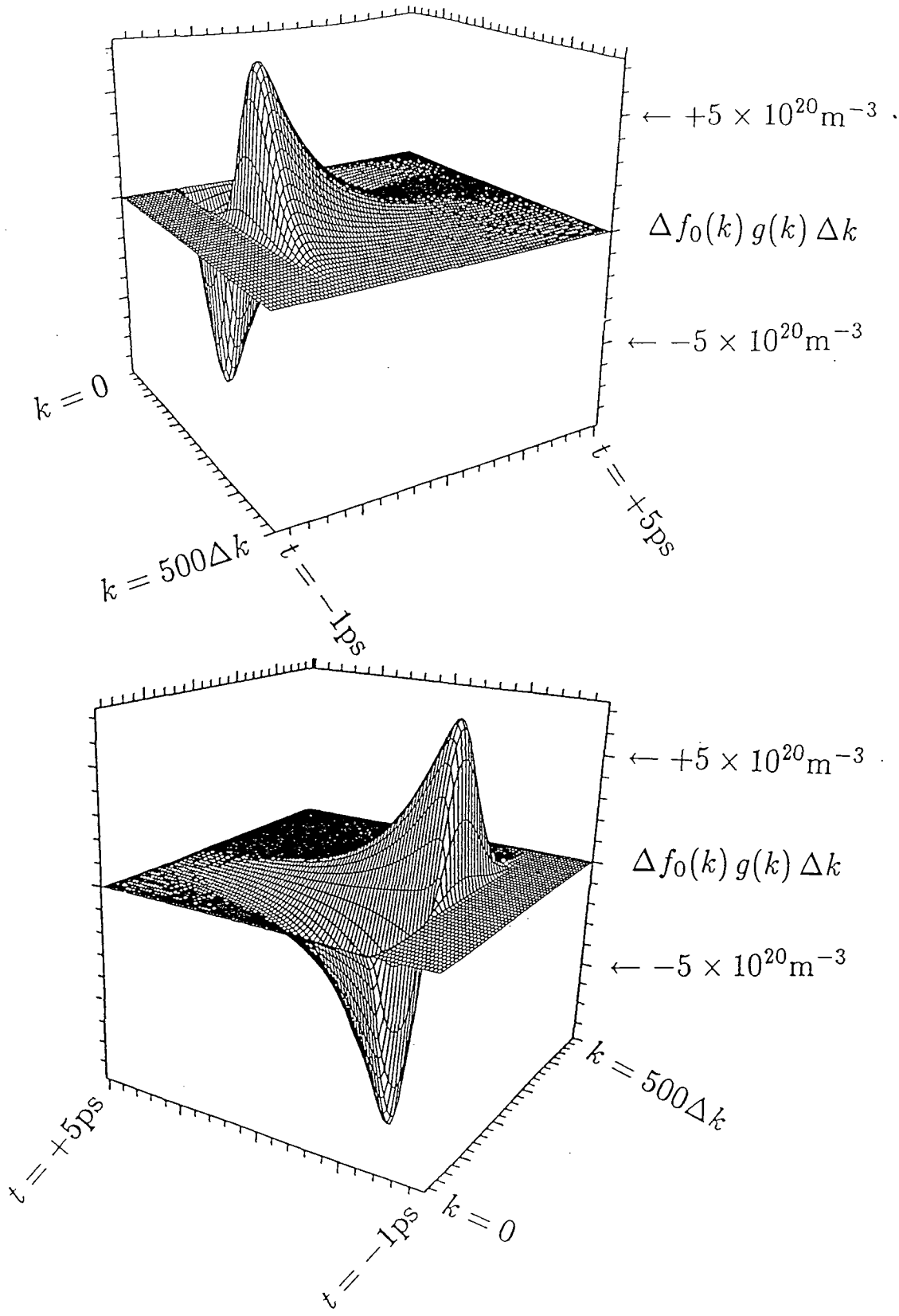

Figure 5.3. Two views of the change in bulk hole density as a function of electron wavevector k and time t. At each value of k the graphs show the density of holes with a wavevector in the range k to $k + \Delta k$.

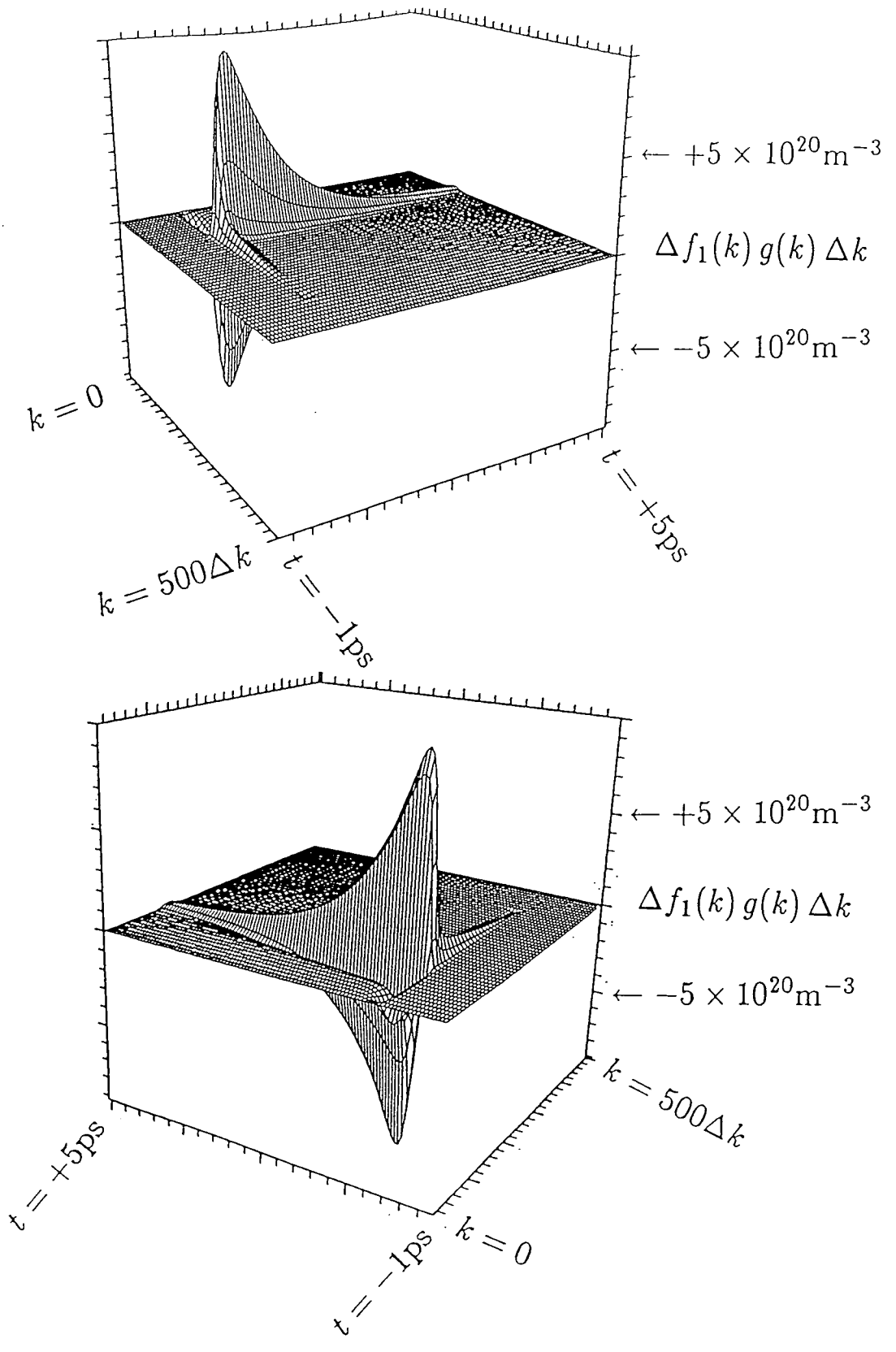

Figure 5.4. Two views of the change in bulk electron density as a function of electron wavevector k and time t. At each value of k the graphs show the density of electrons with a wavevector in the range k to $k + \Delta k$.

temperature T with the lattice temperature T_0. Because figures 5.3 and 5.4 show the response at transparency, the change in the total number of carriers in each band is zero. Hence when T reaches T_0 the initial carrier distribution is restored and the change in carrier density is zero at all values of electronic wavevector. The variation of the carrier temperature as a function of time is shown in figure 5.5. The pump beam excites carriers high in the band and removes carriers lower in the band, thus the average energy of the carriers increases and their temperature rises. Due to the higher curvature of the conduction band the electrons initially reach a higher temperature than the holes, but the inclusion of electron-hole scattering in the model means that the two carrier temperatures are quickly brought together. In the following few picoseconds the carrier temperature drops back to the lattice temperature as the carrier-phonon scattering takes effect. Figure 5.6 shows the changes in the bulk hole density for the injected carrier densities $N_{\mathrm{Bulk}} = 4 \times 10^{24}\mathrm{m}^{-3}$ and $N_{\mathrm{Bulk}} = 8 \times 10^{24}\mathrm{m}^{-3}$. In the first case the injected carrier density is below the transparency value so that more absorption occurs than stimulated emission and there is an increase in the final carrier density of some states. Conversely in the second case more carriers are removed by stimulated emission than are generated by absorption so that there is a decrease in the final carrier density of some states. These changes in the carrier density are eventually removed by recombination (or injection) but this occurs on the much longer timescale of nanoseconds.

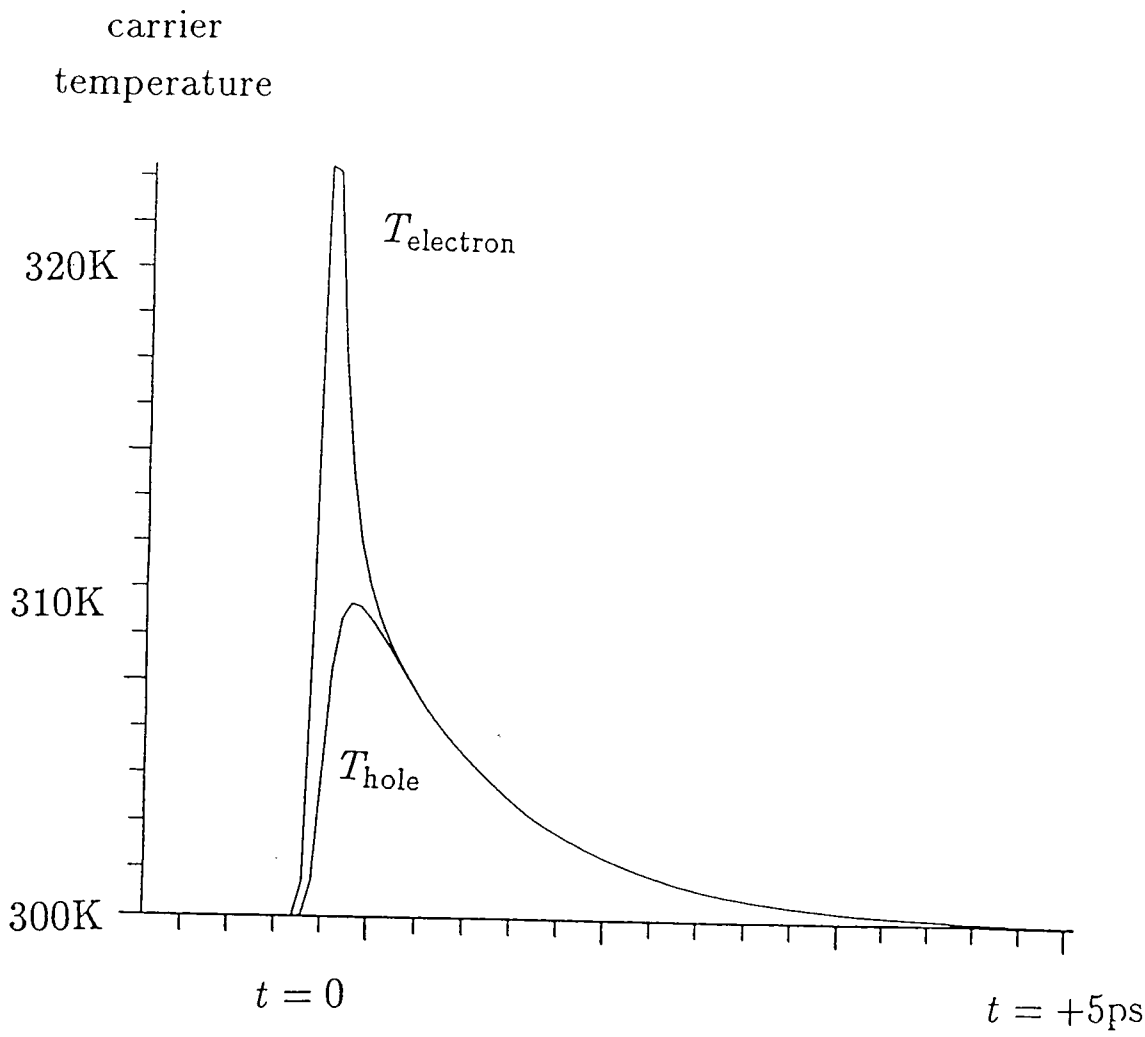

Figure 5.5. The variation in time of the carrier temperatures T_{hole} and T_{electron}. The lattice temperature is $T_0 = 300\text{K}$.

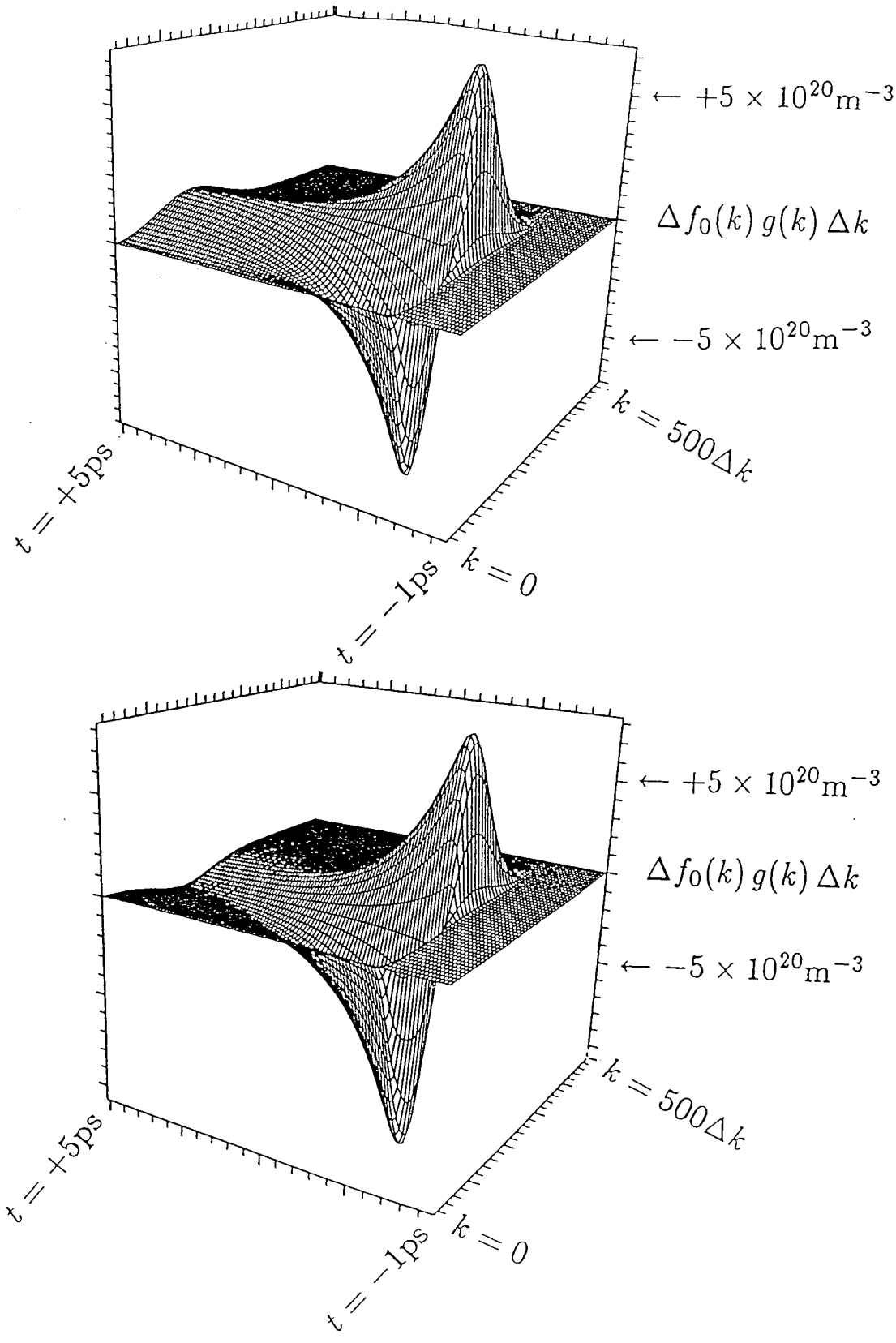

Figure 5.6. The change in bulk hole density as a function of electron wavevector k and time t showing an increase of the total hole density for $N_{\mathrm{Bulk}} = 4 \times 10^{24}\mathrm{m}^{-3}$ (top) and a decrease of the total hole density for $N_{\mathrm{Bulk}} = 8 \times 10^{24}\mathrm{m}^{-3}$ (bottom).

The absorption coefficient α and refractive index n experienced by the probe beam are shown in figures 5.7 and 5.8 for the bulk and in figures 5.9 and 5.10 for the quantum well. The photon energy E_p of both the pump and probe beams is equal to the bandgap energy E_g. The optical response is plotted as a function of time delay between pump and probe beams relative to the response at large negative time delay and the three cases of injected carrrier density above, at and below the transparency value are considered. In all three carrier density regimes the absorption coefficient increases around zero time delay, although the size of this increase becomes smaller as the injected carrier density is reduced. At transparency the absorption coefficient returns to its initial value, but with a lower injected carrier density the final value of the absorption coefficient is reduced and with a higher density it is increased. (Strictly speaking the values are 'final' only on a picosecond timescale as recombination and current injection restore the initial value eventually, but this effect is ignored here). The changes in absorption coefficient are explained by the final changes in carrier density (depicted in figure 5.6) induced by the pump beam which tend to move the absorption coefficient towards its value at transparency. Similarly, in all three regimes the refractive index shows a temporary increase with the formation of the quasi-Fermi distributions at the elevated carrier temperature T. The final value of the refractive index depends on whether the total carrier density has been increased or decreased by the pump beam. In chapter four it was shown that for below-resonance excitation the gen-

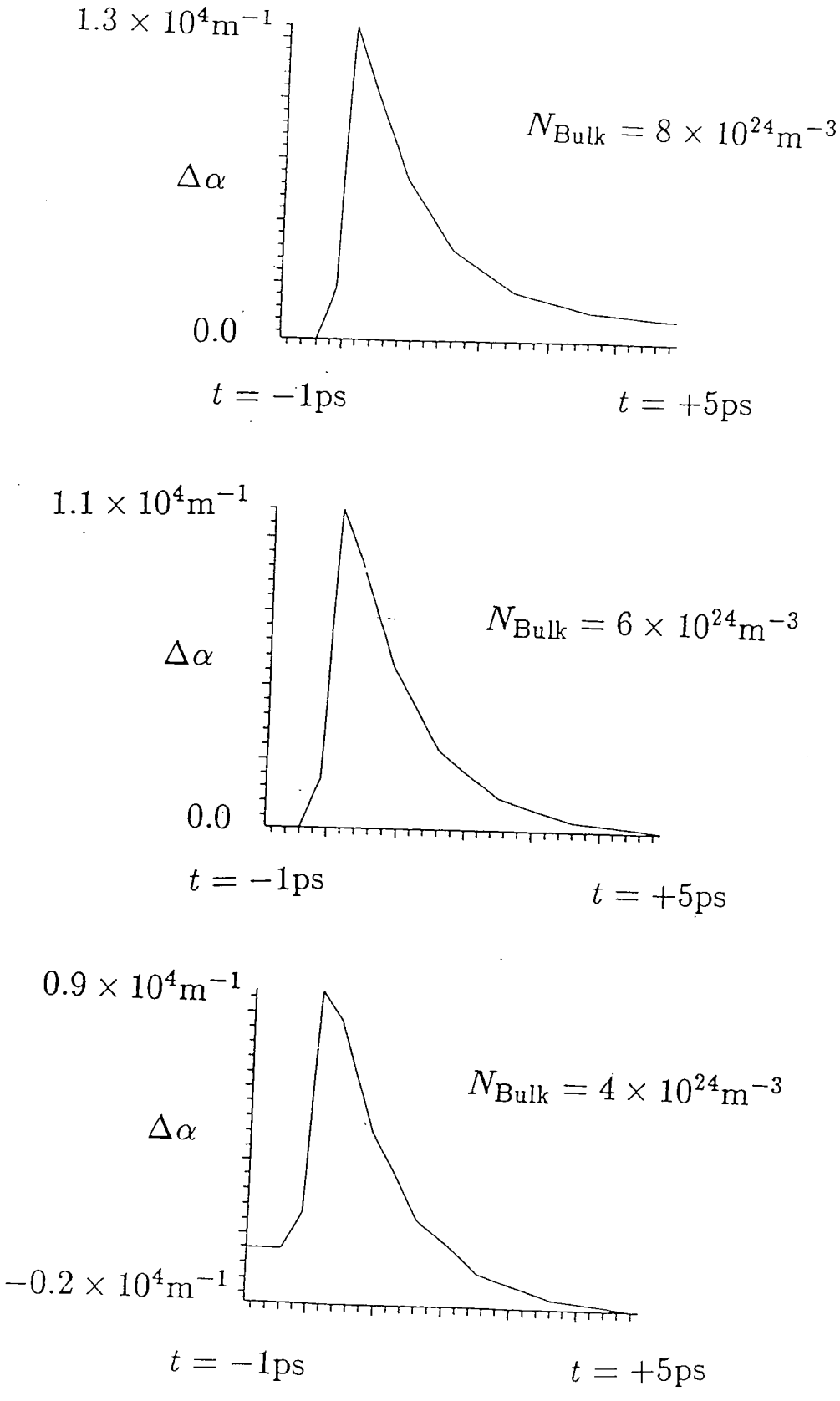

Figure 5.7. The variation of the absorption coefficient experienced by the probe pulse against time delay of the probe relative to the pump.

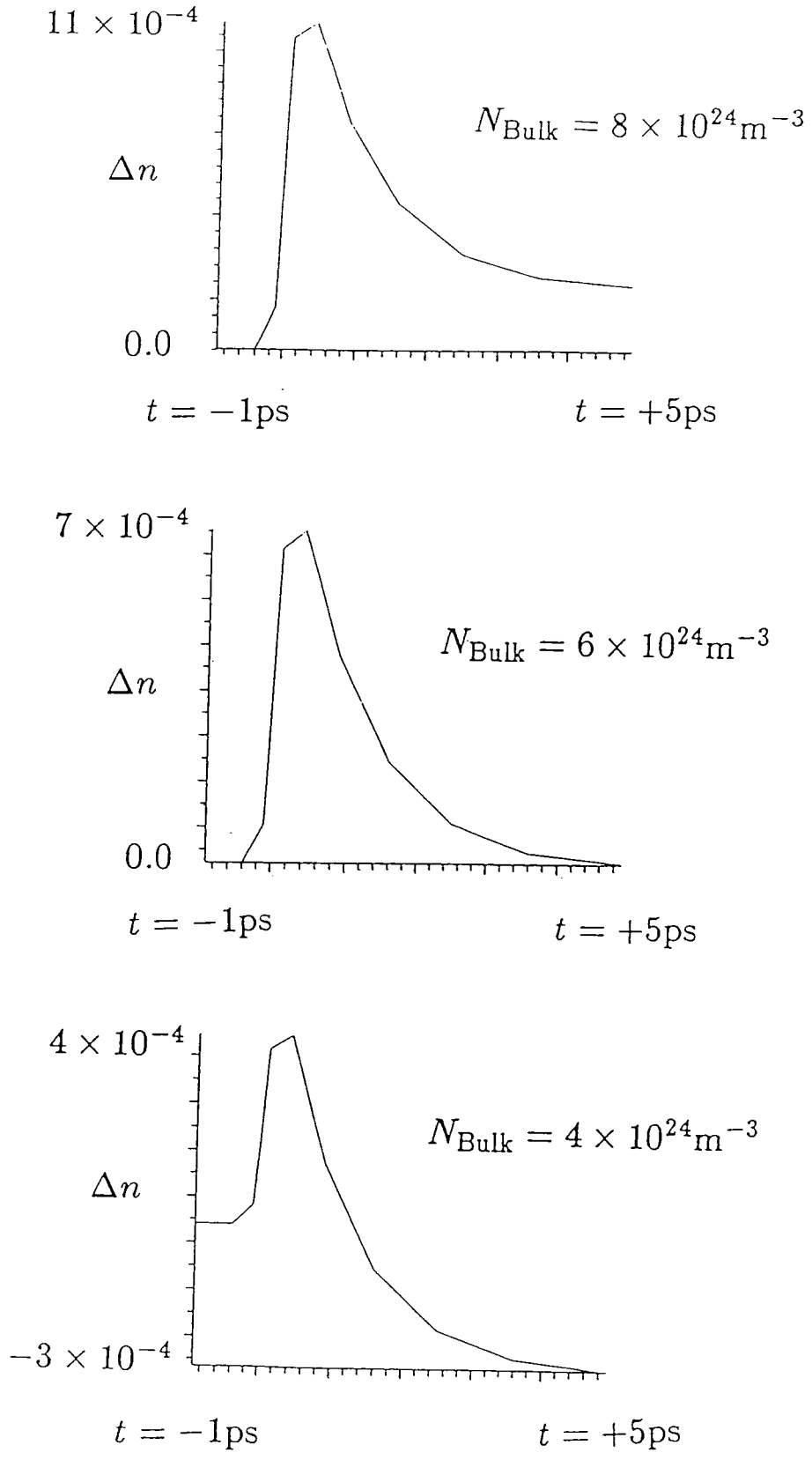

Figure 5.8. The variation of the refractive index experienced by the probe pulse against time delay of the probe relative to the pump.

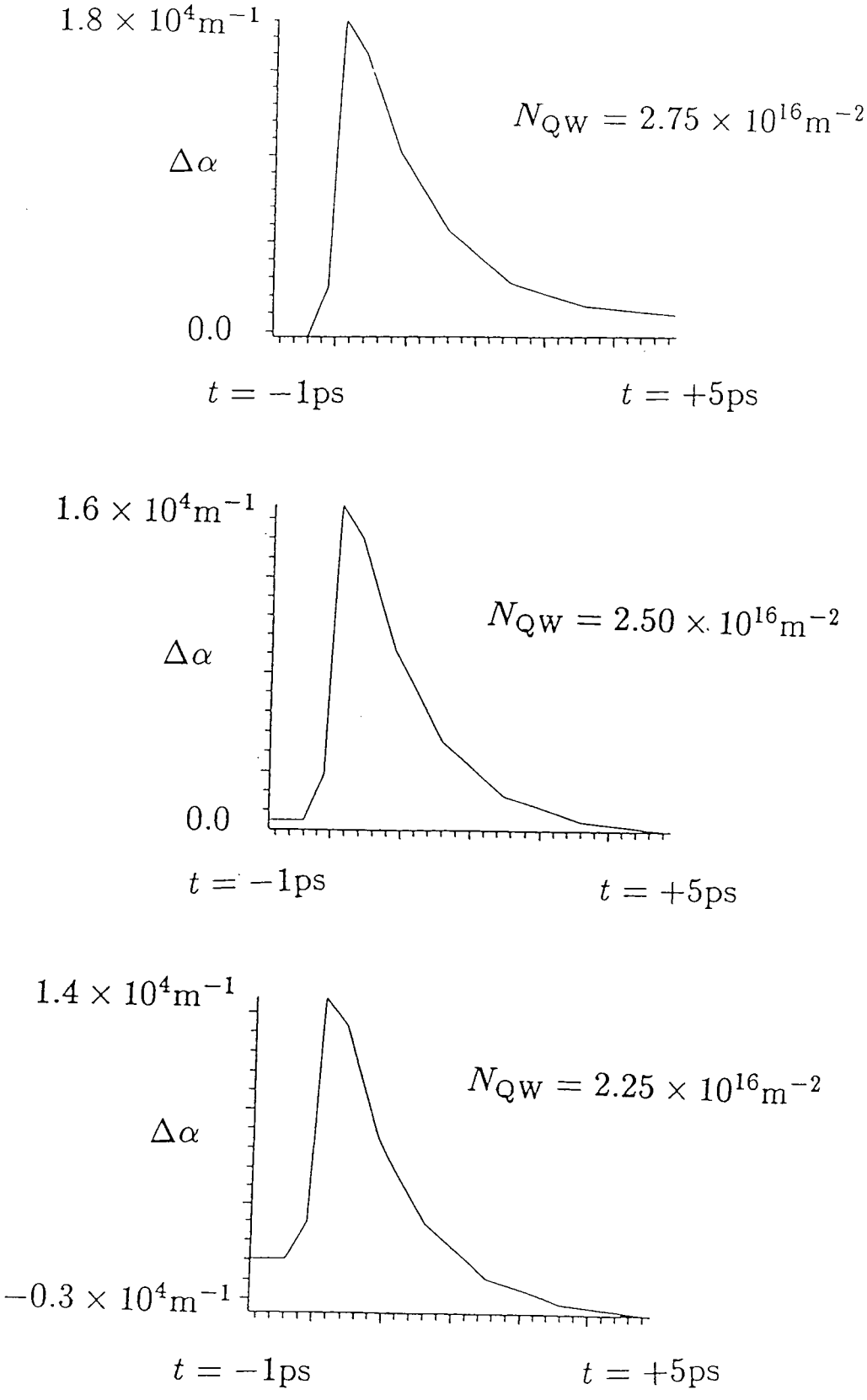

Figure 5.9. The variation of the absorption coefficient experienced by the probe pulse against time delay of the probe relative to the pump.

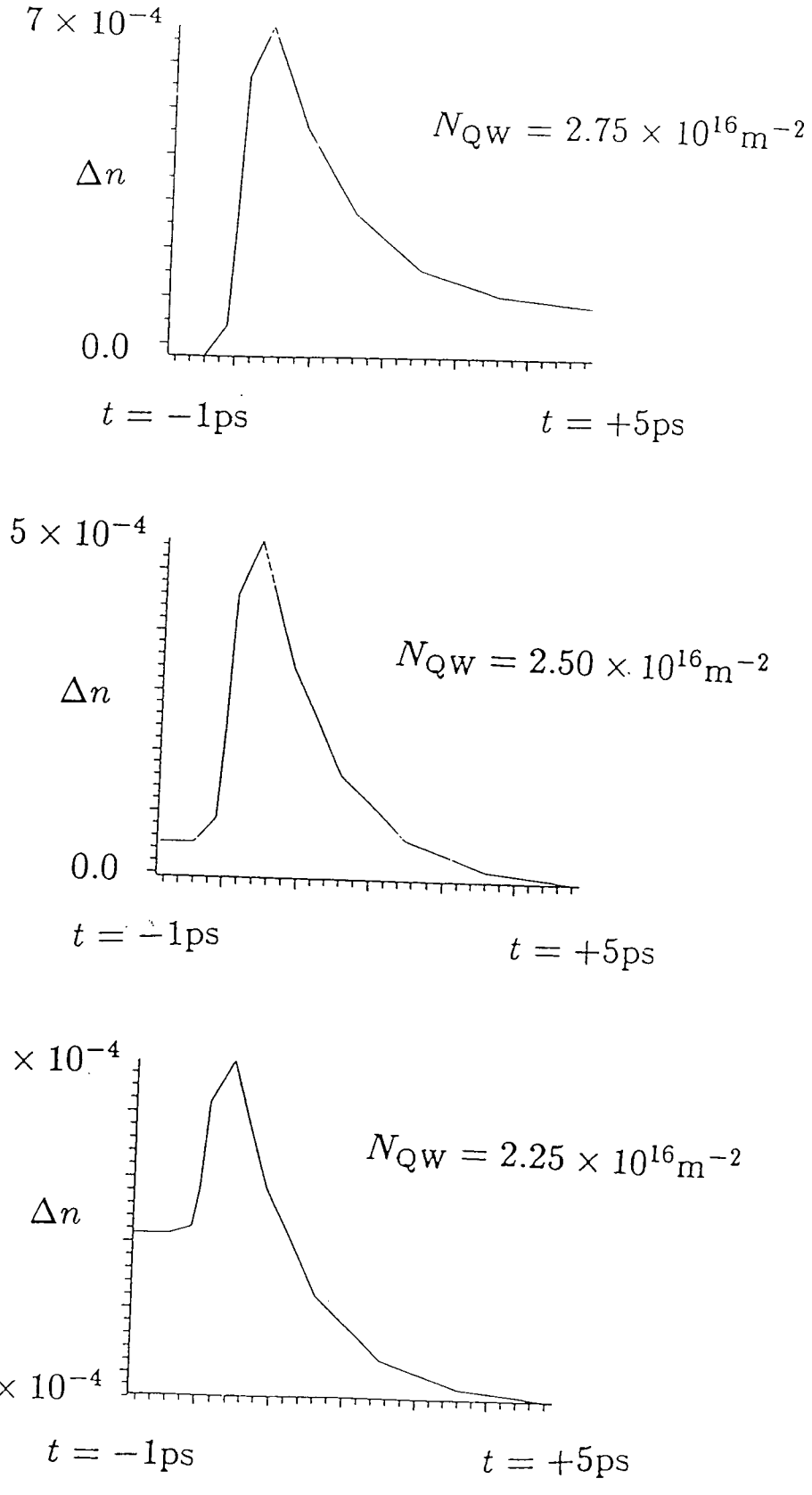

Figure 5.10. The variation of the refractive index experienced by the probe pulse against time delay of the probe relative to the pump.

eration of carriers leads to a decrease in the refractive index whilst a reduction in the number of carriers produces an increase in the refractive index (and that for above-resonance excitation the converse is true). These relationships can also be applied here so that, for example, with an injected carrier density above the transparency value the carrier density is reduced by the pump beam and this leads to a final increase in the refractive index.

The theoretical results may be compared (at least qualitatively) with the experimental measurements of Hultgren and Ippen [53] reproduced in figure 5.11. The figure shows the pulse transmission coefficient and phase shift for propagation through a 300μm AlGaAs diode laser amplifier. All of the features noted above are reproduced in the experimental observations, but there is another feature seen in the experiments which does not appear in the theoretical results presented so far. This is the occurrence of a negative spike in the refractive index at zero time delay. However, this feature is also predicted by the model described here if the photon energy E_p is increased above the bandgap energy E_g so that there is a larger contribution from the absorptive region of the Brillouin zone. The changes in the electron and hole densities near transparency ($N_{\mathrm{QW}} = 2.6 \times 10^{16}\mathrm{m}^{-2}$) are shown in figure 5.12 for the quantum well system with $E_p \simeq 1.03E_g$. An additional feature (cf. figures 5.3 and 5.4) is apparent near $t = 0$ (particularly in the hole distribution) and this is responsible for generating the negative spike in the refractive index before it is destroyed by the carrier-carrier scattering. The absorption

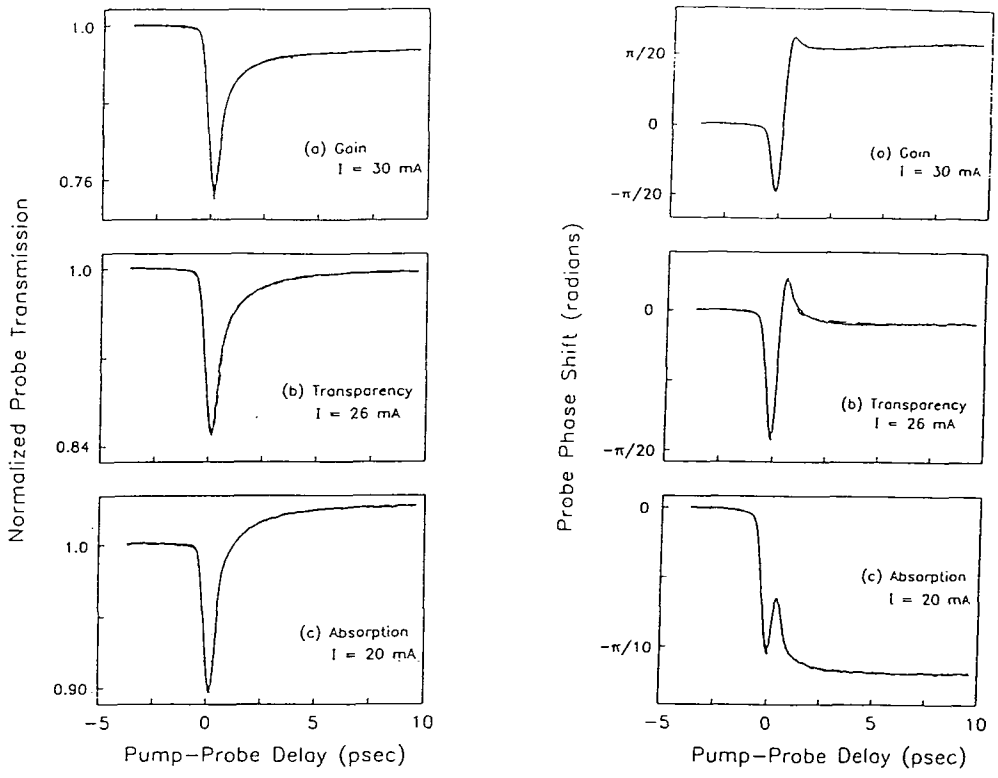

Figure 5.11. Experimental results of Hultgren and Ippen (Appl. Phys. Lett. **59** 635) showing probe transmission coefficient and phase shift for propagation through a 300μm AlGaAs diode laser amplifier.

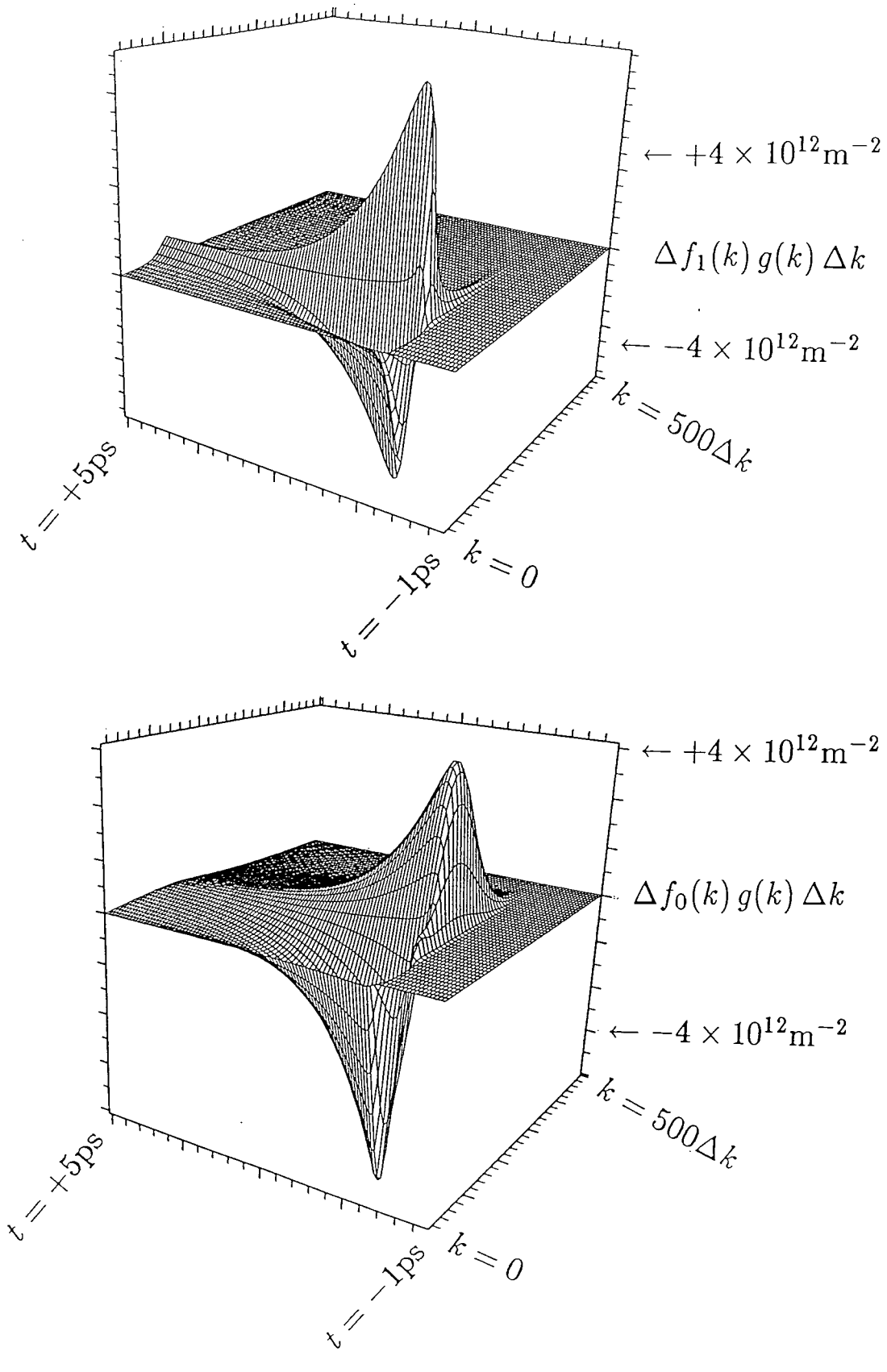

Figure 5.12. The change in quantum well electron (top) and hole (bottom) densities plotted as functions of electronic wavevector k and time t. At each value of k the graphs show the density of carriers with a wavevector in the range k to $k + \Delta k$.

coefficient and refractive index experienced by the probe beam at the new photon energy are shown in figures 5.13 and 5.14 respectively. The theoretical results now display all of the major features exhibited by the experimental observations depicted in figure 5.11.

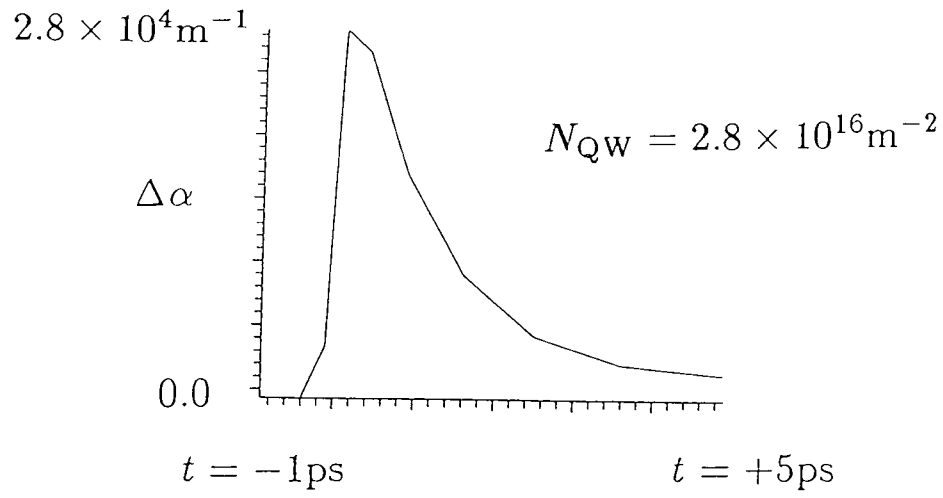

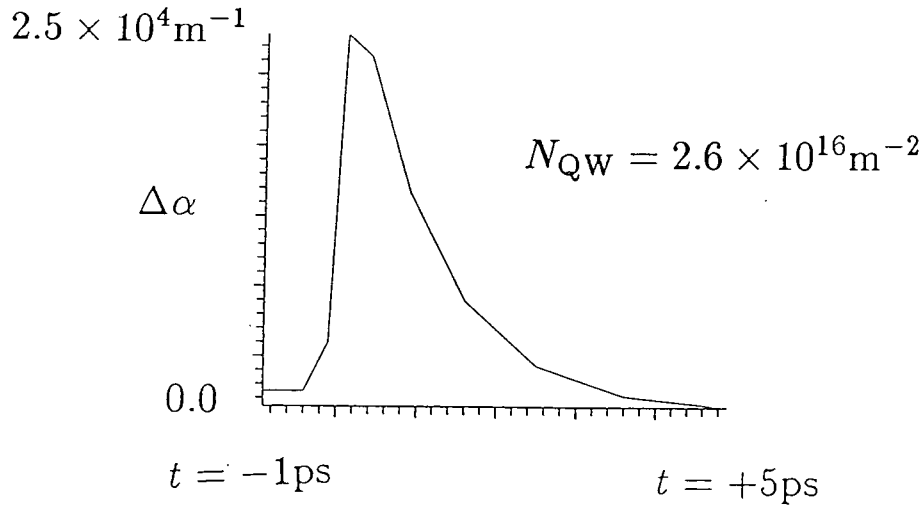

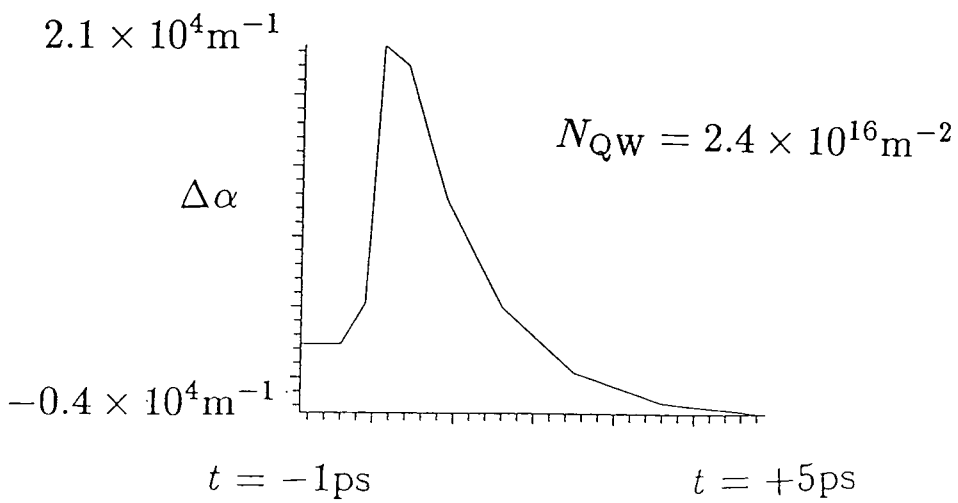

Figure 5.13. The variation of the absorption coefficient experienced by the probe pulse against time delay of the probe relative to the pump.

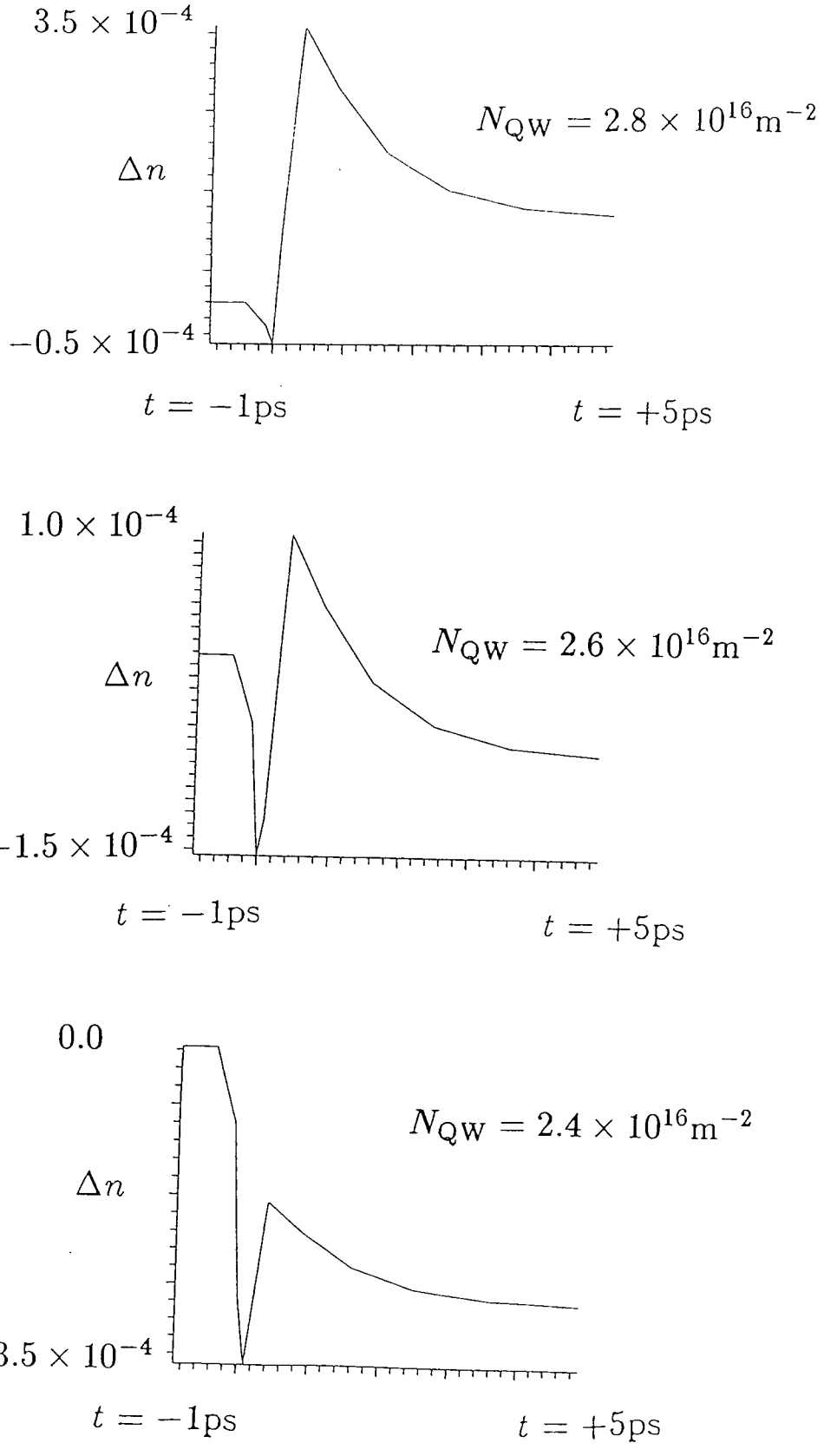

Figure 5.14. The variation of the refractive index experienced by the probe pulse against time delay of the probe relative to the pump.

CHAPTER SIX

The effects of bandstructure on optical response

In previous chapters the ultrafast nonlinear optical response of various semiconductor systems has been examined using a simple parabolic band model for both the valence and conduction bands. Whilst this is a reasonable approximation for the conduction band, the proximity of the heavy and light hole subbands near the valence band edge produces significant mixing of nearby states resulting in a strong non-parabolicity of the energy dispersion for the valence subbands. Further, it has previously been assumed that the optical matrix elements are independent of the in-plane electronic wavevector $\mathbf{k}_{\|}$ and of the orientation of the electric field vector of the illumination. In this chapter two **k.p** based models are described which can provide a more realistic bandstructure. The first model employs an infinite well approximation and has the advantage of being relatively simple to implement computationally, whilst the second model takes into account the penetration of the wavefunctions into the barrier regions that occurs with a finite quantum well. The final section discusses the calculation of optical matrix elements from the wavefunctions obtained using these models and presents a brief investigation into the effects of bandstructure on optical response.

Section 6.1. Infinite well bandstructure.

The two **k.p** models described in this chapter both employ a quantum well of width L grown in the z-direction. The calculations involve the construction of quantum well wavefunctions from linear combinations of bulk wavefunctions. The quantum well bandstructure is determined by fixing the in-plane wavevector $\mathbf{k}_{||}$ and scanning through energy E to find values at which it is possible to construct wavefunctions that satisfy the boundary conditions of the quantum well. The infinite well model described here [66-70] has been developed in collaboration with G. C. Crow. It retains the assumption of parabolic energy dispersion in the conduction band but examines the mixing of light and heavy hole states in the valence band. The spin split-off band is neglected. When the double degeneracy of spin is taken into account this leads to a four band model of the valence subbands. Suppose that X^+, Y^+, Z^+ and X^-, Y^-, Z^- denote p-orbitals oriented along the x-, y- and z-axes with positive and negative spin respectively, then taking the z-axis as the reference direction the basis states

$$u_1 = -\frac{1}{\sqrt{2}}\left(X^+ + iY^+\right) \tag{6.1}$$

$$u_2 = \frac{1}{\sqrt{6}}\left(X^+ - iY^+\right) + \sqrt{\frac{2}{3}}Z^- \tag{6.2}$$

$$u_3 = -\frac{1}{\sqrt{6}}\left(X^- + iY^-\right) + \sqrt{\frac{2}{3}}Z^+ \tag{6.3}$$

$$u_4 = \frac{1}{\sqrt{2}}\left(X^- - iY^-\right) \tag{6.4}$$

represent states with angular momentum quantum numbers $j = 3/2$ and $m_j = \pm 1/2, \pm 3/2$. The **k.p** Hamiltonian in this basis has a full 4×4 matrix but a block

diagonal representation may be obtained through a unitary transformation of the basis set. The new basis $\{v_i\}$ is given by $v_i = T_{mi}u_m$ where [66-68]

$$T = \begin{bmatrix} \alpha & 0 & 0 & \alpha \\ 0 & \beta & \overline{\beta} & 0 \\ 0 & -\overline{\beta} & \overline{\beta} & 0 \\ -\overline{\alpha} & 0 & 0 & \overline{\alpha} \end{bmatrix} \tag{6.5}$$

and

$$\alpha = \frac{1}{\sqrt{2}} \exp\left[i(3\pi/4 - 3\phi/2)\right] \tag{6.6}$$

$$\beta = \frac{1}{\sqrt{2}} \exp\left[i(-\pi/4 + \phi/2)\right] \tag{6.7}$$

with ϕ defining the direction of the in-plane wavevector $\mathbf{k}_{\|} = (k_x, k_y)$ through $k_x = k_{\|}\cos\phi$ and $k_y = k_{\|}\sin\phi$. In the new basis the matrix of the **k.p** Hamiltonian becomes [66-68]

$$H = \begin{bmatrix} H^I & 0 \\ 0 & H^{II} \end{bmatrix} \tag{6.8}$$

with

$$H^I = \frac{\hbar^2}{2m} \begin{bmatrix} (\gamma_1 + \gamma_2)k_{\|}^2 + (\gamma_1 - 2\gamma_2)k_z^2 & (\sqrt{3}/2)\left((\gamma_2 + \gamma_3)k_{\|}^2 - 4i\gamma_3 k_{\|}k_z\right) \\ (\sqrt{3}/2)\left((\gamma_2 + \gamma_3)k_{\|}^2 + 4i\gamma_3 k_{\|}k_z\right) & (\gamma_1 - \gamma_2)k_{\|}^2 + (\gamma_1 + 2\gamma_2)k_z^2 \end{bmatrix} \tag{6.9}$$

and

$$H^{II} = \frac{\hbar^2}{2m} \begin{bmatrix} (\gamma_1 - \gamma_2)k_{\|}^2 + (\gamma_1 + 2\gamma_2)k_z^2 & (\sqrt{3}/2)\left((\gamma_2 + \gamma_3)k_{\|}^2 - 4i\gamma_3 k_{\|}k_z\right) \\ (\sqrt{3}/2)\left((\gamma_2 + \gamma_3)k_{\|}^2 + 4i\gamma_3 k_{\|}k_z\right) & (\gamma_1 + \gamma_2)k_{\|}^2 + (\gamma_1 - 2\gamma_2)k_z^2 \end{bmatrix} \tag{6.10}$$

where $\gamma_1, \gamma_2, \gamma_3$ are the Luttinger parameters [71] and k_z is the perpendicular component of the wavevector. The bulk state $\Psi_j(\mathbf{k}_{\|}, k_z(j))$ at given in-plane wavevector $\mathbf{k}_{\|}$ may be expanded over the basis $\{v_i\}$ as

$$\Psi_j(\mathbf{k}_{\|}, k_z(j)) = \sum_{i=1}^{4} F_{ij} v_i \exp(i\mathbf{k}_{\|}.\mathbf{r}_{\|}) \exp(ik_z(j)z) \qquad \text{for } j = 1, 8 \tag{6.11}$$

where the matrix F_{ij} follows the block diagonal structure of the transformed Hamiltonian so that the states $\Psi_1, \ldots, \Psi_4$ are combinations of the basis states v_1 and v_2 whilst the states $\Psi_5, \ldots, \Psi_8$ are combinations of the basis states v_3 and v_4. The columns $\mathbf{F}_j$ of the matrix F_{ij} are determined by the eigenvalue equations $(H - EI)\mathbf{F}_j = \mathbf{0}$ where H is the Hamiltonian and E is the energy of the state Ψ_j. To obtain a non-zero solution for $\mathbf{F}_j$ requires that $\det(H - EI) = 0$. In the calculation of bulk bandstructure it is usual to fix $\mathbf{k}_{||}$ and k_z and to find E such that the determinant is zero, but here quantum well wavefunctions are constructed from bulk wavefunctions having particular values of $\mathbf{k}_{||}$ and E so that it is more useful to fix $\mathbf{k}_{||}$ and E and to determine k_z. The choice of basis reduces the problem of finding k_z to the solution of two (identical) quadratic equations in k_z^2

$$\begin{aligned}\left[4(\gamma_1^2 - 4\gamma_2^2)\right] k_z^4 + 8\left[(\gamma_1^2 + 2\gamma_2^2 - 6\gamma_3^2)k_{||}^2 - \gamma_1 k^2\right] k_z^2 \\ + \left[\left(4(\gamma_1^2 - \gamma_2^2) - 3(\gamma_2 + \gamma_3)^2\right) k_{||}^4 - 8\gamma_1 k^2 k_{||}^2 + 4k^4\right] = 0 \qquad (6.12)\end{aligned}$$

where $k^2 = 2mE/\hbar^2$. Hence for a fixed value of $\mathbf{k}_{||}$ it is possible to scan through values of energy E and to determine the corresponding values of k_z which are labelled $k_1, \ldots, k_8$ with $k_{j+4} = k_j$.

With the bulk states determined, the quantum well states may be obtained as linear combinations of the bulk states at the chosen in-plane wavevector $\mathbf{k}_{||}$

$$\begin{aligned}\Psi &= \sum_{j=1}^{8} A_j \Psi_j \\ &= \exp(i\mathbf{k}_{||}.\mathbf{r}_{||}) \sum_{i=1}^{4} \sum_{j=1}^{8} F_{ij} A_j v_i \exp(ik_j z) \qquad (6.13)\end{aligned}$$

There are two independent solutions for the vector A_j corresponding to two energy degenerate states. The block diagonal structure of the matrix F allows the first solution to be chosen as a combination of the states $\Psi_1, \ldots, \Psi_4$ whilst the second solution is taken to be a combination of the states $\Psi_5, \ldots, \Psi_8$. Thus

$$\Psi^I = \sum_{j=1}^{4} A_j \Psi_j \tag{6.14}$$

and

$$\Psi^{II} = \sum_{j=5}^{8} A_j \Psi_j \tag{6.15}$$

In the infinite well approximation there is no penetration of the wavefunctions into the barriers so that $\Psi^I(\pm L/2) = 0$ and $\Psi^{II}(\pm L/2) = 0$ where L is the well width. Hence requiring that the coefficients of each v_i should separately vanish gives

$$\sum_{j=1}^{4} F_{ij} A_j \exp\left(\pm i k_j L/2\right) = 0 \qquad \text{for } i = 1, 2 \tag{6.16}$$

and

$$\sum_{j=5}^{8} F_{ij} A_j \exp\left(\pm i k_j L/2\right) = 0 \qquad \text{for } i = 3, 4 \tag{6.17}$$

Each of equations (6.16) and (6.17) leads to a set of four linear equations in the coefficients A_j which may be expressed in matrix form as $M\mathbf{A} = \mathbf{0}$ with

$$M = \begin{bmatrix} F_{11}\exp(ik_1L/2) & F_{12}\exp(ik_2L/2) & F_{13}\exp(ik_3L/2) & F_{14}\exp(ik_4L/2) \\ F_{21}\exp(ik_1L/2) & F_{22}\exp(ik_2L/2) & F_{23}\exp(ik_3L/2) & F_{24}\exp(ik_4L/2) \\ F_{11}\exp(-ik_1L/2) & F_{12}\exp(-ik_2L/2) & F_{13}\exp(-ik_3L/2) & F_{14}\exp(-ik_4L/2) \\ F_{21}\exp(-ik_1L/2) & F_{22}\exp(-ik_2L/2) & F_{23}\exp(-ik_3L/2) & F_{24}\exp(-ik_4L/2) \end{bmatrix} \tag{6.18}$$

for equation (6.16) and similarly for equation (6.17) but with k_{j+4} and $F_{3,j+4}$ and $F_{4,j+4}$ replacing k_j and F_{1j} and F_{2j} respectively. Now except at the zone

centre where the basis states are decoupled it is possible to set $F_{1j} = 1$ and to define $F_j \equiv F_{2j}$ (or to set $F_{3j} = 1$ and to define $F_j \equiv F_{4j}$). Also by ordering the wavevectors k_z so that $k_{j+2} = -k_j$ the value of $\det M$ may be obtained from equation (6.18) as

$$\begin{aligned} \det M = & \, 2\left(F_1 - F_2\right)\left(F_3 - F_4\right)\cos\left[\left(k_1 + k_2\right)L\right] \\ & + 2\left(F_1 - F_3\right)\left(F_4 - F_2\right) \\ & + 2\left(F_1 - F_4\right)\left(F_2 - F_3\right)\cos\left[\left(k_1 - k_2\right)L\right] \end{aligned} \tag{6.19}$$

A point on the quantum well bandstructure may be found by scanning through energy E at a fixed in-plane wavevector $\mathbf{k}_{\|}$ to find values of E for which $\det M = 0$. When a bandstructure point has been found the corresponding wavefunctions may be determined by calculating the A_j coefficients. Firstly choose the indices $\{\alpha, \beta, \gamma, \delta\} = \{1, 2, 3, 4\}$ for the wavefunction Ψ_I or choose the indices $\{\alpha, \beta, \gamma, \delta\} = \{5, 6, 7, 8\}$ for the wavefunction Ψ_{II}. Then set $A_\delta = 1$ and calculate A_α (and equivalently A_β and A_γ) using the formula

$$A_\alpha = -\frac{\left(F_\gamma - F_\delta\right)\sin\left[\left(k_\beta - k_\delta\right)L/2\right]}{\left(F_\gamma - F_\alpha\right)\sin\left[\left(k_\beta - k_\alpha\right)L/2\right]} \tag{6.20}$$

which is obtained from equation (6.16) or (6.17) by elimination. Now transforming back to the original basis $\{u_i\}$ and defining G^I_{ij} and G^{II}_{ij} by

$$\Psi^I = \exp(i\mathbf{k}_{\|}.\mathbf{r}_{\|}) \sum_{i=1}^{4}\sum_{j=1}^{4} G^I_{ij} u_i \exp(ik_j z) \tag{6.21}$$

and

$$\Psi^{II} = \exp(i\mathbf{k}_{\|}.\mathbf{r}_{\|}) \sum_{i=1}^{4} \sum_{j=1}^{4} G_{ij}^{II} u_i \exp(ik_j z) \tag{6.22}$$

the wavefunctions Ψ^I and Ψ^{II} may be combined to give definite parity states

$$\Psi = \exp(i\mathbf{k}_{\|}.\mathbf{r}_{\|}) \sum_{i=1}^{4} \sum_{j=1}^{4} G_{ij} u_i \exp(ik_j z) \tag{6.23}$$

So suppose that the envelope functions are defined as

$$\Phi_i^I = \sum_{j=1}^{4} G_{ij}^I \exp(ik_j z) \tag{6.24}$$

$$\Phi_i^{II} = \sum_{j=1}^{4} G_{ij}^{II} \exp(ik_j z) \tag{6.25}$$

then definite parity envelopes are obtained from the combinations

$$\Phi_i^{\text{even}} = \lambda_i^{\text{even}} \Phi_i^I + \mu_i^{\text{even}} \Phi_i^{II} \tag{6.26}$$

$$\Phi_i^{\text{odd}} = \lambda_i^{\text{odd}} \Phi_i^I + \mu_i^{\text{odd}} \Phi_i^{II} \tag{6.27}$$

by ensuring that $\Phi_i^{\text{even}}(z) = \Phi_i^{\text{even}}(-z)$ and $\Phi_i^{\text{odd}}(z) = -\Phi_i^{\text{odd}}(-z)$. In fact the envelopes form two parity sets $P_1 = \{\Phi_1, \Phi_2\}$ and $P_2 = \{\Phi_3, \Phi_4\}$ such that the ratios $\mu_i^{\text{even}}/\lambda_i^{\text{even}}$ and $\mu_i^{\text{odd}}/\lambda_i^{\text{odd}}$ depend only on whether $\Phi_i \in P_1$ or $\Phi_i \in P_2$. Further if $\Phi_i \in P_1$ and $\Phi_{i'} \in P_2$ then

$$\mu_i^{\text{even}}/\lambda_i^{\text{even}} = \mu_{i'}^{\text{odd}}/\lambda_{i'}^{\text{odd}} \tag{6.28}$$

and

$$\mu_i^{\text{odd}}/\lambda_i^{\text{odd}} = \mu_{i'}^{\text{even}}/\lambda_{i'}^{\text{even}} \tag{6.29}$$

Thus definite parity states Ψ may be obtained with the envelopes Φ_1 and Φ_2 of even parity and the envelopes Φ_3 and Φ_4 of odd parity, or vice versa. The wavefunction

Ψ is normalised using

$$\langle \Psi | \Psi \rangle = A_{\|} \sum_{i=1}^{4} \sum_{j=1}^{4} \sum_{j'=1}^{4} \overline{G}_{ij} G_{ij'} L_{jj'} \tag{6.30}$$

where

$$\begin{aligned} L_{jj'} &= \int_{-L/2}^{+L/2} \exp\left[i(k_{j'} - \overline{k}_j)z\right] dz \\ &= L \operatorname{sinc}\left[(k_{j'} - \overline{k}_j)L/2\right] \end{aligned} \tag{6.31}$$

and $A_{\|} = \int d\mathbf{r}_{\|}$ is the cross-sectional area of the quantum well. From these definite parity wavefunctions the optical matrix elements of the quantum well may be calculated as discussed in section 6.4.

Section 6.2. Finite well bandstructure.

In the finite well model the wavefunctions extend from the well region into the barrier regions so that it is necessary to consider the form of the wavefunctions in each of these regions and to determine the matching conditions which must be met at the interfaces between them. With simplicity no longer paramount it is appropriate to extend the model from four to eight bands with the inclusion of the spin split-off and conduction bands in addition to the light and heavy hole bands. The model presented here develops the earlier work of Wood [72]. The same procedure is used to calculate the bulk wavefunctions as for the infinite well model

$$\Psi_j(\mathbf{k}_\parallel, k_z(j)) = \sum_{i=1}^{8} F_{ij} u_i \exp(i\mathbf{k}_\parallel.\mathbf{r}_\parallel) \exp(ik_z(j)z) \qquad \text{for } j = 1,16 \qquad (6.32)$$

where the basis states

$$u_1 = S^+ \qquad (6.33)$$

$$u_2 = \frac{1}{\sqrt{2}}(X^+ + iY^+) \qquad (6.34)$$

$$u_3 = \frac{1}{\sqrt{6}}(X^- + iY^-) - \sqrt{\frac{2}{3}}Z^+ \qquad (6.35)$$

$$u_4 = \frac{1}{\sqrt{3}}(X^- + iY^-) + \sqrt{\frac{1}{3}}Z^+ \qquad (6.36)$$

$$u_5 = S^- \qquad (6.37)$$

$$u_6 = \frac{1}{\sqrt{2}}(X^- - iY^-) \qquad (6.38)$$

$$u_7 = -\frac{1}{\sqrt{6}}(X^+ - iY^+) - \sqrt{\frac{2}{3}}Z^- \qquad (6.39)$$

$$u_8 = -\frac{1}{\sqrt{3}}(X^+ - iY^+) + \sqrt{\frac{1}{3}}Z^- \qquad (6.40)$$

of the well and barrier materials are expressed in terms of the appropriate p-orbitals $X^{\pm}, Y^{\pm}, Z^{\pm}$ and s-orbitals $S^{\pm}$. The additions to the basis set u_1, u_5 and u_4, u_8 are the zone centre conduction states and spin split-off states respectively. Now in comparison to the infinite well calculations it is rather more difficult to determine the values of k_z corresponding to given values of energy E and in-plane wavevector $\mathbf{k}_{\|}$. The columns $\mathbf{F}_j$ of the matrix F_{ij} may be determined from the matrix equation

$$(H_2 k_z^2 + H_1 k_z + H_0 - EI)\mathbf{F}_j = \mathbf{0} \tag{6.41}$$

where the Hamiltonian H has been written to explicitly show its dependence on the powers of k_z. Together with the trivial relation $k_z\mathbf{F}_j = k_z\mathbf{F}_j$ this equation may be rewritten in the form

$$\begin{bmatrix} 0 & 1 \\ -H_2^{-1}(H_0 - EI) & -H_2^{-1}H_1 \end{bmatrix} \begin{bmatrix} \mathbf{F}_j \\ k_z\mathbf{F}_j \end{bmatrix} = k_z \begin{bmatrix} \mathbf{F}_j \\ k_z\mathbf{F}_j \end{bmatrix} \tag{6.42}$$

which is an eigenvalue problem for k_z that can be solved by the usual methods. The matrix $-H_2^{-1}$ is block diagonal

$$-H_2^{-1} = \begin{bmatrix} H_{\text{block}} & 0 \\ 0 & H_{\text{block}} \end{bmatrix} \tag{6.43}$$

where

$$H_{\text{block}} = \frac{2m}{\hbar^2}\begin{bmatrix} H_{\text{inv}}^{(1)} & 0 & 0 & 0 \\ 0 & H_{\text{inv}}^{(2)} & 0 & 0 \\ 0 & 0 & H_{\text{inv}}^{(3)} & H_{\text{inv}}^{(5)} \\ 0 & 0 & H_{\text{inv}}^{(5)} & H_{\text{inv}}^{(4)} \end{bmatrix} \tag{6.44}$$

The components of H_{block} are given by the relations

$$H_{\text{inv}}^{(0)} = (\gamma_1 + 4\gamma_2)^{-1} \tag{6.45}$$

$$H_{\text{inv}}^{(1)} = -s^{-1} \tag{6.46}$$

$$H_{\text{inv}}^{(2)} = (\gamma_1 - 2\gamma_2)^{-1} \tag{6.47}$$

$$H_{\text{inv}}^{(3)} = \gamma_1 H_{\text{inv}}^{(0)} H_{\text{inv}}^{(2)} \tag{6.48}$$

$$H_{\text{inv}}^{(4)} = (\gamma_1 + 2\gamma_2) H_{\text{inv}}^{(0)} H_{\text{inv}}^{(2)} \tag{6.49}$$

$$H_{\text{inv}}^{(5)} = 2\sqrt{2}\gamma_2 H_{\text{inv}}^{(0)} H_{\text{inv}}^{(2)} \tag{6.50}$$

where s is the conduction band s-parameter and $\gamma_1, \gamma_2, \gamma_3$ are modified Luttinger parameters [73,74] which explicitly include the influence of the conduction band in the Hamiltonian. The product matrix $-H_2^{-1}H_0$ may be written as the sum of a block diagonal matrix with

$$H_{\text{block}} = \frac{2m}{\hbar^2}\begin{bmatrix} E_g H_{\text{inv}}^{(1)} & 0 & 0 & 0 \\ 0 & 0 & 0 & 0 \\ 0 & 0 & 0 & -\Delta H_{\text{inv}}^{(5)} \\ 0 & 0 & 0 & -\Delta H_{\text{inv}}^{(4)} \end{bmatrix} \tag{6.51}$$

which is independent of $\mathbf{k}_{\|} = (k_x, k_y)$ plus the product matrix $-H_2^{-1}\tilde{H}_0$ shown overleaf.

$$-H_2^{-1}\tilde{H}_0 =$$

$$\left[\begin{array}{cccc}
s|k_{\rm par}|^2 H_{\rm inv}^{(1)} & \sqrt{\tfrac{1}{2}}i\alpha P k_{\rm par} H_{\rm inv}^{(1)} & 0 & 0 \\
-\sqrt{\tfrac{1}{2}}i\alpha P \bar{k}_{\rm par} H_{\rm inv}^{(2)} & -(\gamma_1+\gamma_2)|k_{\rm par}|^2 H_{\rm inv}^{(2)} & 0 & 0 \\
0 & 0 & |k_{\rm par}|^2\left(-\gamma_1 H_{\rm inv}^{(0)} - \gamma_2 H_{\rm inv}^{(2)}\right) & -3\sqrt{2}\gamma_1\gamma_2|k_{\rm par}|^2 H_{\rm inv}^{(0)} H_{\rm inv}^{(2)} \\
0 & 0 & -3\sqrt{2}\gamma_1\gamma_2|k_{\rm par}|^2 H_{\rm inv}^{(0)} H_{\rm inv}^{(2)} & |k_{\rm par}|^2\left(-\gamma_1 H_{\rm inv}^{(2)} + 2\gamma_2 H_{\rm inv}^{(0)}\right) \\
0 & 0 & \sqrt{\tfrac{1}{6}}i\alpha P k_{\rm par} H_{\rm inv}^{(1)} & \sqrt{\tfrac{1}{3}}i\alpha P k_{\rm par} H_{\rm inv}^{(1)} \\
0 & 0 & \sqrt{3}\big(-\gamma_2 \Re{\rm e}\, k_{\rm par}^2 & \sqrt{6}\big(-\gamma_2 \Re{\rm e}\, k_{\rm par}^2 \\
 & & -i\gamma_3 \Im{\rm m}\, k_{\rm par}^2\big) H_{\rm inv}^{(2)} & -i\gamma_3 \Im{\rm m}\, k_{\rm par}^2\big) H_{\rm inv}^{(2)} \\
\sqrt{\tfrac{1}{6}}i\alpha P k_{\rm par} H_{\rm inv}^{(2)} & \sqrt{3}\big(\gamma_2 \Re{\rm e}\, k_{\rm par}^2 & 0 & 0 \\
 & +i\gamma_3 \Im{\rm m}\, k_{\rm par}^2\big) H_{\rm inv}^{(2)} & & \\
\sqrt{\tfrac{1}{3}}i\alpha P k_{\rm par} H_{\rm inv}^{(2)} & \sqrt{6}\big(\gamma_2 \Re{\rm e}\, k_{\rm par}^2 & 0 & 0 \\
 & +i\gamma_3 \Im{\rm m}\, k_{\rm par}^2\big) H_{\rm inv}^{(2)} & &
\end{array}\right.$$

$$\left.\begin{array}{cccc}
0 & 0 & -\sqrt{\tfrac{1}{6}}i\alpha P \bar{k}_{\rm par} H_{\rm inv}^{(1)} & -\sqrt{\tfrac{1}{3}}i\alpha P \bar{k}_{\rm par} H_{\rm inv}^{(1)} \\
0 & 0 & \sqrt{3}\big(\gamma_2 \Re{\rm e}\, k_{\rm par}^2 & \sqrt{6}\big(\gamma_2 \Re{\rm e}\, k_{\rm par}^2 \\
 & & -i\gamma_3 \Im{\rm m}\, k_{\rm par}^2\big) H_{\rm inv}^{(2)} & -i\gamma_3 \Im{\rm m}\, k_{\rm par}^2\big) H_{\rm inv}^{(2)} \\
-\sqrt{\tfrac{1}{6}}i\alpha P \bar{k}_{\rm par} H_{\rm inv}^{(2)} & \sqrt{3}\big(-\gamma_2 \Re{\rm e}\, k_{\rm par}^2 & 0 & 0 \\
 & +i\gamma_3 \Im{\rm m}\, k_{\rm par}^2\big) H_{\rm inv}^{(2)} & & \\
-\sqrt{\tfrac{1}{3}}i\alpha P \bar{k}_{\rm par} H_{\rm inv}^{(2)} & \sqrt{6}\big(-\gamma_2 \Re{\rm e}\, k_{\rm par}^2 & 0 & 0 \\
 & +i\gamma_3 \Im{\rm m}\, k_{\rm par}^2\big) H_{\rm inv}^{(2)} & & \\
s|k_{\rm par}|^2 H_{\rm inv}^{(1)} & \sqrt{\tfrac{1}{2}}i\alpha P \bar{k}_{\rm par} H_{\rm inv}^{(1)} & 0 & 0 \\
-\sqrt{\tfrac{1}{2}}i\alpha P k_{\rm par} H_{\rm inv}^{(2)} & -(\gamma_1+\gamma_2)|k_{\rm par}|^2 H_{\rm inv}^{(2)} & 0 & 0 \\
0 & 0 & |k_{\rm par}|^2\left(-\gamma_1 H_{\rm inv}^{(0)} - \gamma_2 H_{\rm inv}^{(2)}\right) & -3\sqrt{2}\gamma_1\gamma_2|k_{\rm par}|^2 H_{\rm inv}^{(0)} H_{\rm inv}^{(2)} \\
0 & 0 & -3\sqrt{2}\gamma_1\gamma_2|k_{\rm par}|^2 H_{\rm inv}^{(0)} H_{\rm inv}^{(2)} & |k_{\rm par}|^2\left(-\gamma_1 H_{\rm inv}^{(2)} + 2\gamma_2 H_{\rm inv}^{(0)}\right)
\end{array}\right] \qquad (6.52)$$

where $\alpha = 2m/\hbar^2$ and $k_{\rm par}$ is the complex quantity $k_{\rm par} = k_x + ik_y$. The constant E_g is the bandgap energy, Δ is the spin orbit splitting and P is the Kane momentum parameter [75] with $P = -(i\hbar/m)\langle S^+|p^x|X^+\rangle$. Similarly the product matrix $-H_2^{-1}H_1$ can be written as the sum of a block diagonal matrix with

$$H_{\rm block} = \frac{2m}{\hbar^2}\begin{bmatrix} 0 & 0 & -\sqrt{\frac{2}{3}}iPH_{\rm inv}^{(1)} & \sqrt{\frac{1}{3}}iPH_{\rm inv}^{(1)} \\ 0 & 0 & 0 & 0 \\ \sqrt{\frac{2}{3}}iPH_{\rm inv}^{(0)} & 0 & 0 & 0 \\ -\sqrt{\frac{1}{3}}iPH_{\rm inv}^{(0)} & 0 & 0 & 0 \end{bmatrix} \tag{6.53}$$

which is independent of $\mathbf{k}_{\|}$ plus the product matrix

$$-H_2^{-1}\tilde{H}_1 = \begin{bmatrix} 0 & 0 & 0 & 0 \\ 0 & 0 & 2\sqrt{3}\gamma_3\overline{k}_{\rm par}H_{\rm inv}^{(2)} & -\sqrt{6}\gamma_3\overline{k}_{\rm par}H_{\rm inv}^{(2)} \\ 0 & 2\sqrt{3}\gamma_3 k_{\rm par}H_{\rm inv}^{(0)} & 0 & 0 \\ 0 & -\sqrt{6}\gamma_3 k_{\rm par}H_{\rm inv}^{(0)} & 0 & 0 \\ 0 & 0 & 0 & 0 \\ 0 & 0 & 0 & 0 \\ 0 & 0 & -3\sqrt{2}\gamma_3 k_{\rm par}H_{\rm inv}^{(5)} & 3\sqrt{2}\gamma_3 k_{\rm par}H_{\rm inv}^{(3)} \\ 0 & 0 & -3\sqrt{2}\gamma_3 k_{\rm par}H_{\rm inv}^{(4)} & 3\sqrt{2}\gamma_3 k_{\rm par}H_{\rm inv}^{(5)} \end{bmatrix} \cdots$$

$$\cdots \begin{bmatrix} 0 & 0 & 0 & 0 \\ 0 & 0 & 0 & 0 \\ 0 & 0 & 3\sqrt{2}\gamma_3\overline{k}_{\rm par}H_{\rm inv}^{(5)} & -3\sqrt{2}\gamma_3\overline{k}_{\rm par}H_{\rm inv}^{(3)} \\ 0 & 0 & 3\sqrt{2}\gamma_3\overline{k}_{\rm par}H_{\rm inv}^{(4)} & -3\sqrt{2}\gamma_3\overline{k}_{\rm par}H_{\rm inv}^{(5)} \\ 0 & 0 & 0 & 0 \\ 0 & 0 & 2\sqrt{3}\gamma_3 k_{\rm par}H_{\rm inv}^{(2)} & -\sqrt{6}\gamma_3 k_{\rm par}H_{\rm inv}^{(2)} \\ 0 & 2\sqrt{3}\gamma_3\overline{k}_{\rm par}H_{\rm inv}^{(0)} & 0 & 0 \\ 0 & -\sqrt{6}\gamma_3\overline{k}_{\rm par}H_{\rm inv}^{(0)} & 0 & 0 \end{bmatrix} \tag{6.54}$$

The bulk wavefunctions for the well and barrier materials may be obtained from the eigenvector equation (6.42). As the barriers are semi-infinite in extent a restriction must be placed on the bulk solutions used in each barrier and only those wavefunctions whose k_z value ensures a decay with distance from the well are retained. The set of sixteen values of k_z derived from the eigenvalue problem are

thus separated into two sets of eight, one set for each of the barriers on either side of the well. The wavevectors on the negative z side of the well have $\Im\mathrm{m}\, k_z < 0$ and are labelled $k_1^B, \ldots, k_8^B$ whilst those on the positive z side of the well have $\Im\mathrm{m}\, k_z > 0$ and are labelled $k_9^B, \ldots, k_{16}^B$. A similar division of k_z values is also made in the well region with the set of wavevectors for which $\Im\mathrm{m}\, k_z \geq 0$ being labelled $k_1^W, \ldots, k_{j_{\mathrm{mid}}}^W$ and those for which $\Im\mathrm{m}\, k_z < 0$ being labelled $k_{j_{\mathrm{mid}}+1}^W, \ldots, k_{16}^W$. This division is made to assist in the avoidance of a numerical problem which is further discussed in section 6.3. With the well extending from $z = z_{\mathrm{left}}$ to $z = z_{\mathrm{right}}$, the barrier wavefunctions $\Psi_{\mathrm{left}}(z \leq z_{\mathrm{left}})$ and $\Psi_{\mathrm{right}}(z \geq z_{\mathrm{right}})$ and the well wavefunction $\Psi_{\mathrm{well}}(z_{\mathrm{left}} \leq z \leq z_{\mathrm{right}})$ may be written in the form

$$\Psi_{\mathrm{left}} = \exp(i\mathbf{k}_{\|}.\mathbf{r}_{\|}) \sum_{i=1}^{8} \sum_{j=1}^{8} \exp\left[ik_j^B (z - z_{\mathrm{left}})\right] F_{ij}^B A_j^B u_i \tag{6.55}$$

$$\Psi_{\mathrm{right}} = \exp(i\mathbf{k}_{\|}.\mathbf{r}_{\|}) \sum_{i=1}^{8} \sum_{j=9}^{16} \exp\left[ik_j^B (z - z_{\mathrm{right}})\right] F_{ij}^B A_j^B u_i \tag{6.56}$$

$$\begin{aligned}\Psi_{\mathrm{well}} = {} & \exp(i\mathbf{k}_{\|}.\mathbf{r}_{\|}) \sum_{i=1}^{8} \sum_{j=1}^{j_{\mathrm{mid}}} \exp\left[ik_j^W (z - z_{\mathrm{left}})\right] F_{ij}^W A_j^W u_i \\ & + \exp(i\mathbf{k}_{\|}.\mathbf{r}_{\|}) \sum_{i=1}^{8} \sum_{j=j_{\mathrm{mid}}+1}^{16} \exp\left[ik_j^W (z - z_{\mathrm{right}})\right] F_{ij}^W A_j^W u_i\end{aligned} \tag{6.57}$$

where the superscripts B and W denote values in the barrier and well respectively.

The first boundary matching condition is that the wavefunctions match at the two interfaces so that $\Psi_{\mathrm{left}}(z_{\mathrm{left}}) = \Psi_{\mathrm{well}}(z_{\mathrm{left}})$ and $\Psi_{\mathrm{right}}(z_{\mathrm{right}}) = \Psi_{\mathrm{well}}(z_{\mathrm{right}})$. Thus assuming that the basis states u_i (for $i = 1$ to 8) are comparable in the well and barrier materials

$$\sum_{j=1}^{8} F_{ij}^B A_j^B = \sum_{j=1}^{j_{\mathrm{mid}}} F_{ij}^W A_j^W + \sum_{j=j_{\mathrm{mid}}+1}^{16} F_{ij}^W A_j^W \exp\left(-ik_j^W L\right) \tag{6.58}$$

$$\sum_{j=9}^{16} F_{ij}^{B} A_j^{B} = \sum_{j=1}^{j_{\mathrm{mid}}} F_{ij}^{W} A_j^{W} \exp\left(ik_j^{W} L\right) + \sum_{j=j_{\mathrm{mid}}+1}^{16} F_{ij}^{W} A_j^{W} \tag{6.59}$$

where $L = z_{\mathrm{right}} - z_{\mathrm{left}}$ is the well width. The second boundary condition is that the derivatives of the wavefunctions with respect to z match at the interfaces. With one complete basis set applicable to both materials this is satisfied if the derivatives of the envelope functions match at the interfaces [76], and although used in conjunction with two incomplete basis sets the relations

$$\sum_{j=1}^{8} D_{ij}^{B} A_j^{B} = \sum_{j=1}^{j_{\mathrm{mid}}} D_{ij}^{W} A_j^{W} + \sum_{j=j_{\mathrm{mid}}+1}^{16} D_{ij}^{W} A_j^{W} \exp\left(-ik_j^{W} L\right) \tag{6.60}$$

$$\sum_{j=9}^{16} D_{ij}^{B} A_j^{B} = \sum_{j=1}^{j_{\mathrm{mid}}} D_{ij}^{W} A_j^{W} \exp\left(ik_j^{W} L\right) + \sum_{j=j_{\mathrm{mid}}+1}^{16} D_{ij}^{W} A_j^{W} \tag{6.61}$$

are nevertheless applied here with $D_{ij} = ik_j F_{ij}$. Indeed calculations with other matching conditions [72] suggest that the exact choice of the derivative matching condition does not have much effect on those subbands employed in section 6.4 for the calculation of optical matrix elements. The equations (6.58) to (6.61) may be written in a more compact matrix form

$$F_B \mathbf{A}_B = F_W \mathbf{A}_W \tag{6.62}$$

$$D_B \mathbf{A}_B = D_W \mathbf{A}_W \tag{6.63}$$

where

$$F_B = \begin{bmatrix} F_{ij}^{B}\left(\substack{i=1,8 \\ j=1,8}\right) & 0 \\ 0 & F_{ij}^{B}\left(\substack{i=1,8 \\ j=9,16}\right) \end{bmatrix} \tag{6.64}$$

and

$$F_W = \begin{bmatrix} F_{ij}^{W}\left(\substack{i=1,8 \\ j=1,j_{\mathrm{mid}}}\right) & F_{ij}^{W} \exp(-ik_j^{W} L)\left(\substack{i=1,8 \\ j=j_{\mathrm{mid}}+1,16}\right) \\ F_{ij}^{W} \exp(ik_j^{W} L)\left(\substack{i=1,8 \\ j=1,j_{\mathrm{mid}}}\right) & F_{ij}^{W}\left(\substack{i=1,8 \\ j=j_{\mathrm{mid}}+1,16}\right) \end{bmatrix} \tag{6.65}$$

and similarly for D_B and D_W. The two boundary matching equations (6.62) and (6.63) may be combined to give

$$F_W^{-1} F_B D_B^{-1} D_W \mathbf{A}_W = \mathbf{A}_W \tag{6.66}$$

and by defining $M = F_W^{-1} F_B D_B^{-1} D_W - I$ the bandstructure at a given value of in-plane wavevector $\mathbf{k}_\parallel$ may be determined by scanning through energy E and looking for $\det M = 0$ as in the case of the infinite quantum well model. This produces doubly degenerate states Ψ^I and Ψ^{II} which may be combined to obtain definite parity states of the form

$$\Psi_{\text{left}} = \exp(i\mathbf{k}_\parallel.\mathbf{r}_\parallel) \sum_{i=1}^{8} \sum_{j=1}^{8} \exp\left[ik_j^B(z - z_{\text{left}})\right] G_{ij}^B u_i \tag{6.67}$$

$$\Psi_{\text{right}} = \exp(i\mathbf{k}_\parallel.\mathbf{r}_\parallel) \sum_{i=1}^{8} \sum_{j=9}^{16} \exp\left[ik_j^B(z - z_{\text{right}})\right] G_{ij}^B u_i \tag{6.68}$$

$$\begin{aligned}\Psi_{\text{well}} = {} & \exp(i\mathbf{k}_\parallel.\mathbf{r}_\parallel) \sum_{i=1}^{8} \sum_{j=1}^{j_{\text{mid}}} \exp\left[ik_j^W(z - z_{\text{left}})\right] G_{ij}^W u_i \\ & + \exp(i\mathbf{k}_\parallel.\mathbf{r}_\parallel) \sum_{i=1}^{8} \sum_{j=j_{\text{mid}}+1}^{16} \exp\left[ik_j^W(z - z_{\text{right}})\right] G_{ij}^W u_i\end{aligned} \tag{6.69}$$

As with the infinite well, the envelope functions form parity sets $P_1 = \{\Phi_1, \Phi_2, \Phi_7, \Phi_8\}$ and $P_2 = \{\Phi_3, \Phi_4, \Phi_5, \Phi_6\}$ so that a definite parity state Ψ has envelopes from one set that are of even parity whilst those from the other set have odd parity. The wavefunction Ψ may be normalised using the relation

$$\langle \Psi | \Psi \rangle = A_\parallel \sum_{\text{region}} \sum_{i=1}^{8} \sum_{j,j'} \overline{G}_{ij} G_{ij'} L_{jj'} \tag{6.70}$$

with

$$L_{jj'} = \int_{\text{region}} \exp\left[ik_{j'}(z - z_{j'}) - i\overline{k}_j(z - z_j)\right] dz \tag{6.71}$$

where $z_j = z_{j'} = z_{\text{left}}$ if the region is the left barrier and $z_j = z_{j'} = z_{\text{right}}$ if it is the right barrier. For the well region the values of z_j and $z_{j'}$ depend on whether $j \leq j_{\text{mid}}$ or $j > j_{\text{mid}}$. Hence defining $k_{\text{diff}} = k_{j'} - \overline{k}_j$ then for the left barrier

$$L_{jj'} = \frac{1}{ik_{\text{diff}}} \tag{6.72}$$

and for the right barrier

$$L_{jj'} = -\frac{1}{ik_{\text{diff}}} \tag{6.73}$$

In the well $L_{jj'}$ takes the values

$$L_{jj'} = \left\{ \begin{array}{cc} \left[\exp(ik_{\text{diff}}L) - 1\right]/ik_{\text{diff}} & \text{for } j, j' \leq j_{\text{mid}} \\ \left[\exp(-i\overline{k}_j L) - \exp(-ik_{j'}L)\right]/ik_{\text{diff}} & \text{for } j \leq j_{\text{mid}} < j' \\ \left[\exp(ik_{j'}L) - \exp(i\overline{k}_j L)\right]/ik_{\text{diff}} & \text{for } j' \leq j_{\text{mid}} < j \\ \left[1 - \exp(-ik_{\text{diff}}L)\right]/ik_{\text{diff}} & \text{for } j_{\text{mid}} < j, j' \end{array} \right] \tag{6.74}$$

but it is possible that $k_{\text{diff}} = 0$ in the well and then

$$L_{jj'} = L \exp\left[-ik_{j'}(z_{j'} - z_j)\right] \tag{6.75}$$

The use of the normalised wavefunctions to calculate optical matrix elements is considered in section 6.4.

Section 6.3. Numerical considerations.

The first problem in implementing the bandstructure techniques described above is to determine a method to search for $\det M = 0$. As $\det M$ is a complex quantity it is not possible to look for zero crossings directly (although for the infinite well case $\det M$ makes abrupt changes from being wholly real to wholly imaginary and vice versa which simplifies the problem). An alternative is to look for minimum values of $|\det M|$ and then check that these occur for $\det M = 0$. The search procedure is divided into two steps. Firstly the energy range of interest is scanned through in small steps of energy ~ 0.1 eV. Then a bisection technique is used to narrow down the accuracy of the energy value for the bandstructure to the order of micro-electronvolts. This degree of accuracy is required to avoid numerical inaccuracies in the calculation of the wavefunctions. Assume that three values $f(a), f(b), f(c)$ of $|\det M|$ have been calculated at equally spaced points a, b, c such that $f(b) \leq f(a)$ and $f(b) \leq f(c)$. This is a region where a minimum value occurs and so the bisection technique is started by calculating two new values $f(d)$ and $f(e)$ at the points $d = (a+b)/2$ and $e = (b+c)/2$. If $f(d) \leq f(b)$ then the three initial values may be replaced by $f(a), f(d), f(b)$. Otherwise if $f(e) \leq f(b)$ then the three initial values may be replaced by $f(b), f(e), f(c)$. If neither of these inequalities hold then the three new values are $f(d), f(b), f(e)$. In any case the size of the interval has been halved and the procedure may be iterated to increase the accuracy to the desired level.

One numerical difficulty in the finite well calculations is the evaluation of exponential terms $\exp(ik_z z)$ at the well edges $z = z_{\text{left}}$ and $z = z_{\text{right}}$ for wavevectors with large values of $|\Im\text{m}\, k_z|$ and the avoidance of this problem is the reason that the form of the wavefunctions given in equations (6.55) to (6.57) is adopted. However, as the wavevectors k_z change with changing energy E this approach constantly redefines the coefficients $\mathbf{A}_B$ and $\mathbf{A}_W$ which appear in equations (6.62) and (6.63). So suppose that $\mathbf{A}_B$ and $\mathbf{A}_W$ are subject to the linear transformations

$$\hat{\mathbf{A}}_B = \Lambda_B \mathbf{A}_B \tag{6.76}$$

$$\hat{\mathbf{A}}_W = \Lambda_W \mathbf{A}_W \tag{6.77}$$

This requires that the matrices F and D used for the boundary matching also be transformed as

$$\hat{F}_B = F_B \Lambda_B^{-1} \tag{6.78}$$

$$\hat{F}_W = F_W \Lambda_W^{-1} \tag{6.79}$$

$$\hat{D}_B = D_B \Lambda_B^{-1} \tag{6.80}$$

$$\hat{D}_W = D_W \Lambda_W^{-1} \tag{6.81}$$

Then

$$\begin{aligned}
\det \hat{M} &= \det \left[\hat{F}_W^{-1} \hat{F}_B \hat{D}_B^{-1} \hat{D}_W - I \right] \\
&= \det \left[\Lambda_W F_W^{-1} F_B \Lambda_B^{-1} \Lambda_B D_B^{-1} D_W \Lambda_W^{-1} - I \right] \\
&= \det \left[F_W^{-1} F_B D_B^{-1} D_W - I \right] \\
&= \det M
\end{aligned} \tag{6.82}$$

so that the transformation does not affect the value of $\det M$. Hence, the introduction of the arbitrary phase factors $\exp(-ik_z z_{\text{left}})$ and $\exp(-ik_z z_{\text{right}})$ (and even the re-ordering of the wavevectors k_z) has no effect on $\det M$ and thus does not interfere with the scanning technique described above.

Finally a well-known numerical problem appears in the finite well bandstructure calculation where the value of $|\det M|$ becomes very large at particular values of energy E. In general the function $|\det M|$ is very smooth but spurious spikes appear at unpredictable energy values. If the value of E is changed by an extremely small amount (on the order of nano-electronvolts) the spike is avoided and the solution adopted was to calculate a number of values for $|\det M|$ near to the chosen value of E and then to pick a value which produced a smooth function. The three previously calculated points $f(a), f(b), f(c)$ were used to obtain a parabolic extrapolation (or interpolation) to predict the value of the next point to be calculated. Whilst stepping through in equal energy steps the value nearest to $f(a) - 3f(b) + 3f(c)$ was chosen and during the bisection phase the values of $(3f(a) + 6f(b) - f(c))/8$ and $(-f(a) + 6f(b) + 3f(c))/8$ where used to pick the values for $f(d)$ and $f(e)$ respectively.

Section 6.4. Calculation of optical matrix elements.

In this section the wavefunctions obtained using the techniques of the previous sections are used to investigate the effects of bandstructure on the optical response of a semiconductor quantum well. Of particular interest are the non-parabolicity of the energy subbands and the variation of the optical matrix elements in relation to the in-plane electronic wavevector $\mathbf{k}_{\|}$ and to the orientation of the electric field **E** of the light. For definiteness an 80Å (unstrained) quantum well of $In_{0.53}Ga_{0.47}As$ sandwiched between barriers of $In_{0.75}Ga_{0.25}As_{0.55}P_{0.45}$ is investigated. This system is of practical interest as it emits light in the 1.55μm window suitable for optical fibre communications. The material parameters used for the well and barriers are tabulated below [77,78].

	$In_{0.53}Ga_{0.47}As$	$In_{0.75}Ga_{0.25}As_{0.55}P_{0.45}$
E_g	0.75eV	0.99eV
Δ	0.33eV	0.25eV
$m_h^*[001]$	0.42	0.47
$\hat{m}_h^*[111]$	0.95	0.90
m_l^*	0.052	0.078
m_{so}^*	0.16	0.17
m_e^*	0.041	0.059

The effective masses m_h^* and $\hat{m}_h^*$ (heavy hole), m_l^* (light hole), m_{so}^* (spin split-off), m_e^* (electron) are used in the calculation of the parameters s, γ_1, γ_2, γ_3, P for the

finite quantum well model [73,74].

$$s = \frac{1}{m_e^*} - \left(1 + \frac{3E_g}{2\Delta}\right)\left[\frac{1}{m_h^*} + \frac{1}{m_l^*} - \frac{2}{m_{so}^*}\right] \tag{6.83}$$

$$\gamma_1 = -\frac{E_g}{2\Delta}\left[\frac{1}{m_h^*} + \frac{1}{m_l^*} - \frac{2}{m_{so}^*}\left(1 + \frac{\Delta}{E_g}\right)\right] \tag{6.84}$$

$$\gamma_2 = \frac{1}{2}\left[-\frac{E_g}{2\Delta}\left(\frac{1}{m_h^*} + \frac{1}{m_l^*}\right) + \frac{1}{m_{so}^*}\left(1 + \frac{E_g}{\Delta}\right) - \frac{1}{m_h^*}\right] \tag{6.85}$$

$$\gamma_3 = \frac{1}{2}\left[\gamma_1 - \frac{1}{\hat{m}_h^*}\right] \tag{6.86}$$

$$\lambda = \left(1 + \frac{E_g}{\Delta}\right)\left[\frac{1}{m_h^*} + \frac{1}{m_l^*} - \frac{2}{m_{so}^*}\right] \tag{6.87}$$

$$P = \left[\frac{\hbar^2}{2m}\frac{3\lambda E_g}{2}\right]^{1/2} \tag{6.88}$$

The data values above are used in conjunction with equations (6.83) to (6.88) to obtain the following parameter values used in the calculations.

	$In_{0.53}Ga_{0.47}As$	$In_{0.75}Ga_{0.25}As_{0.55}P_{0.45}$
s	-14.2	-2.7
P	1.76×10^{-28}Jm	1.42×10^{-28}Jm
γ_1	-3.52	0.36
γ_2	-2.94	-0.89
γ_3	-2.28	-0.38

The bandstructure near the band edges is shown in figure 6.1. The interband energy gap is 0.80eV which corresponds to a wavelength of 1.55μm. The conduction subband is essentially parabolic whilst the valence subbands display strong non-parabolicity with the first two subbands anti-crossing at a parallel wavevector of $k_{\|} \simeq 0.02\text{Å}^{-1}$. Figure 6.2 depicts the envelope functions of states at the Brillouin

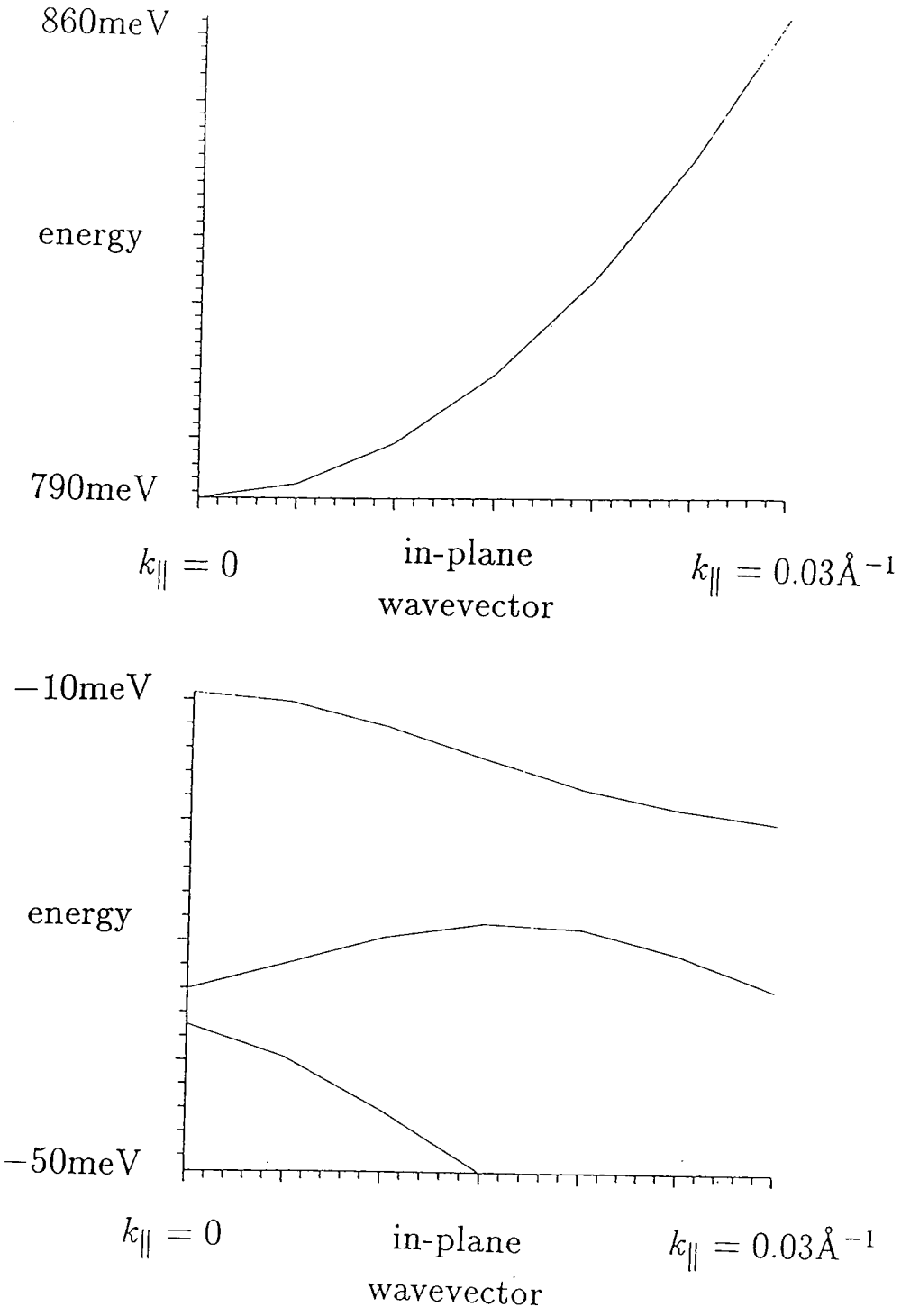

Figure 6.1. Bandstructure of an 80Å $In_{0.53}Ga_{0.47}As$ – $In_{0.75}Ga_{0.25}As_{0.55}P_{0.45}$ quantum well showing conduction subbands (top) and valence subbands (bottom) near the band edge.

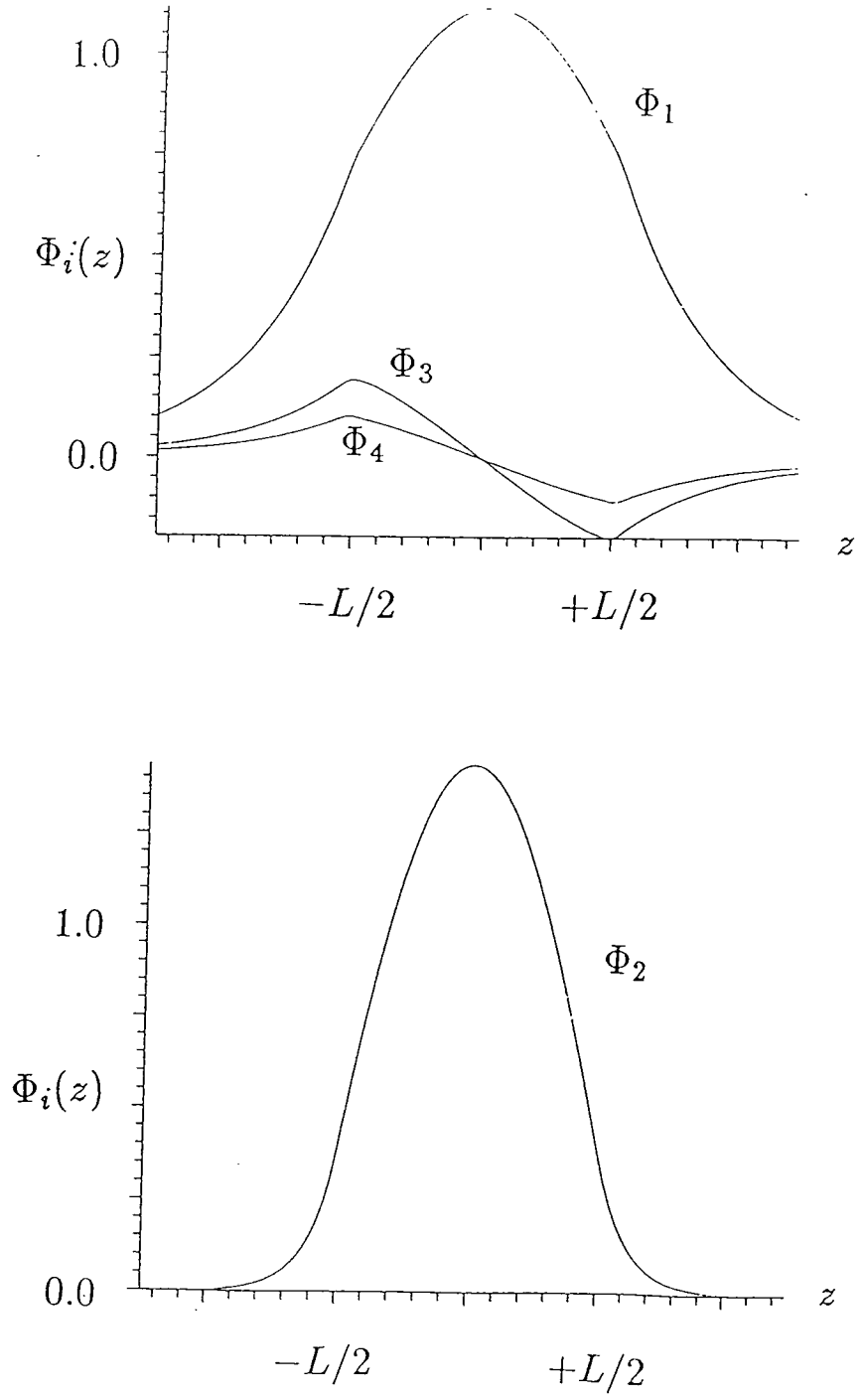

Figure 6.2. Envelope functions of zone centre states from the first conduction subband (top) and from the first valence subband (bottom) of figure 6.1 plotted against distance z in the growth direction (with the well edges at $\pm L/2$). The units are arbitrary but common to figures 6.2 and 6.3.

zone centre and shows that the conduction subband state consists principally of the conduction envelope Φ_1 with smaller contributions from the valence envelopes Φ_3 and Φ_4. As a result of the energy degeneracy there is a complementary state (not shown) comprising of the envelopes Φ_5, Φ_7 and Φ_8. Figure 6.2 also shows that the only significant envelope function of the zone centre state from the first valence subband is Φ_2. (The other energy degenerate state has Φ_6 as the only significant envelope). Further from the zone centre the states of the first valence subband exhibit increasingly large contributions from the envelopes Φ_7, Φ_3 and Φ_6 (see figure 6.3) as the anti-crossing of valence subbands results in a mixing of adjacent energy states.

Now to calculate some optical matrix elements using the **A**.**p** approach discussed in chapter two. Consider two normalised wavefunctions

$$\Psi_{\text{region}} = \exp(i\mathbf{k}_{\|}.\mathbf{r}_{\|}) \sum_{i,j} G_{ij} u_i \exp\left[ik_j(z - z_j)\right] \tag{6.89}$$

and

$$\hat{\Psi}_{\text{region}} = \exp(i\mathbf{k}_{\|}.\mathbf{r}_{\|}) \sum_{i',j'} \hat{G}_{i'j'} u_{i'} \exp\left[i\hat{k}_{j'}(z - \hat{z}_{j'})\right] \tag{6.90}$$

which have the same in-plane wavevector $\mathbf{k}_{\|}$. For the infinite well model the z co-ordinate is measured relative to $z_j = 0$, whilst for the finite well model it is measured relative to $z_j = z_{\text{left}}$ or $z_j = z_{\text{right}}$ dependent on the value of $\Im\text{m}\, k_j$ as described in section 6.2. The momentum matrix element may be calculated from

$$\langle \Psi_{\text{region}} | \mathbf{p} | \hat{\Psi}_{\text{region}} \rangle \simeq \sum_{i,j,i',j'} \overline{G}_{ij} \hat{G}_{i'j'} \sum_{\mathbf{r}_n} \exp\left[i\hat{k}_{j'}(z_n - \hat{z}_{j'}) - i\overline{k}_j(z_n - z_j)\right] \int_{\text{cell}} \overline{u}_i(\mathbf{p} + \hbar\hat{\mathbf{k}}_{j'}) u_{i'} d^3\mathbf{r}$$

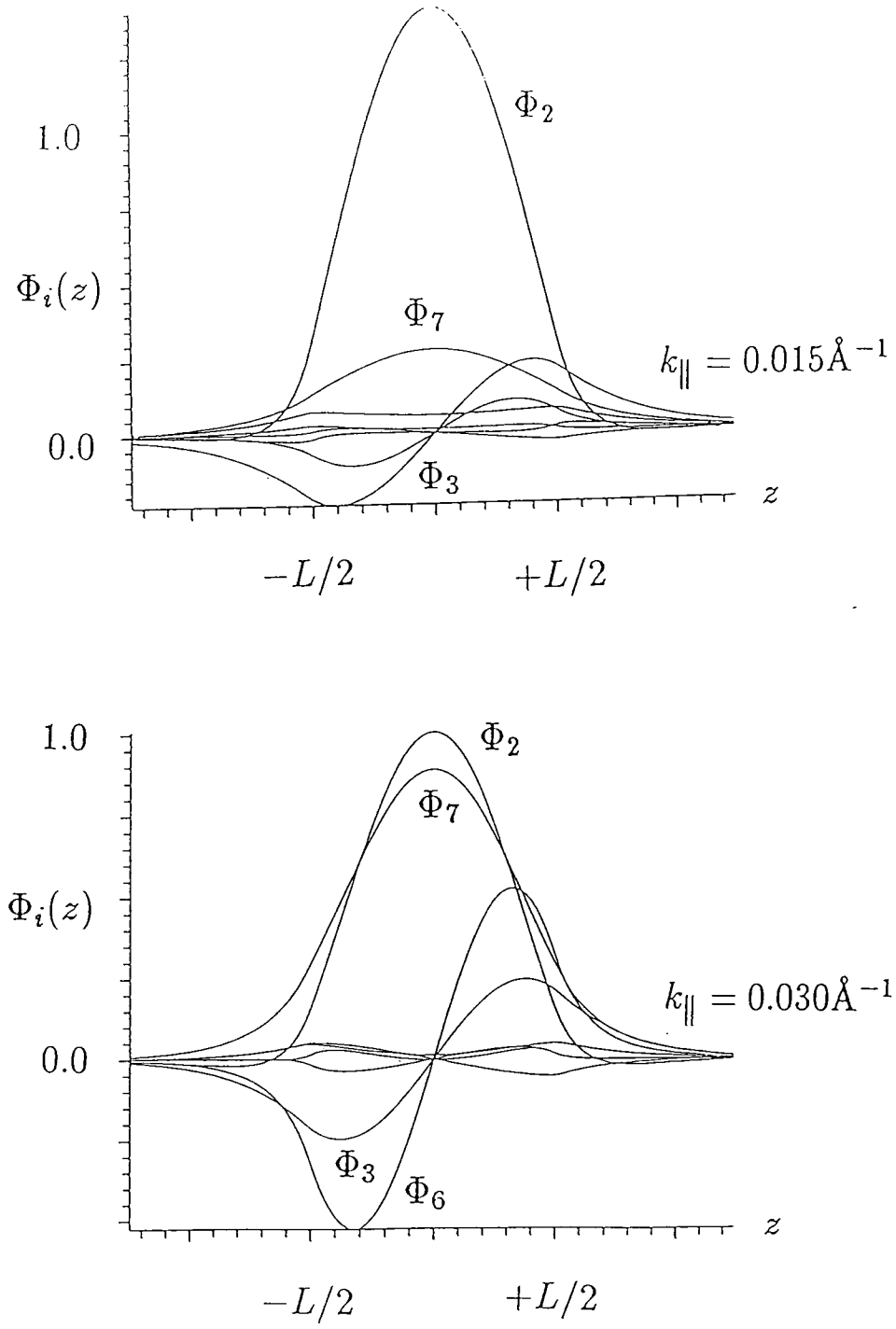

Figure 6.3. Influence of energy anti-crossing on first valence subband state showing increasing mixing with second valence subband state at larger values of $k_{\|}$.

$$\simeq A_{\|} \sum_{i,j,i',j'} \overline{G}_{ij} \hat{G}_{i'j'} L_{jj'} (\hbar \mathbf{k}_{ii'} + \hbar \hat{\mathbf{k}}_{j'} \delta_{ii'}) \tag{6.91}$$

where

$$L_{jj'} = \int_{\text{region}} \exp\left[i\hat{k}_{j'}(z - \hat{z}_{j'}) - i\overline{k}_j (z - z_j) \right] dz \tag{6.92}$$

may be evaluated by substituting $\hat{k}_{j'}$ for $k_{j'}$ in equations (6.31) and (6.72) to (6.75). Also $\hat{\mathbf{k}}_{j'} = \mathbf{k}_{\|} + \hat{k}_{j'} \mathbf{e}_z$ and the momentum matrix element for the unit cell is defined by $\hbar \mathbf{k}_{ii'} = \langle u_i | \mathbf{p} | u_{i'} \rangle_{\text{cell}}$. The values of $\hbar \mathbf{k}_{ii'}$ are determined from the basis states in equations (6.1) to (6.4) for the infinite well and in equations (6.33) to (6.40) for the finite well using the relations

$$\begin{aligned} &\langle S^+ | p^x | X^+ \rangle = \langle S^+ | p^y | Y^+ \rangle = \langle S^+ | p^z | Z^+ \rangle \\ &= \langle S^- | p^x | X^- \rangle = \langle S^- | p^y | Y^- \rangle = \langle S^- | p^z | Z^- \rangle = -\frac{mP}{i\hbar} \end{aligned} \tag{6.93}$$

where P is the Kane momentum parameter and with all other momentum matrix elements between $S^{\pm}, X^{\pm}, Y^{\pm}, Z^{\pm}$ being zero. The term containing $\hbar \mathbf{k}_{ii'}$ is the dominant term in equation (6.91). The momentum matrix element $\langle \Psi | \mathbf{p} | \hat{\Psi} \rangle$ is calculated using wavefunctions Ψ and $\hat{\Psi}$ obtained for the $In_{0.53}Ga_{0.47}As$ – $In_{0.75}Ga_{0.25}As_{0.55}P_{0.45}$ quantum well presented above. Although the energy dispersion is essentially isotropic in $\mathbf{k}_{\|}$ space, the value of $\langle \Psi | \mathbf{p} | \hat{\Psi} \rangle$ does depend on the orientation of $\mathbf{k}_{\|}$. For $\mathbf{k}_{\|}$ taken along the k_x direction and with the states $\Psi(\mathbf{k}_{\|})$ and $\hat{\Psi}(\mathbf{k}_{\|})$ taken from the first conduction and valence subbands respectively, the values of $|\langle \Psi | \hat{\mathbf{E}}.\mathbf{p} | \hat{\Psi} \rangle|$ are shown in figure 6.4 for $\hat{\mathbf{E}}$ (the electric field direction of the light) oriented along the x-, y-, and z-axes. The scale of the graphs

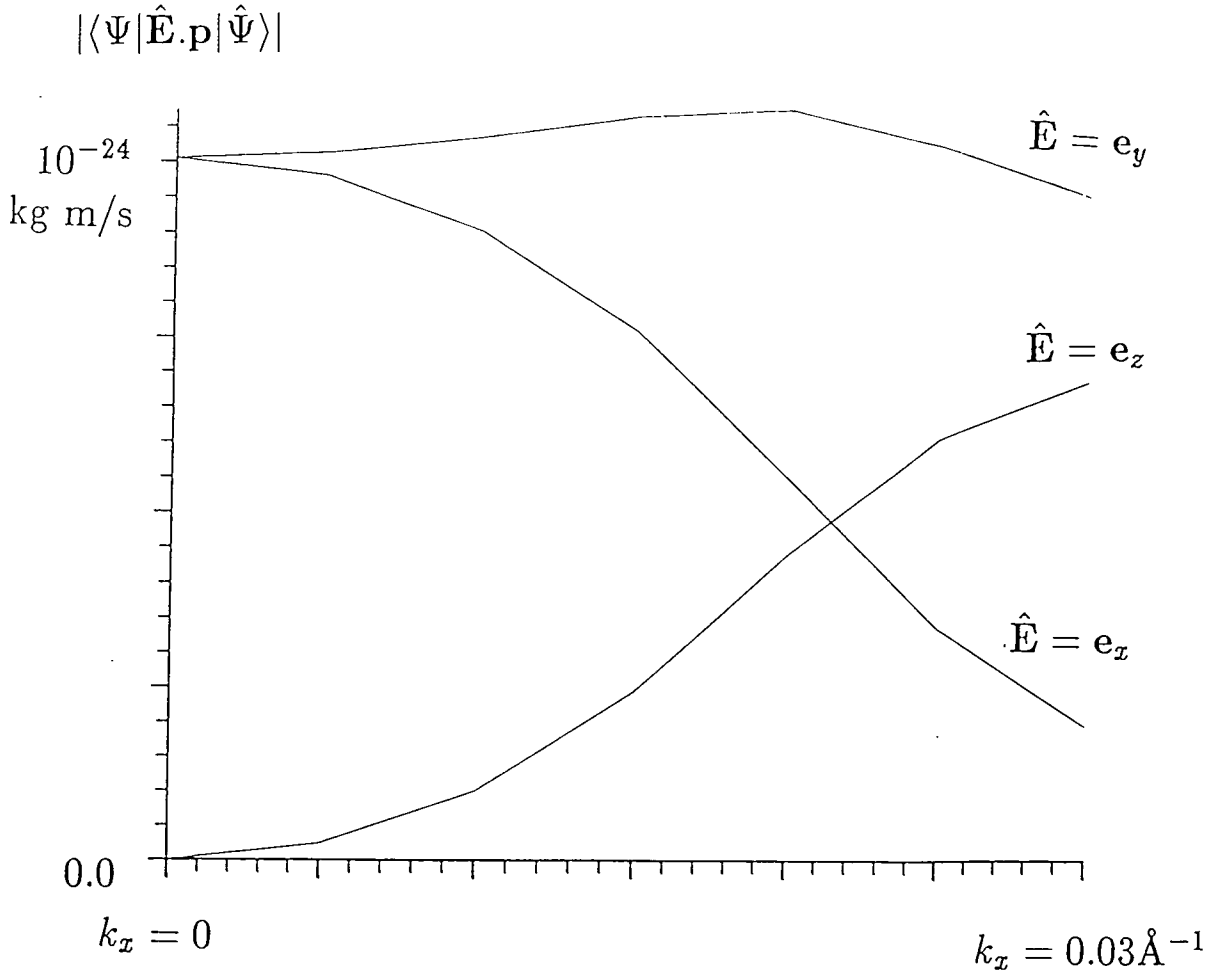

Figure 6.4. Variation with in-plane wavevector (along the k_x axis) of the magnitude of the optical matrix element for three orientations of the electric field vector.

is of the order 10^{-24} kg m s^{-1} which corresponds to an electronic displacement of the order of 10Å. For $\hat{\mathbf{E}} = \mathbf{e}_z$ the magnitude of the optical matrix element is zero at the Brillouin zone centre. Figure 6.2 shows that the valence state $\hat{\Psi}(\mathbf{0})$ comprises only the envelope Φ_2 (or Φ_6) and hence only the p-orbitals X and Y but $\langle S|p^z|X\rangle = \langle S|p^z|Y\rangle = 0$ so that for $\hat{\mathbf{E}} = \mathbf{e}_z$ the optical matrix element $\langle\Psi(\mathbf{0})|\hat{\mathbf{E}}.\mathbf{p}|\hat{\Psi}(\mathbf{0})\rangle$ must be zero. As the in-plane wavevector is increased along the k_x axis, the magnitude of optical matrix element increases for $\hat{\mathbf{E}} = \mathbf{e}_z$, whilst for $\hat{\mathbf{E}} = \mathbf{e}_x$ the magnitude decreases and for $\hat{\mathbf{E}} = \mathbf{e}_y$ it remains approximately constant over the range considered. If $\mathbf{k}_{||}$ is instead taken along the k_y direction, the graphs for $\hat{\mathbf{E}} = \mathbf{e}_x$ and $\hat{\mathbf{E}} = \mathbf{e}_y$ appearing in figure 6.4 are interchanged whilst that for $\hat{\mathbf{E}} = \mathbf{e}_z$ is unaffected, as would be expected from symmetry considerations. This behaviour has been described [79] for a simple parabolic band model which yields the relations

$$\langle\Psi|p^x|\hat{\Psi}\rangle = M\left(\cos\theta\cos\phi - i\sin\phi\right) \tag{6.94}$$

$$\langle\Psi|p^y|\hat{\Psi}\rangle = M\left(\cos\theta\sin\phi + i\cos\phi\right) \tag{6.95}$$

$$\langle\Psi|p^z|\hat{\Psi}\rangle = -M\sin\theta \tag{6.96}$$

where θ and ϕ are the polar and azimuthal angles of the wavevector $\mathbf{k} = \mathbf{k}_{||} + k_z\mathbf{e}_z$ and M is constant. For example, along the k_x direction $\phi = 0$ and

$$|\langle\Psi|p^x|\hat{\Psi}\rangle| = |M|\cos\theta \tag{6.97}$$

$$|\langle\Psi|p^y|\hat{\Psi}\rangle| = |M| \tag{6.98}$$

$$|\langle\Psi|p^z|\hat{\Psi}\rangle| = |M|\sin\theta \tag{6.99}$$

At the zone centre $\theta = 0$, and θ increases with k_x so that equations (6.97) to (6.99) describe qualitatively the behaviour seen in figure 6.4.

The non-parabolicity of the valence subbands causes the first valence subband to be relatively flat over the region shown in figure 6.1. The effect on the optical response is to reduce the detuning in this region and hence to increase the magnitude of the contributions for these values of wavevector. Figure 6.4 shows that the orientation of the electric field does influence the optical response and further investigations are necessary to determine, for example, the nonlinear effects achievable with several light beams oriented in different directions. A number of studies with this arrangement of light beams have been performed by Jaros and co-workers [26,29,95-96] using pseudopotential bandstructure calculations. Finally, the equations (6.94) to (6.96) show that different regions of the Brillouin zone can contribute responses with different phases and the influence of this on second order mixing, for example, offers another possibility for investigation.

CHAPTER SEVEN

Conclusion

The work presented in this thesis has been directed at establishing a clear physical picture of the ultrafast nonlinear optical phenomena which occur in semiconductor materials. In particular the two main regimes of operation have been examined, namely off-resonance excitation where virtual processes are important and on-resonance excitation where real carriers are photogenerated.

The difficulties in obtaining gauge invariant results when using the so called **A.p** and **E.r** gauges were investigated in chapter three, and the equivalence of first order susceptibilities obtained using the two gauges was explicitly demonstrated. The study of off-resonance phenomema in chapter four centered on two- and three-level quantum well systems, and it was shown that the concept of state-filling which is commonly used to describe a two-level system can be extended to the three-level model provided that second order mixing contributions can be neglected. The modelling of recent experimental investigations into the ultrafast optical properties of semiconductor laser amplifiers presented in chapter five provides a clear physical picture of a mechanism which predicts the observed behaviour. However, other theoretical explanations for the experimental observations have recently appeared

in the literature [80,81]. Whatever its origins, the nonlinear optical response of the laser amplifier promises the development of practical all-optical switching systems based on these devices. Finally, in chapter six a brief exploration of the effects of bandstructure on optical response has been made, and this has prompted a number of suggestions for further research.

The model of thermal relaxation processes developed in chapter five employed a number of phenomenological time constants, but it is possible to formulate theories of the scattering rates for these processes which start from first principles [82-84]. A deeper study of the scattering mechanisms and their relation to the optical response would be of interest, especially on the origins of the destruction of phase coherence (dephasing). A more complex description of spectral broadening than that provided by a Lorentzian line-shape has also been proposed [85-86].

Throughout this thesis, the influence of excitonic effects arising from Coulombic interactions has been neglected. In the study of the three-level systems proposed by Morrison and Jaros [25-29], this can be justified by arguing that such effects are small in the narrow bandgap materials capable of providing the equal spacing of energy levels required. Whilst with the work on laser amplifiers, the high carrier densities will substantially screen the influence of the Coulombic attractions between electron-hole pairs. Nevertheless, there has been much work devoted to investigating many-body effects and their influence on the optical properties of semiconductors [34-36,55,87-94] and these include the use of a density matrix de-

scription which could be employed to extend the model presented here.

REFERENCES

1. P. Lorrain and D.R. Corson, 'Electromagnetism – principles and applications' Freeman (1979).

2. A.M. Portis, 'Electromagnetic fields' Wiley (1978).

3. V. Rossiter, 'Electromagnetism' Heyden (1979).

4. P.N. Butcher and D. Cotter, 'The elements of nonlinear optics' Cambridge (1990).

5. N. Bloembergen, 'Nonlinear optics' Benjamin (1965).

6. P.N. Butcher and T.P. McLean, Proc. Phys. Soc. **81** 219 (1963).

7. Y.R. Shen, 'The principles of nonlinear optics' Wiley (1984).

8. L.I. Schiff, 'Quantum Mechanics' McGraw-Hill (1968).

9. E. Merzbacher, 'Quantum Mechanics' Wiley (1970).

10. R.D. Mattuck, 'A guide to Feynman diagrams in the many-body problem' McGraw-Hill (1976).

11. J.P. Uyemura, IEEE J. Quant. Elec. **QE-16** 472 (1980).

12. T.K. Yee and T.K. Gustafson, Phys. Rev. A **18** 1597 (1978).

13. J.G. Fujimoto and T.K. Yee, IEEE J. Quant. Elec. **QE-19** 861 (1983).

14. J.G. Fujimoto and T.K. Yee, IEEE J. Quant. Elec. **QE-22** 1215 (1986).

15. B.K. Ridley, 'Quantum Processes in semiconductors' Oxford (1988).

16. T.E. Feuchtwang, E. Kazes, P.H. Cutler and H. Grotch, J. Phys. A **17** 151 (1984).

17. D.H. Kobe and K.H. Yang, Phys. Rev. A **32** 952 (1985).

18. D.H. Kobe and K.H. Yang, Am. J. Phys. **51** 163 (1983).

19. D.H. Kobe and A.L. Smirl, Am. J. Phys. **46** 624 (1978).

20. K.H. Yang, Annals of Physics **101** 62 (1976).

21. K.H. Yang, J. Phys. A **15** 1201 (1982).

22. Z. Fried, Phys. Rev. A **8** 2835 (1973).

23. M.F. Reid, J. Phys. Chem. Solids **49** 185 (1988).

24. D.H. Kobe, Am. J. Phys. **50** 128 (1982).

25. I. Morrison, M. Jaros and A.W. Beavis, Appl. Phys. Lett. **55** 1609 (1989).

26. I. Morrison and M. Jaros, Phys. Rev. B **42** 3749 (1990).

27. I. Morrison and M. Jaros, J. Phys. Condens. Matter **2** 4879 (1990).

28. R.J. Turton and M. Jaros, IEE Proc. J **138** 323 (1991).

29. B.M. Adderley and M. Jaros, Opt. Materials **1** 141 (1992).

30. C. Cohen-Tannoudji and S. Reynaud, J. Phys. B **10** 345 (1977).

31. A. Mysyrowicz, D. Hulin, A. Antonetti, A. Migus, W.T. Masselink and H. Morkoç, Phys. Rev. Lett. **56** 2748 (1986).

32. M. Joffre, D. Hulin, J.P. Foing, J.P. Chambaret, A. Migus and A. Antonetti, IEEE J. Quant. Elec. **QE-25** 2505 (1989).

33. R. Zimmermann and M. Hartmann, Phys. Stat. Sol. B **150** 365 (1988).

34. S. Schmitt-Rink, D.S. Chemla and H. Haug, Phys. Rev. B **37** 941 (1988).

35. N. Peyghambarian, S.W. Koch, M. Lindberg, B. Fluegel and M. Joffre, Phys.

Rev. Lett. **62** 1185 (1989).

36. W.H. Knox, D.S. Chemla, D.A.B. Miller, J.B. Stark and S. Schmitt-Rink, Phys. Rev. Lett. **62** 1189 (1989).

37. M.G. Burt, Semicond. Sci. Technol. **5** 1215 (1990).

38. J.H. Shirley, Phys. Rev. **138** B979 (1965).

39. Y.B. Zel'dovich, Sov. Phys. JETP **24** 1006 (1967).

40. N.L. Manakov, V.D. Ovsiannikov and L.P. Rapoport, Phys. Reports **141** 319 (1986).

41. H.P. Breuer, K. Dietz and M. Holthaus, Z. Phys. D **8** 349 (1988).

42. H.P. Breuer, K. Dietz and M. Holthaus, Z. Phys. D **10** 13 (1988).

43. H.P. Breuer and M. Holthaus, Z. Phys. D **11** 1 (1989).

44. H.P. Breuer, K. Dietz and M. Holthaus, J. Phys. France **51** 709 (1990).

45. H.P. Breuer, K. Dietz and M. Holthaus, Il Nuovo Cimento **105** 53 (1990).

46. M.S. Stix, M.P. Kesler and E.P. Ippen, Appl. Phys. Lett. **48** 1722 (1986).

47. M.P. Kesler and E.P. Ippen, Appl. Phys. Lett. **51** 1765 (1987).

48. M.P. Kesler and E.P. Ippen, Elec. Lett. **24** 1102 (1988).

49. R.S. Grant and W. Sibbert, Appl. Phys. Lett. **58** 1119 (1991).

50. K.L. Hall, E.P Ippen and G. Eisenstein, Appl. Phys. Lett. **57** 129 (1990).

51. K.L. Hall, J. Mark, E.P. Ippen and G. Eisenstein, Appl. Phys. Lett. **56** 1740 (1990).

52. K.L. Hall, Y. Lai, E.P. Ippen, G. Eisenstein and U.Koren, Appl. Phys. Lett.

57 2888 (1990).

53. C.T. Hultgren and E.P. Ippen, Appl. Phys. Lett. **59** 635 (1991).

54. M.D. Crisp, Phys. Rev. A **8** 2128 (1973).

55. R. Binder, S.W. Koch, M. Lindberg and N. Peyghambarian, Phys. Rev. Lett. **65** 899 (1990).

56. W.Z. Lin, R.W. Schoenlein, J.G. Fujimoto and E.P Ippen, IEEE J. Quant. Elec. **QE-24** 267 (1988).

57. W.Z. Lin, J.G. Fujimoto, E.P. Ippen and R.A. Logan, Appl. Phys. Lett. **51** 161 (1987).

58. M. Yamada, IEEE J. Quant. Elec. **QE-19** 1365 (1983).

59. M. Yamada and Y. Suematsu, J. Appl. Phys. **52** 2653 (1981).

60. D. Ahn and S.L. Chuang, IEEE J. Quant. Elec. **QE-26** 13 (1990).

61. R.F. Kazarinov, C.H. Henry and R.A. Logan, J. Appl. Phys. **53** 4631 (1982).

62. W.E. Lamb, Phys. Rev. **134** A1429 (1964).

63. G.P. Agrawal, IEEE J. Quant. Elec. **QE-23** 860 (1987).

64. M.J. LaGasse, K.K. Anderson, H.A. Haus and J.G. Fujimoto, Appl. Phys. Lett. **54** 2068 (1989).

65. M.J. LaGasse, K.K. Anderson, C.A. Wang, H.A. Haus and J.G. Fujimoto, Appl. Phys. Lett. **56** 417 (1990).

66. D. Ahn and S.L. Chuang, IEEE J. Quant. Elec. **QE-24** 2400 (1988).

67. D.A. Broido and L.J. Sham, Phys. Rev. B **31** 888 (1985).

68. A. Twardowski and C. Herman, Phys. Rev. B **35** 8144 (1987).

69. S.S. Nedorezov, Sov. Phys. Solid State **12** 1814 (1971).

70. B.K. Ridley, J. Appl. Phys. **68** 4667 (1990).

71. J.M. Luttinger, Phys. Rev. **102** 1030 (1956).

72. A.C.G. Wood, Ph.D. Thesis, University of Durham (1990).

73. M.F.H. Schuurmans and G.W. t'Hooft, Phys. Rev. B **31** 8041 (1985).

74. R. Eppenga, M.F.H. Schuurmans and S. Colak, Phys. Rev. B **36** 1554 (1987).

75. E.O. Kane, J. Phys. Chem. Solids **1** 249 (1957).

76. M.G. Burt, J. Phys. Condens. Matter **4** 6651 (1992).

77. N.K. Dutta and R.J. Nelson, J. Appl. Phys. **53** 74 (1981).

78. Landolt-Börnstein,'Numerical Data and Functional Relationships in Science and Technology' Springer-Verlag (1982).

79. M. Asada, A. Kameyama and Y. Suematsu, IEEE J. Quant. Elec. **QE-20** 745 (1984).

80. M. Sheik-Bahae, D.C. Hutchings, D.J. Hagan and E.W. Van Stryland, IEEE J. Quant. Elec. **QE-27** 1296 (1991).

81. D.C. Hutchings, M. Sheik-Bahae, D.J. Hagan and E.W. Van Stryland, Opt. Quant. Elec. **24** 1 (1992).

82. M. Asada, IEEE J. Quant. Elec. **QE-25** 2019 (1989).

83. A.I. Kucharska and D.J. Robbins, IEEE J. Quant. Elec. **QE-26** 443 (1990).

84. P.T. Landsberg and D.J. Robbins, Solid State Elec. **28** 137 (1985).

85. M. Yamanishi and Y. Lee, IEEE J. Quant. Elec. **QE-23** 367 (1987).

86. T. Ohtoshi and M. Yamanishi, IEEE J. Quant. Elec. **QE-27** 46 (1991).

87. Y.H. Lee, A. Chavez-Pirson, S.W. Koch *et al.*, Phys. Rev. Lett. **57** 2446 (1986).

88. S.W. Koch, N. Peyghambarian and H.M. Gibbs, J. Appl. Phys. **63** R1 (1988).

89. S.H. Park, J.F. Morhange, A.D. Jeffery *et al.*, Appl. Phys. Lett. **52** 1201 (1988).

90. C. Ell, J.F. Müller, K. El Sayed and H. Haug, Phys. Rev. Lett. **62** 304 (1989).

91. S. Schmitt-Rink and D.S. Chemla, Phys. Rev. Lett. **57** 2752 (1986).

92. M. Lindberg and S.W. Koch, Phys. Rev. B **38** 3342 (1988).

93. I. Balslev, R. Zimmermann and A. Stahl, Phys. Rev. B **40** 4095 (1989).

94. S.W. Koch, N. Peyghambarian and M. Lindberg, J. Phys. C **21** 5229 (1988).

95. M.J. Shaw, D.Ninno, B.M. Adderley and M. Jaros, Phys. Rev. B **45** 11031 (1992).

96. M.J. Shaw, K.B. Wong and M. Jaros, Phys. Rev. B **48** 2001 (1993).